Dynamical Core Model Intercomparison Project (DCMIP)
Test Case Document

Paul Aaron Ullrich
Christiane Jablonowski
James Kent
Peter Hjort Lauritzen
Ramachandran D. Nair
Mark A. Taylor

DCMIP Summer School: July/30/2012 - August/10/2012

Version 1.7
January 14, 2013

Email questions to **dcmip@ucar.edu**

OVERVIEW OF THE TEST CASE SUITE

The set of test cases collected in this document has been developed for the Dynamical Core Model Intercomparison Project (DCMIP) in an effort to understand the broad treatment of the equations of motion within a variety of atmospheric General Circulation Models (GCMs). The majority of these dynamical core tests have either been drawn from the recent literature or have been inspired by existing ideas for 2D (x-z) and 3D tests. In particular, we made existing 2D Cartesian-geometry tests viable for 3D dynamical core assessments in spherical geometry, and extended existing 3D tests by adding dynamic tracer fields and including simplified moisture feedbacks. In some cases, the analytic expressions of the initial data and forcing mechanisms are completely new. All formulations are based on analytic initial conditions that have been formulated for hydrostatic and non-hydrostatic shallow-atmosphere equation sets. If models provide both a shallow-atmosphere and deep-atmosphere configuration, we recommend the shallow-atmosphere setup to avoid imbalances in the initial conditions. The preferred choice is to test the models in their non-hydrostatic formulations (if available). If models can be configured both as a hydrostatic and non-hydrostatic dynamical core, additional hydrostatic simulations might be conducted to evaluate the direct impact of the hydrostatic approximation.

Table I provides an overview of all test cases described in this document. The test cases are listed in order of increasing complexity, beginning with pure advection tests and non-rotating model configurations, dry baroclinic waves, and extending to test cases of intermediate complexity, incorporating moisture and very simplified physical parameterizations. In addition, an optional 10-day aqua-planet simulation with the model's own physical parameterization package is suggested.

0. PRACTICAL CONSIDERATIONS

0.1. List of Symbols

Throughout this test case document we will use $\lambda \in [0, 2\pi)$ to denote longitude, $\varphi \in [-\pi/2, \pi/2]$ to represent latitude, z to represent the height with respect to the mean sea level (assumed to be zero), and p to symbolize the pressure. Table II lists the symbols used for the initialization of the model variables in sections 1 through 5.

0.2. List of Physical Constants

A list of physical constants which are used throughout this document is given in Table III. Constants which are specific to each test case are similarly tabulated at the beginning of each section.

0.3. Small-Planet Experiments

The test case suite makes extensive use of small-planet experiments that have the potential to expose the differences between hydrostatic and non-hydrostatic modeling approaches at reasonable computational cost. In particular, the small-planet setups allow the evaluation of the model behavior with physical grid spacings down to a few hundred meters. In some instances, we suggest small planets with circumferences of about 40 km and a vertical extent of 30 km which raises questions

Table I. A list of test cases described in this document.

Test Case	Description
Pure advection	
1-1	3D deformational flow
1-2	3D Hadley-like meridional circulation
1-3	2D solid-body rotation of thin cloud-like tracer in the presence of orography
Impact of orography on a non-rotating steady-state at rest: Hydrostatic scales	
2-0-x	optional: Accuracy of the pressure-gradient calculation in presence of a mountain
Orographic and non-orographic gravity waves on a non-rotating small-planet: Non-hydrostatic scales	
2-1	Mountain waves over a Schär-type mountain on a small planet
2-2	Mountain waves over a Schär-type mountain on a small planet with wind shear
3-1	Non-orographic gravity waves on a small planet
Rotating planet: From hydrostatic to non-hydrostatic scales	
4-1-x	Dry baroclinic instability on a shrinking planet with dynamic tracers EPV and Θ reduction factors 1, 10, 100, 1000 to enable extreme grid spacings down to $\Delta x \approx 110$ m
Simple moist interactions	
4-2	Moist baroclinic instability with large-scale condensation
4-3	optional: Moist baroclinic instability with simplified physics forcings
5-1	Idealized tropical cyclone with simplified physics forcings
Complex moist interactions	
5-2	optional: Idealized tropical cyclone with full physics package

concerning the validity of the shallow-atmosphere approximation. However, since the experiments are not compared to observations, we still ask for the use of the shallow-atmosphere approach to allow for intercomparisons among the DCMIP models and to avoid imbalances of the initial conditions.

When a non-unity reduction factor X is applied in order to shrink the size of the Earth and thereby the physical grid spacing of the computational grid, a variety of model adjustments become necessary. Most prominently these include the scaling of the radius, the rotational speed, the model time step and explicit viscosity parameters (if applied). The adjustment steps for small-planet simulations are:

- Divide the radius of the Earth a_{ref} by X to obtain the rescaled radius $a = \frac{a_{\mathrm{ref}}}{X}$.
- Divide the length of the dynamics time step Δt by X, especially if a CFL condition needs to be obeyed.
- In case of rotating planets: multiply the Earth's angular velocity Ω_{ref} by the factor X to obtain the rescaled angular speed $\Omega = \Omega_{\mathrm{ref}} X$. This guarantees that the characteristics of Rossby waves are comparable in unscaled and scaled model experiments since the Rossby number stays constant.
- In case of explicit diffusion of type $K_{2k} \nabla^{2k}$ with a prescribed diffusion coefficient K_{2k} (and $k = 1, 2 \ldots$) divide K_{2k} by the factor X^{2k-1}. This accounts for a reduction of the e-folding time τ and the horizontal grid spacing Δx according to the relationship $\frac{(\Delta x)^{2k}/X^{2k}}{\tau/X}$. The K_{2k}

Table II. List of symbols for the model initialization

Symbol	Description
λ	Longitude (in radians)
φ	Latitude (in radians)
z	Height with respect to mean sea level (set to zero)
p_s	Surface pressure (p_s of moist air if $q > 0$)
Φ_s	Surface geopotential
z_s	Surface elevation with respect to mean sea level (set to zero)
u	Zonal wind
v	Meridional wind
w	Vertical velocity
ω	Vertical pressure velocity
δ	Divergence
ζ	Relative vorticity
p	Pressure (pressure of moist air if $q > 0$)
ρ	Density (density of moist air if $q > 0$)
T	Temperature
T_v	Virtual temperature
Θ	Potential temperature
Θ_v	Virtual potential temperature
q	Specific humidity
P_{ls}	Large-scale precipitation rate
q_1, q_2, q_3, q_4, q_5	Passive tracers

Table III. A list of physical constants used in this document.

Constant	Description	Value
a_{ref}	Radius of the Earth	6.37122×10^6 m
Ω_{ref}	Rotational speed of the Earth	7.292×10^{-5} s^{-1}
X	Reduced-size Earth reduction factor	variable (default $= 1$)
a	Scaled radius of the Earth	a_{ref}/X
Ω	Scaled rotational speed of the Earth	$\Omega_{\text{ref}} \cdot X$
g	Gravity	9.80616 m s^{-2}
p_0	Reference pressure	1000 hPa
c_p	Specific heat capacity of dry air at constant pressure	1004.5 J kg^{-1} K^{-1}
c_v	Specific heat capacity of dry air at constant volume	717.5 J kg^{-1} K^{-1}
R_d	Gas constant for dry air	287.0 J kg^{-1} K^{-1}
R_ν	Gas constant for water vapor	461.5 J kg^{-1} K^{-1}
κ	Ratio of R_d to c_p	$R_d/c_p = 2/7$
ε	Ratio of R_d to R_ν	$R_d/R_\nu \approx 0.622$
ρ_{water}	Density of water	1000 kg m^{-3}

diffusion coefficient is typically based on such a relationship. Note that some models might provide an automatic scaling of the diffusion coefficients according to the actual dynamics time step and grid spacing. If a model applies Rayleigh friction as a sponge near the model top, the friction coefficient needs to be multiplied by X. Again, this corresponds to a reduction of the e-folding frictional time scale $\frac{1}{\tau/X} = \frac{X}{\tau}$ in small-planet experiments.

- If physical forcing mechanisms are present on the right hand side of the equations of motion the strengths of the physical forcing must be increased (multiplied) by the factor X. This will

not be applicable to the test cases presented here unless Rayleigh friction is considered as such a forcing as outlined above.

0.4. Notes on the Requested Model Output

0.4.1. NetCDF

A fundamental requirement for the exchange of scientific data is the ability to precisely describe the physical quantities being represented. Therefore, special attention needs to be paid to the representation of the model data in the output files. We require data in the 'Network Common Data Form' (netCDF) [1] that adhere to the netCDF Climate and Forecast (CF) metadata convention (if possible to version 1.6 from Dec. 2011 [2]). All netCDF files should have the file name extension '.nc'. We specify details of the netCDF requirements in Appendix G and will also provide help via NCO operators before the DCMIP event to make the data CF-compliant if necessary. Please communicate your output constraints or concerns (if any) to the DCMIP organizers as soon as possible. We will also ask for example data sets before the DCMIP event.

0.4.2. Computational grid

Most DCMIP models utilize non-orthogonal computational grids like cubed-sphere grids, icosahedral grids, hexagonal grid, Voronoi grids or Yin-Yang grids. Among the mix of DCMIP GCMs are even models that provide provisions for variable-resolution grids. We encourage the use of the variable-resolution configurations as an additional test option whenever possible. This raises questions concerning the desired representation of the data in the netCDF output files.

If models on non-traditional (non latitude-longitude) grids are used, we ask for two output files that represent the identical model run. The first output file should be written on the native computational grid without any interpolations. In addition, most models will likely provide built-in provisions for interpolated output to a regular (equidistant in degrees) latitude-longitude grid. We therefore also ask for a second output file that represents the data on model levels on the interpolated latitude-longitude grid. We ask for co-located (Arakawa-A type) data on the interpolated grid regardless of the GCM's staggering options. The grid spacing of the interpolated grid should be comparable to the actual resolution of the model run, which might be for example $1° \times 1°$. Using this example, the interpolated grid will have 180×360 horizontal grid points if the equator and pole points are not part of the interpolated grid. If the equator and pole points are included it yields 181×360 horizontal grid points. If models can freely choose their interpolation points, we suggest the 180×360 configuration for the given example. If models need to include the equator and pole points, we ask for the 181×360 horizontal grid.

Models on regular latitude-longitude or Gaussian grids should only provide a single output file using their native horizontal resolution and model levels. If reduced Gaussian grids are utilized a second file on the full Gaussian grid is requested. If models are run with variable-resolution grids, we leave the choice of the best suitable interpolation grid to the modeling group. We ask to write all output variables for each experiment to the same file.

0.4.3. Naming convention for output file names

The naming convention for the final output file names is:

model.test_case.horizontal_resolution.levels.grid.equation.description.nc

NetCDF-CF compliant files with these naming conventions will be uploaded to the Earth System Grid on a NOAA server. The optional free-text character string at the end of the file name ("description") might be used to denote a special setting, such as a varied non-default diffusion coefficient or the selection of a variable-resolution configuration. The standard keywords for the DCMIP models are listed in the left columns of Tables IV and V. The keyword for the number of vertical levels, e.g. "L30", denotes the number of the full model levels (here 30). In case a model also employs interface levels, this setting indirectly implies that the model has one more interface level . Examples are

cam-fv.11.medium.L60.latlon.hydro.4th_order_div_damping.nc
mcore.12.high.L120.interp_latlon.nonhydro.nc
cam-se.51.high.L30.cubed.hydro.nc
cam-se.410.medium.L30.interp_latlon.hydro.double_K4_2e15.nc
cam-se.51.ultra.L30.interp_latlon.hydro.variable_220_25km.nc

The last example expresses the suggested naming convention for a variable-resolution simulation. The keyword 'ultra' denotes the finest grid spacing in the variable-resolution run which is, in this example, interpolated to a regular latitude-longitude grid with the same fine grid spacing of about 28 km. The free-text 'description' contains the suggested keyword 'variable' and specifies details about the resolution range in the variable-resolution run. In addition to such an interpolated data set, the original output file of a variable-resolution simulation should also be archived. Its name should be 'cam-se.51.ultra.L30.cubed.hydro.variable_220_25km.nc' for the example above, where the specification 'cubed' for the underlying base grid has been chosen.

Table IV. Keywords for the output file naming convention.

model	Organization
cam-fv	NCAR
cam-se	Sandia National Laboratories & NCAR
dynamico	LMD
endgame	UK Met Office
fim	NOAA ESRL
gem-latlon	Environment Canada
gem-yinyang	Environment Canada
fv3-gfdl	NOAA GFDL
icon-iap	IAP
icon-mpi-dwd	MPI & DWD
ifs	ECMWF
mcore	University of Michigan
nicam	RIKEN & University of Tokyo
nim	NOAA ESRL
mpas	NCAR & Los Alamos National Laboratory
olam	University of Miami
puma	University of Hamburg
uzim	Colorado State University

Table V. Continuation of the list of keywords for the output file naming convention: Grid specifications.

test_case	Description of the test case number
11	3D deformational flow
12	3D Hadley-like meridional circulation
13	2D transport of thin cloud-like tracer in the presence of orography
200	Accuracy of the pressure-gradients over a moderately-steep Schär-type mountain
201	Accuracy of the pressure-gradients over a steep single mountain
21	Mountain waves over a Schär-type mountain on a small planet
22	Mountain waves over a Schär-type mountain on a small planet with shear
31	Nonorographic gravity waves on a small planet, along the equator
410	Dry baroclinic instability with dynamic tracers EPV and Θ and X=1
411	Dry baroclinic instability with dynamic tracers EPV and Θ and X=10
412	Dry baroclinic instability with dynamic tracers EPV and Θ and X=100
413	Dry baroclinic instability with dynamic tracers EPV and Θ and X=1000
42	Moist baroclinic instability (with large-scale condensation)
43	optional: Moist baroclinic instability (with simplified physics forcing)
51	Idealized tropical cyclone (with simplified physics forcing)
52	optional: Idealized tropical cyclone (with full physics forcing)

horizontal_resolution	Approximate grid spacing in degrees or equatorial grid spacing (unscaled)
low	between 2°-2.5° or 220-275 km (on unscaled planet)
medium	between 1°-1.5° or 110-165 km (on unscaled planet)
high	between 0.5°-0.7° or 55-78 km (on unscaled planet)
ultra	between 0.25°-0.35° or 28-39 km (on unscaled planet)

levels	Number of vertical levels (full model levels)
L10	10 levels
L15	15 levels
L20	20 levels
L30	30 levels
L60	60 levels
L120	120 levels

grid	Type of native grid or indicator of interpolated grid
cubed	cubed sphere
hex	hexagonal grid based on an icosahedron, maybe optimized via spring dynamics
gauss	Gaussian grid
tri	triangular grid based on an icosahedron, maybe optimized via spring dynamics
interp_latlon	interpolated latitude-longitude grid
latlon	latitude-longitude
oct	octagonal
red_latlon	reduced latitude-longitude grid
red_gauss	reduced Gaussian grid
voronoi	spherical centriodal Voronoi tessellation
yinyang	Yin-Yang

equation	Indicator for hydrostatic or non-hydrostatic simulation
hydro	hydrostatic
nonhydro	non-hydrostatic

0.5. Short Note on Data Analysis and Visualization

We will provide NCAR Command Language (NCL) scripts to help visualize the model results and provide analysis functions. In addition, the DCMIP participants will have access to interactive Graphical User Interfaces (GUIs) to support the visualization and model intercomparison. Among the GUIs are the netCDF viewers Ncview and Panoply which are public domain tools and locally installed on the NCAR mirage server. In addition, we expect to provide some basic online visualization capabilities via NOAA's Live Access Server (LAS) software. A key to the successful visualization is the adherence of the output data sets to the netCDF-CF standard (see Appendix G).

0.6. Short Note on the Fortran Templates

We have provided a set of stand-alone Fortran routines that compute the initial conditions for all test cases. They are named

- dcmip_initial_conditions_test_1_2_3_v4.f90 (please disregard earlier versions)
  Change log for version 3 (v3, June/8/2012), version 4 (v4, July/8/2012), and version 5 (v5, July/20/2012):

  - v2: bug fixes in the tracer initialization for height-based models
  - v3: test 3-1: the density is now initialized with the unperturbed background temperature (not the perturbed temperature), equation (101)
  - v3: constants converted to double precision
  - v4: modified tracers in test 1-1 with cutoff altitudes. This change was reversed in version 5 that no longer required this adjustment.
  - v4: modified cos-term in vertical velocity (now $\cos(2\pi t/\tau)$) in test 1-1, now completing one full up and down cycle, equation (16)
  - v4: added subroutine test1_advection_orography for test 1-3
  - v4: added subroutine test2_steady_state_mountain for test 2-0-0
  - v4: modified parameter list for tests 2-1 and 2-2 (routine test2_schaer_mountain): addition of parameters hybrid_eta, hyam, hybm
    if the logical flag "hybrid_eta" is true then the pressure in pressure-based model with hybrid sigma-p (η) coordinates is computed internally. In that case the hybrid coefficients hyam and hybm need to be supplied via the parameter list, otherwise they are not used.
  - v5: test 1-1: modified vertical velocity and zonal velocity. The vertical velocity has a new tapering function (17), and an adjustment is added to the zonal velocity (23) to fulfill the continuity equation. This ensures that the advection process written in the advective or conservative form is equivalent.
  - v5: no cutoff altitude for the tracers in test 1-1 (reverses a change from version v4)
  - v5: test 1-2: modified meridional wind (37) and vertical velocity equation (38) with a new amplitude w_0 and positions z_1 and z_2 that determine the initial location of the tracer.

- dcmip_initial_conditions_test_4_v3.f90 (please disregard earlier versions)
  Change log for version 2 (v2, June/8/2012) and version 3 (v3, July/20/2012):

- – v2: correction of a typo (removal of 1/a) on the right-hand side of the $\frac{\partial \theta}{\partial \varphi}$, equation (137)
  - – v2: initialization of q_2 with the absolute value of Ertel's Potential Vorticity (EPV), equations (131) and (132)
  - – v3: additional if-construct that prevents division by zero in relative vorticity (ζ) calculation (133) in case the perturbation center point, its antipode, or the north or south poles are part of the computational grid

- dcmip_initial_conditions_test_5_v1.f90

These updates are also marked in the Fortran codes. Their inline documentation makes these routines self-explanatory. The input parameter list needs to be supplied with the position of a single grid point. The routines can either be included into the GCM source code or be used to compute an initial data file. Some output parameters might not be needed, depending on the model design.

In addition, we have provided a template Fortran routine

- simple_physics_v5.90 (please disregard earlier versions)
  Change log for version 4 and before (v4, June/8/2012) and version 5 (v5, July/8/2012):

  - – v2: removal of some NCAR CAM-specific "use" associations
  - – v3: corrected $precl(i)$ computation, the precipitation rate is now computed via a vertical integral, the previous single-level computation in v2 was a bug
  - – v3: corrected $dtdt(i, 1) =$ computation, the term $-(i, 1)$ was missing the temperature variable: $-t(i, 1)$
  - – v4: modified and enhanced parameter list to make the routine truly standalone, the number of columns and vertical levels have been added: pcols, pver
  - – v4: "ncol" has been removed, "pcols" is used instead
  - – v5: the sea surface temperature (SST) field $Tsurf$ is now an array, the SST now depends on the latitude
  - – v5: addition of the latitude array "lat" and the flag "test" in the parameter list
    if $test = 0$: constant SST is used, correct setting for the tropical cyclone test case 5-1
    if $test = 1$: newly added latitude-dependent SST is used, correct setting for the moist baroclinic wave test with simple-physics (test 4-3)

that implements suggested simplified physical forcing mechanisms [3] in the recommended order (1) large-scale condensation, (2) surface fluxes, and (3) boundary-layer mixing. These processes are coupled in a time-split manner [4] so that each mechanism already updates the state variables that are used for the next parameterization step. The template routine has been developed for NCAR's Community Atmosphere Model (CAM). It therefore needs to be tailored to match model-specific requirements such as the choice of the prognostic variables. The template routine assumes that the state variables u, v, T, p and q are co-located at full model levels. In addition, it assumes that the level indices follow a top-down approach with level index 1 located at the topmost level. If the vertical ordering of the levels is reversed, with level index 1 denoting the lowermost level, adjustments of the template routine are needed. In addition, all partial height derivatives have been expressed as pressure derivatives with the help of the hydrostatic equation as CAM is a pressure-based model. This could potentially be changed for models with height-based vertical coordinates.

0.7. Short Note on the Virtual, Shared DCMIP Workspace

We are building a 'virtual DCMIP community' via a shared Wiki-driven virtual workspace: http://earthsystemcog.org/projects/dcmip-2012/ We would like to ask you to create an account on this Commodity Governance (CoG) webpage (see 'create account' button in the upper left corner). CoG is a newly created cyberinfrastructure software hosted on a NOAA server that facilitates connections between projects and people. Please create a CoG account and after pressing 'submit', logon with your selected user name and password. Then navigate to DCMIP-2012, e.g. via http://earthsystemcog.org/projects/dcmip-2012/ and ask for membership in the DCMIP-2012 project (upper left corner, press 'Join the DCMIP-2012 project'). You will get an email shortly afterwards that will confirm that you have become a member. This will now enable you to edit the Wiki functionality within DCMIP-2012. We will utilize the DCMIP-2012 workspace before and during (and after) the summer school to share information, model documentation, metadata, model results, discussion points, online visualization, etc. The shared workspace will be a resource not just for the 2012 summer school, but for all researchers interested in dynamical cores, test cases and the dynamical core data in the future. The software will also build a bridge/links to the Earth System Grid where our intercomparison data will be hosted.

0.8. Summary of All DCMIP Model Experiments

This section provides an overview of all suggested experiments in Tables VI and VII. The tables list the specific settings for each experiment like the small-planet scaling coefficient, the suggested horizontal and vertical resolutions, the position of the model top, the length of the simulation, the desired output quantities and their output frequency. These pieces of information are also repeated in each of the test case descriptions below. Table VIII summarizes the necessary model adjustments, e.g. the rescaling of physical constants. It is desirable to supply such parameters or design choices (e.g. switch for the activation or deactivation of Rayeigh friction) through an input namelist file to minimize the actual modifications of the GCM course code.

All models should be run in their operational configurations which includes the typical diffusion mechanisms and coefficients, filters, time steps and other tunable parameters. In addition, the runs should utilizes their standard *a posteriori* fixers like mass or energy fixers if applicable. We ask to document all parameters and fixers to foster the model intercomparison. In addition, the modeling groups are also invited to test their models in non-operational configurations that, for example, use a reduced explicit diffusion coefficient. Such non-operational settings need to be clearly marked.

We also invite the modeling groups to test their variable-resolution grids, e.g. the nested- or stretched-grid options (if available), in addition to running the experiments on their native non-adapted grids. The choice of the non-uniform grid is left to the modeling group and should be documented.

Table VI. List of all DCMIP model experiments:
Test case, small-planet reduction factor X, horizontal grid spacing in degrees in both horizontal directions and the approximate physical grid spacing at the equator, levels, model top and vertical grid spacing.

Label	Test	X	Grid spacing	Levels	Model top	Δz
11.medium.L60	1-1	1	$1° \approx 110$ km	60	12 km ≈ 254.944 hPa	200 m
12.low.L30	1-2	1	$2° \approx 220$ km	30	12 km ≈ 254.944 hPa	400 m
12.medium.L60	1-2	1	$1° \approx 110$ km	60	12 km ≈ 254.944 hPa	200 m
12.high.L120	1-2	1	$0.5° \approx 55$ km	120	12 km ≈ 254.944 hPa	100 m
13.medium.L30	1-3	1	$1° \approx 110$ km	30	12 km ≈ 254.944 hPa	400 m
13.medium.L60	1-3	1	$1° \approx 110$ km	60	12 km ≈ 254.944 hPa	200 m
13.medium.L120	1-3	1	$1° \approx 110$ km	120	12 km ≈ 254.944 hPa	100 m
optional:						
200.medium.L15	2-0-0	1	$1° \approx 110$ km	15	12 km ≈ 205.448 hPa	800 m
200.medium.L30	2-0-0	1	$1° \approx 110$ km	30	12 km ≈ 205.448 hPa	400 m
201.low.L30	2-0-1	500	$2° \approx 440$ m	30	12 km	400 m
21.medium.L60	2-1	500	$1.5° \approx 333.6$ m	60	30 km ≈ 32.818 hPa	500 m
22.medium.L60	2-2	500	$1.5° \approx 333.6$ m	60	30 km ≈ 32.818 hPa	500 m
31.medium.L10	3-1	125	$1.125° \approx 1$ km	10	10 km ≈ 273.759 hPa	1000 m
410.medium.L30	4-1-0	1	$1° \approx 110$ km	30	≈ 44 km / 2.26 hPa	stretched
411.medium.L30	4-1-1	10	$1° \approx 11$ km	30	≈ 44 km / 2.26 hPa	stretched
412.medium.L30	4-1-2	100	$1° \approx 1.1$ km	30	≈ 44 km / 2.26 hPa	stretched
413.medium.L30	4-1-3	1000	$1° \approx 110$ m	30	≈ 44 km / 2.26 hPa	stretched
42.medium.L30	4-2	1	$1° \approx 110$ km	30	≈ 44 km / 2.26 hPa	stretched
42.high.L30	4-2	1	$0.5° \approx 55$ km	30	≈ 44 km / 2.26 hPa	stretched
optional:						
43.medium.L30	4-3	1	$1° \approx 110$ km	30	≈ 44 km / 2.26 hPa	stretched
43.high.L30	4-3	1	$0.5° \approx 55$ km	30	≈ 44 km / 2.26 hPa	stretched
51.medium.L30	5-1	1	$1° \approx 110$ km	30	≈ 44 km / 2.26 hPa	stretched
51.high.L30	5-1	1	$0.5° \approx 55$ km	30	≈ 44 km / 2.26 hPa	stretched
51.ultra.L30	5-1	1	$0.25° \approx 28$ km	30	≈ 44 km / 2.26 hPa	stretched
optional:						
52.high.L30	5-2	1	$0.5° \approx 55$ km	30	≈ 44 km / 2.26 hPa	stretched

Table VII. List of all DCMIP model experiments: Simulation length, output variables and output frequency.

Label	Length (unscaled)	Output variables	Output frequency
11.medium.L60	12 days	q_1, q_2, q_3, q_4, (q_5 optional)	daily (86400 s)
12.low.L30	1 day	q_1	hourly (3600 s)
12.medium.L60	1 day	q_1	hourly (3600 s)
12.high.L120	1 day	q_1	hourly (3600 s)
13.medium.L30	12 days	$q_1, q_2, q_3, q_4, p_s, p, \Phi_s$	daily (86400 s)
13.medium.L60	12 days	$q_1, q_2, q_3, q_4, p_s, p, \Phi_s$	daily (86400 s)
13.medium.L120	12 days	$q_1, q_2, q_3, q_4, p_s, p, \Phi_s$	daily (86400 s)
optional:			
200.medium.L15	6 days	u, v, w or $\omega, T, p_s, p, \Phi_s,$ T_{500}, w_{500} or ω_{500}	6-hourly (21600 s)
200.medium.L30	6 days	u, v, w or $\omega, T, p_s, p, \Phi_s,$ T_{500}, w_{500} or ω_{500}	6-hourly (21600 s)
201.low.L30	0.5 hr $\equiv 250$ hr (scaled)	u, v, w or $\omega, T, p_s, p, \Phi_s,$ T_{500}, w_{500} or ω_{500}	100 s (unscaled) $\equiv 50000$ s (scaled)
21.medium.L60	2 hr $\equiv 1000$ hr (scaled)	u, v, w or $\omega, T, p_s, p, \Phi_s$	100 s (unscaled) $\equiv 50000$ s (scaled)
22.medium.L60	2 hr $\equiv 1000$ hr (scaled)	u, v, w or $\omega, T, p_s, p, \Phi_s$	100 s (unscaled) $\equiv 50000$ s (scaled)
31.medium.L10	1 hr $\equiv 125$ hr (scaled)	u, v, w or ω, T, p_s, p	100 s (unscaled) $\equiv 12500$ s (scaled)
410.medium.L30	30 days	q_1, q_2, u, v, w or $\omega, T, p_s, p,$ $\Phi_s, u_{850}, v_{850}, T_{850}, \omega_{850}$ or w_{850}	daily (86400 s)
411.medium.L30	3 days $\equiv 30$ days (scaled)	q_1, q_2, u, v, w or $\omega, T, p_s, p,$ $\Phi_s, u_{850}, v_{850}, T_{850}, \omega_{850}$ or w_{850}	8640 s (unscaled) $\equiv$ daily (scaled)
412.medium.L30	25920 s $\equiv 30$ days (scaled)	q_1, q_2, u, v, w or ω, T, p_s, p $\Phi_s, u_{850}, v_{850}, T_{850}, \omega_{850}$ or w_{850}	864 (unscaled) $\equiv$ daily (scaled)
413.medium.L30	2592 s $\equiv 30$ days (scaled)	q_1, q_2, u, v, w or $\omega, T, p_s, p,$ $\Phi_s, u_{850}, v_{850}, T_{850}, \omega_{850}$ or w_{850}	86.4 s (unscaled) $\equiv$ daily (scaled)
42.medium.L30	15 days	q, u, v, w or $\omega, T, p_s, p, P_{ls}$ $\Phi_s, u_{850}, v_{850}, T_{850}, \omega_{850}$ or w_{850}	6-hourly (21600 s)
42.high.L30	15 days	q, u, v, w or $\omega, T, p_s, p, P_{ls}$ $\Phi_s, u_{850}, v_{850}, T_{850}, \omega_{850}$ or w_{850}	6-hourly (21600 s)
optional:			
43.medium.L30	15 days	q, u, v, w or $\omega, T, p_s, p, P_{ls}, SST$ $\Phi_s, u_{850}, v_{850}, T_{850}, \omega_{850}$ or w_{850}	6-hourly (21600 s)
43.high.L30	15 days	q, u, v, w or $\omega, T, p_s, p, P_{ls}, SST$ $\Phi_s, u_{850}, v_{850}, T_{850}, \omega_{850}$ or w_{850}	6-hourly (21600 s)
51.medium.L30	10 days	q, u, v, w or $\omega, T, p_s, p, P_{ls}$ $\Phi_s, u_{850}, v_{850}, T_{850}, \omega_{850}$ or w_{850}	6-hourly (21600 s)
51.high.L30	10 days	q, u, v, w or $\omega, T, p_s, p, P_{ls}$ $\Phi_s, u_{850}, v_{850}, T_{850}, \omega_{850}$ or w_{850}	6-hourly (21600 s)
51.ultra.L30	10 days	q, u, v, w or $\omega, T, p_s, p, P_{ls}$ $\Phi_s, u_{850}, v_{850}, T_{850}, \omega_{850}$ or w_{850}	6-hourly (21600 s)
optional:			
52.high.L30	10 days	q, u, v, w or $\omega, T, p_s, p,$ $\Phi_s, u_{850}, v_{850}, T_{850}, \omega_{850}$ or w_{850} surface fluxes, large-scale, convective and total precip. rate	6-hourly (21600 s)

Table VIII. A list of all model adjustments.

Test Case	Adjustments
Pure advection	
1-1, 1-2	suppress dynamic updates of the flow field, except for the tracers introduce counter that counts the elapsed seconds since the start of run prescribe time-dependent 3D velocities
1-3	suppress dynamic updates of the flow field, except for the tracers prescribe time-independent (initial) 3D velocities
Impact of orography on a non-rotating steady-state at rest: Hydrostatic scales	
2-0-0	set the rotational speed to zero
2-0-1	rescale the Earth, set the rotational speed to zero rescale the time step, diffusion coefficients
Orographic and non-orographic gravity waves on a non-rotating small-planet: Non-hydrostatic scales	
2-1, 2-2	rescale the Earth, set the rotational speed to zero rescale the time step, diffusion coefficients add Rayleigh friction to the uppermost 10 km of the domain
3-1	rescale the Earth, set the rotational speed to zero rescale the time step, diffusion coefficients
Rotating planet: From hydrostatic to non-hydrostatic scales	
4-1-0	no adjustment
4-1-1, 4-1-2, 4-1-3	rescale the Earth and rotational speed rescale the time step, diffusion coefficients
Simple moist interactions	
4-2	add large-scale condensation process
4-3, 5-1	add simplified physics forcings
Complex moist interactions	
5-2	set sea surface temperature (SST) to 29 °C switch to the model's aqua-planet mode

1. TEST CATEGORY 1-X: TRACER TRANSPORT EXPERIMENTS

This section includes three 3D passive advection tests with prescribed wind fields. To ensure that an analytic solution is known at the end of the simulation we apply time reversal to return the original profile to its original position (with some zonal offset) in two of the suggested tests. The third test utilizes a 2D solid-body rotation and returns the tracer to its initial position after one revolution around the sphere. These tests are used to assess consistency, monotonicity preservation, convergence rates and other properties which are relevant to the problem of tracer transport.

The tracer transport tests presented in this document make use of prescribed 3D velocities and an isothermal temperature field. Consequently, dynamic updates of the velocity, temperature, pressure and density fields need to be disabled, and prescribed (analytic) updates of the time-dependent velocity fields need to be included into the model code for test 1-1 and 1-2. Test 1-3 utilizes time-independent velocities that can be provided via the initial data set.

The pressure field is prescribed and needs to remain constant for the duration of the simulation except if floating Lagrangian pressure-based coordinates are used in the vertical direction [5] as explained below. The latter might require prescribed variations of the pressure thicknesses Δp between two model interface levels to account for deforming layers. Such a deformation for floating Lagrangian coordinates will only be valid for one time step before a vertical remapping algorithm restores the initial pressure values at the model levels.

The initial pressure field is given by

$$p(\lambda, \varphi, z) = p_0 \exp\left(\frac{-gz}{R_d T_0}\right), \tag{1}$$

where $T_0 \equiv 300$ K is the isothermal atmospheric temperature which yields $T(\lambda, \varphi, z) = T_0$ for all three test variants. The reference pressure at $z = 0$ m is set to $p_0 = 1000$ hPa. The surface pressure p_s can be computed when evaluating (1) at the surface elevation z_s which is specified later. The specific humidity field q is set to zero in all advection tests. Note that (1) can also be expressed as

$$z(\lambda, \varphi, p) = H \ln\left(\frac{p_0}{p}\right) \tag{2}$$

which utilizes the scale height

$$H = \frac{R_d T_0}{g}. \tag{3}$$

Equation (2) transforms the pressure into the height z in an isothermal atmosphere.

The advection process can be represented in many forms. If the advective form for the tracer q is selected it can be expressed as

$$\frac{dq}{dt} = 0 \tag{4}$$

$$\frac{\partial q}{\partial t} + \vec{v} \cdot \nabla q = 0 \tag{5}$$

for a Lagrangian and Eulerian framework, respectively. Here, $\vec{v}$ symbolizes the 3D wind vector, ∇ is the 3D gradient operator and d/dt stands for the material time (t) derivative.

If an advection scheme utilizes the conservation form

$$\frac{\partial}{\partial t}\left(\rho\, q\right) + \nabla \cdot \left(\vec{v}\, \rho\, q\right) = 0 \tag{6}$$

the density ρ needs to be present. In order to avoid solving a second transport equation for ρ and to simplify the test setup, the stratified density

$$\rho(\lambda, \varphi, p) \;=\; \frac{p}{R_d\, T_0} \tag{7}$$

$$\rho(\lambda, \varphi, z) \;=\; \frac{p_0}{R_d T_0} \exp\left(\frac{-z}{H}\right) \tag{8}$$

should be prescribed and held constant ($\partial \rho / \partial t = 0$) for the duration of the experiment. This will ensure that models with pressure-based and height-based vertical coordinates will resemble each other since isothermal conditions are used to determine the placement of the initial pressure levels. For the transport experiments provided in this document, the advective form (5) and conservation form (6) should produce nearly identical results, up to model error. This result holds since for all tests we require that $(\rho\,\vec{v})$ is a divergence-free field, i.e. that the continuity equation is analytically satisfied with

$$\frac{\partial \rho}{\partial t} = 0. \tag{9}$$

As a third variant, if an advection scheme utilizes a floating Lagrangian coordinate without explicit vertical transport the conservation law for the advection takes the form

$$\frac{\partial}{\partial t}\left(\Delta p\, q\right) + \nabla \cdot \left(\vec{v}_h\, \Delta p\, q\right) = 0 \tag{10}$$

where $\vec{v}_h$ denotes the horizontal wind vector. The vertical transport then needs to be mimicked by a vertical remapping algorithm after the horizontal advection step.

Normalized error norms are used in all three sets of tests, and defined by

$$\ell_1(q) \;=\; \frac{I\left[|q - q_T|\right]}{I\left[|q_T|\right]}, \tag{11}$$

$$\ell_2(q) \;=\; \sqrt{\frac{I\left[(q - q_T)^2\right]}{I\left[q_T^2\right]}}, \tag{12}$$

$$\ell_\infty(q) \;=\; \frac{\max|q - q_T|}{\max|q_T|}, \tag{13}$$

where q_T is the tracer field at the initial time (due to periodicity of the test cases, this is also the exact solution). Here I denotes an approximation to the global integral, given by

$$I[x] = \sum_{\text{all elements } j} x_j V_j, \tag{14}$$

where V_j denotes the volume of element j.

Table IX. List of constants used for the 3D Deformational Flow test case (Test $1-1$)

Constant	Value	Description
z_{top}	12000 m	Height position of the model top
p_{top}	≈ 254.944 hPa	Pressure at the model top
X	1	Small-planet scaling factor (regular-size Earth)
T_0	300 K	Isothermal atmospheric temperature
p_0	1000 hPa	Reference pressure
τ	1036800 s	Period of motion (here 12 days)
ω_0	$23000\,\pi/\tau$ Pa	Maximum of the vertical pressure velocity in units Pa/s
b	0.2	Normalized pressure depth of divergent layer
λ_{c1}	$5\pi/6$	Initial longitude of first tracer
λ_{c2}	$7\pi/6$	Initial longitude of second tracer
φ_c	0	Initial latitude of tracers
z_c	5000 m	Initial altitude of tracers
R_t	$a/2$	Horizontal half-width of tracers
Z_t	1000 m	Vertical half-width of tracers

1.1. Test 1-1: 3D Deformational Flow

The 3D deformational flow test is based on the 2D approach by [6], with a prescribed vertical wind velocity which makes the test truly 3D. An unscaled planet (with scale parameter $X = 1$) is selected. The test utilizes a translational longitude, defined by

$$\lambda' = \lambda - 2\pi t/\tau \tag{15}$$

where t denotes the elapsed time since the start of the simulation. The vertical pressure velocity is specified as

$$\omega(\lambda, \varphi, p, t) = \omega_0 \sin \lambda' \cos \varphi \cos \left(\frac{2\pi t}{\tau} \right) s(p), \tag{16}$$

where

$$s(p) = 1 + \exp \left(\frac{p_{top} - p_0}{b\,p_{top}} \right) - \exp \left(\frac{p - p_0}{b\,p_{top}} \right) - \exp \left(\frac{p_{top} - p}{b\,p_{top}} \right) \tag{17}$$

is a tapering function that tapers the vertical velocity to zero at the top and bottom of the domain. Since pressure and height surfaces are aligned, the pressure position p_{top} of the model top is

$$p_{top} = p(z_{top}), \tag{18}$$

where pressure is determined by (1). In terms of the translational longitude, the horizontal zonal and meridional velocities $\vec{u} = (u, v)$ are given as the sum of a horizontal deformational component $\vec{u}_a = (u_a, v_a)$ and a horizontally divergent component $\vec{u}_d = (u_d, 0)$,

$$\vec{u} = \vec{u}_a + \vec{u}_d. \tag{19}$$

The deformational zonal and meridional wind components follow from [6],

$$u_a(\lambda, \varphi, p, t) = k \sin^2 \lambda' \sin(2\varphi) \cos(\pi t/\tau) + \frac{2\pi a}{\tau} \cos \varphi, \tag{20}$$

$$v_a(\lambda, \varphi, p, t) = k \sin(2\lambda') \cos \varphi \cos(\pi t/\tau). \tag{21}$$

Here the magnitude of the velocity is specified as

$$k = \frac{10a}{\tau}. \tag{22}$$

The divergent zonal wind component is given by

$$u_d(\lambda, \varphi, p, t) = \frac{\omega_0 a}{b\, p_{\text{top}}} \cos \lambda' \cos^2 \phi \cos \left(\frac{2\pi t}{\tau} \right) \left[-\exp \left(\frac{p - p_0}{b\, p_{\text{top}}} \right) + \exp \left(\frac{p_{\text{top}} - p}{b\, p_{\text{top}}} \right) \right]. \tag{23}$$

This velocity field is chosen to satisfy the continuity equation exactly, i.e. in pressure-coordinates it yields

$$\frac{1}{a \cos \varphi} \left[\frac{\partial u}{\partial \lambda} + \frac{\partial}{\partial \varphi} (v \cos \varphi) \right] + \frac{\partial \omega}{\partial p} = 0. \tag{24}$$

The continuity equation is also fulfilled in height-based coordinates. The time-independent density is given by (7) or (8). The surface is flat with $z_s = 0$ m which yields the surface geopotential $\Phi_s = 0$ m^2 s^{-2}. The surface pressure does not depend on time, and is held constant with $p_s(\lambda, \varphi) = p_0$. Therefore, the vertical velocities for models with vertical σ [7] or hybrid σ-pressure (η) coordinates [8] yield

$$\dot{\eta}(\lambda, \varphi, \eta, t) = \dot{\sigma}(\lambda, \varphi, \sigma, t) = \frac{\omega}{p_0} = \frac{\omega_0}{p_0} \sin \lambda' \cos \varphi \cos \left(\frac{2\pi t}{\tau} \right) s(p) \tag{25}$$

where η and σ are given by $\eta = \sigma = p/p_0$ due to the choice of the constant surface pressure $p_s = p_0$. Note that this formulation assumes that the reference pressure for the hybrid η coordinate is set to 1000 hPa as also specified in Appendix F.1. Since there are neither time variations nor horizontal variations of the pressure field the vertical velocity in height coordinates takes the simple form

$$w(\lambda, \varphi, z, t) = -\frac{\omega(\lambda, \varphi, p(z), t)}{g\, \rho(z)} \tag{26}$$

with the density equation (8).

In case pressure-based floating Lagrangian coordinates are used the following discrete algorithm is suggested to prescribe the time-dependent deforming pressure surfaces. First, we recommend calculating the pressure values $p(t_2)$ at the future time $t_2 = t_1 + \Delta t$ where Δt symbolizes the time step length and t_1 is the current time counted in seconds since the start of the advection test. The new pressure values are then discretely given by

$$
\begin{aligned}
p(t_2) &= p(t_1) + \Delta t\, \omega \left(\lambda, \varphi, p, t_1 + \frac{\Delta t}{2} \right) \\
&= p(t_1) + \Delta t\, \omega_0 \, \sin \left[\lambda - \frac{2\pi}{\tau} \left(t_1 + \frac{\Delta t}{2} \right) \right] \cos(\varphi) \cos \left[\frac{2\pi}{\tau} \left(t_1 + \frac{\Delta t}{2} \right) \right] s \left[p \left(t_1 + \frac{\Delta t}{2} \right) \right]
\end{aligned} \tag{27}
$$

where a time-centered evaluation of the time-dependent expressions is selected. The time dependent Δp variation can then be computed as the difference of the pressures at model interfaces at time t_2, and set back to its initial value as part of a remapping algorithm.

Four tracer fields are specified for this test. The first tracer field represents two cosine bells, and is specified as

$$q_1(\lambda, \varphi, z) = \frac{1}{2} \left(1 + \cos(\pi d_1) \right) + \frac{1}{2} \left(1 + \cos(\pi d_2) \right), \tag{28}$$

where d_i $(i = 1, 2)$ denote the scaled distance functions,

$$d_i(\lambda, \varphi, z) = \min\left[1, \left\{\left(\frac{r_i(\lambda, \varphi)}{R_t}\right)^2 + \left(\frac{z - z_c}{Z_t}\right)^2\right\}\right], \tag{29}$$

and $r_i(\lambda, \varphi)$ $(i = 1, 2)$ denotes the great circle distance,

$$r_i(\lambda, \varphi) = a \arccos\left(\sin\varphi_c \sin\varphi + \cos\varphi_c \cos\varphi \cos(\lambda - \lambda_{ci})\right). \tag{30}$$

The second tracer is chosen to correlate with the first tracer,

$$q_2(\lambda, \varphi, z) = 0.9 - 0.8q_1(\lambda, \varphi, z)^2. \tag{31}$$

The third tracer is a slotted ellipse,

$$q_3(\lambda, \varphi, z) = \begin{cases} 1 & \text{if } d_1 < 1/2, \\ 1 & \text{if } d_2 < 1/2, \\ 0.1 & \text{otherwise.} \end{cases} \tag{32}$$

In order to cut the slot out of the cylinder an additional condition is imposed:

$$q_3(\lambda, \varphi, z) = 0.1 \quad \text{if } z > z_c \text{ and } \varphi_c - 1/8 < \varphi < \varphi_c + 1/8. \tag{33}$$

The final tracer is chosen that, in combination with the other tracer fields with weight (3/10), the sum is equal to one

$$q_4(\lambda, \varphi, z) = 1 - \frac{3}{10}\left[q_1(\lambda, \varphi, z) + q_2(\lambda, \varphi, z) + q_3(\lambda, \varphi, z)\right]. \tag{34}$$

For models that utilize the conservation of the advection equation, we also suggest running this test with the optional tracer field

$$q_5(\lambda, \varphi, z) = 1, \tag{35}$$

which tests how well the model is able to satisfy the 3D continuity equation (24) using this velocity field.

Grid spacings, simulation time, output and diagnostics

This test should be run at $1°$ resolution (~ 110 km equatorial grid spacing) in both horizontal directions with 60 uniformly spaced vertical levels (in height coordinates) for 12 days. For models using height levels a model top of $z_{\text{top}} = 12000$ m is suggested, which leads to a vertical grid spacing of $\Delta z = 200$ m. This means that the model interfaces are positioned at 0 m, 200 m, 400 m, etc. and that the full model levels are placed at 100 m, 300 m, 500 m, etc.. From (1) the height position of the model top corresponds to $p_{\text{top}} \approx 254.944$ hPa. Appendix F.3 outlines how pressure-based levels should be positioned in order to correspond to the equidistant grid spacing Δz.

Output should be recorded daily (every 86400 s) and needs to include the initial state (13 time snapshots). The desired output variables on model levels are the instantaneous snapshots of $q_1, q_2, q_3,$ and q_4 (and optionally q_5). The following analysis results are suggested:

- Latitude-longitude plots of q_1, q_2, q_3 and q_4 (and additionally q_5) should be produced at $t = 6$ days and 12 days at the height $z = 4900$ m.
- Longitude-height plots of all tracers should be produced at $t = 12$ days along the equator.
- Normalized l_1, l_2 and l_∞ error norms should be computed for q_1, q_3 and q_4 at $t = 12$ days against the initial conditions.
- Mixing diagnostics l_r, l_u and l_o should be computed at $t = 6$ days. These are described in Appendix A.
- Correlation plots should be produced for q_1 and q_2 at $t = 6$ days at the five levels around 4900 m (4500, 4700, 4900, 5100 and 5300 m). The approach for producing correlation plots is described in Appendix A.

1.2. Test 1-2: Hadley-like Meridional Circulation

Table X. List of constants used for the 3D Hadley-like Meridional Circulation test case (Test $1 - 2$).

Constant	Value	Description
z_{top}	12000 m	Height position of the model top
p_{top}	≈ 254.944 hPa	Pressure at the model top
X	1	Small-planet scaling factor (regular-size Earth)
T_0	300 K	Isothermal atmospheric temperature
p_0	1000 hPa	Reference pressure
τ	86400 s	Period of motion (here 1 day)
K	5	Number of overturning cells
u_0	40 m s^{-1}	Reference zonal velocity
w_0	0.15 m s^{-1}	Reference vertical velocity
z_1	2000 m	Lower boundary of tracer layer
z_2	5000 m	Upper boundary of tracer layer

The zonal, meridional and vertical velocity field for this test is specified as

$$u(\lambda, \varphi, z, t) = u_0 \cos\varphi, \tag{36}$$

$$v(\lambda, \varphi, z, t) = -\frac{a\, w_0\, \pi\, \rho_0}{K\, z_{\text{top}}\, \rho} \cos\varphi \sin(K\varphi) \cos\left(\frac{\pi z}{z_{\text{top}}}\right) \cos\left(\frac{\pi t}{\tau}\right), \tag{37}$$

$$w(\lambda, \varphi, z, t) = \frac{w_0\, \rho_0}{K\, \rho} \left(-2\sin(K\varphi)\sin\varphi + K\cos\varphi\cos(K\varphi)\right) \sin\left(\frac{\pi z}{z_{\text{top}}}\right) \cos\left(\frac{\pi t}{\tau}\right). \tag{38}$$

where the density equation (8) is used in the formulation of the vertical velocity w for height-based coordinates. The symbol ρ_0 denotes the density at the surface with $\rho_0 = p_0/(R_d T_0)$. The surface pressure is constant with $p_s(\lambda, \varphi) = p_0$. Since the pressure field p neither varies in time nor in the horizontal directions the vertical pressure velocity ω for pressure-based coordinates is easily obtained from (1), (26) and (38),

$$\omega(\lambda, \varphi, p, t) = -g\, \rho\, w(\lambda, \varphi, z(p), t). \tag{39}$$

The density ρ vanishes in this equation when plugging in (38). As in test $1-1$ the velocity components are chosen to satisfy the continuity equation exactly which yields

$$\frac{1}{a\cos\varphi}\left[\frac{\partial u}{\partial\lambda}+\frac{\partial}{\partial\varphi}(v\cos\varphi)\right]+\frac{\partial\omega}{\partial p} = 0 \tag{40}$$

$$\frac{1}{a\cos\varphi}\left[\frac{\partial(\rho u)}{\partial\lambda}+\frac{\partial}{\partial\varphi}(\rho v\cos\varphi)\right]+\frac{\partial(\rho w)}{\partial z} = 0 \tag{41}$$

in pressure- and height-coordinates, respectively. The density equation (7) or (8) is time independent and needs to be kept constant for advection schemes in conservation form. This design thereby guarantees that the test is equivalent for tracer advection schemes written in both the advective or conservation form.

The vertical velocities for models with vertical σ or hybrid σ-pressure (η) coordinates are given by

$$\dot{\eta}(\lambda,\varphi,\eta,t)=\dot{\sigma}(\lambda,\varphi,\sigma,t)=-\frac{g\,\rho}{p_0}\,w(\lambda,\varphi,z(p),t), \tag{42}$$

where η and σ are given by $\eta=\sigma=p/p_0$ due to the choice of the constant surface pressure $p_s=p_0$. As in test $1-1$ note that this formulation assumes that the reference pressure for the hybrid η coordinate is set to $p_0=1000$ hPa as also specified in Appendix F.1. If a floating Lagrangian coordinate is used on the basis of varying pressure thicknesses we recommend a mechanism that utilizes (39) in combination with the discrete approach described in (27).

The surface is flat with $z_s=0$ m which sets the surface geopotential $\Phi_s=0$ m^2 s^{-2}. The tracer field consists of a single layer which is deformed over the duration of the simulation. It is given by

$$q_1(\lambda,\varphi,z)=\begin{cases} \frac{1}{2}\left[1+\cos\left(\frac{2\pi(z-z_0)}{z_2-z_1}\right)\right] & \text{if } z_1<z<z_2, \\ 0 & \text{otherwise,} \end{cases} \tag{43}$$

where $z_0=\frac{1}{2}(z_1+z_2)$. For models with pressure-based coordinates (1) and (2) need to be used to convert between height and pressure positions.

Grid spacings, simulation time, output and diagnostics

This test should be run at $2°$ with 30 uniformly spaced vertical levels, $1°$ with 60 uniformly spaced vertical levels and $0.5°$ with 120 uniformly spaced vertical levels. For models using height levels a maximum altitude of $z_{\text{top}}=12000$ m is suggested. These resolutions correspond to an approximate horizontal grid spacing of about 220 km, 110 km and 55 km with a vertical grid spacing of $\Delta z=400$ m, $\Delta z=200$ m and $\Delta z=100$ m, respectively. From (1) the position of the model top yields the pressure $\sim p_{\text{top}}=254.944$ hPa. Appendix F.3 outlines how pressure-based levels should be positioned in order to correspond to the equidistant grid spacing Δz.

The simulation is run for $t=1$ day, until the tracer field returns to its original configuration. We suggest recording hourly model-level output (every 3600 s) of q_1 from each simulation. The output files needs to contain the initial state. For each of these resolutions normalized error norms ℓ_1, ℓ_2 and ℓ_∞ should be computed by comparing the results at $t=1$ day against the initial configuration. In addition, we suggest plotting a latitude-height cross section (at $\lambda=180°$) of the tracer field $q1$ at $t=12$ hr and $t=24$ hr.

1.3. Test 1-3: Horizontal advection of thin cloud-like tracers in the presence of orography

Table XI. List of constants used for the Horizontal advection of thin cloud-like tracers in the presence of orography test case (Test $1 - 3$).

Constant	Value	Description
z_{top}	12000 m	Height position of the model top
p_{top}	≈ 254.944 hPa	Pressure at the model top
X	1	Small-planet scaling factor (regular-size Earth)
T_0	300 K	Isothermal atmospheric temperature
p_0	1000 hPa	Reference surface pressure
u_0	$2\pi a_{\text{ref}}/\tau$	Maximum wind speed
τ	1036800 s	Period of motion (here 12 days)
α	$\pi/6$	Advection angle (radians, 30°)
λ_m	$3\pi/2$	Mountain longitude center point
φ_m	0	Mountain latitude center point
h_0	2000 m	Maximum mountain height
R_m	$3\pi/4$	Mountain radius (radians)
ζ_m	$\pi/16$	Mountain oscillation half-width (radians)
λ_p	$\pi/2$	Cloud-like tracer longitude center point
φ_p	0	Cloud-like tracer latitude center point
$z_{p,1}$	3050 m	First cloud-like tracer altitude
$z_{p,2}$	5050 m	Second cloud-like tracer altitude
$z_{p,3}$	8200 m	Third cloud-like tracer altitude
$\Delta z_{p,1}$	1000 m	First cloud-like tracer thickness
$\Delta z_{p,2}$	1000 m	Second cloud-like tracer thickness
$\Delta z_{p,3}$	400 m	Third cloud-like tracer thickness
R_p	$\pi/4$	Cloud-like deck radius (radians)

For this test the zonal, meridional and vertical velocity fields along surfaces of constant height (above the mean sea level) are specified as

$$u(\lambda, \varphi, z, t) = u_0 \left(\cos\varphi \cos\alpha + \sin\varphi \cos\lambda \sin\alpha\right), \tag{44}$$

$$v(\lambda, \varphi, z, t) = -u_0 \sin\lambda \sin\alpha, \tag{45}$$

$$w(\lambda, \varphi, z, t) = 0. \tag{46}$$

The velocity field transports the cloud-like tracer horizontally (at a constant height) once around the sphere over a duration of 12 days. If orography-following coordinates are used the vertical velocity needs to be translated into the new coordinate system due to the variation of the height along coordinate surfaces. Such a generalized vertical velocity becomes non-zero in this case. The exact description of the vertical velocity for orography-following coordinates is specified below and in Appendix B.

The surface elevation is a 3D variant of a Schär-like [9] mountain with compact support, centered around the point (λ_m, φ_m). The great circle distance from the mountain center point (in radians) is defined as

$$r_m(\lambda, \varphi) = \arccos\left[\sin\varphi_m \sin\varphi + \cos\varphi_m \cos\varphi \cos(\lambda - \lambda_m)\right]. \tag{47}$$

The surface elevation is then given by

$$
z_s(\lambda, \varphi) = \begin{cases} \dfrac{h_0}{2} \left[1 + \cos \left(\dfrac{\pi r_m}{R_m} \right) \right] \cos^2 \left(\dfrac{\pi r_m}{\zeta_m} \right), & \text{if } r_m < R_m, \\ 0, & \text{otherwise.} \end{cases} \tag{48}
$$

This choice ensures that the topography is flat away from the mountain, but strongly oscillates over the mountain range itself. The surface geopotential is then given by $\Phi_s(\lambda, \varphi) = g z_s(\lambda, \varphi)$. As before in tests 1-1 and 1-2, an isothermal atmosphere with $T = T_0$ is selected which leads to the pressure equation (1). The surface pressure is obtained by substituting $z = z_s(\lambda, \varphi)$ into (1).

Three thin cloud-like passive tracers are defined to represent lower-level, medium-level and upper-level cloud decks. These three cloud-like layers are initially placed away from the mountain in a region of flat topography so as to more easily evaluate error norms. The lateral great circle distance from the cloud center point (in radians) is defined as

$$
r_p(\varphi, \lambda) = \arccos \left[\sin \varphi_p \sin \varphi + \cos \varphi_p \cos \varphi \cos(\lambda - \lambda_p) \right]. \tag{49}
$$

Similarly we define a vertical distance from the center of each cloud level,

$$
r_{z,i}(z) = |z - z_{p,i}|, \tag{50}
$$

where $i \in \{1, 2, 3\}$. If pressure-based vertical coordinates are used the height $z(p)$ needs to be computed according to (2) first before applying (50). The lower-level and medium-level cloud-like tracers are disk-shaped, with the 3D mixing ratio

$$
q_i(\varphi, \lambda, z) = \begin{cases} \dfrac{1}{4} \left[1 + \cos \left(\dfrac{2\pi r_{z,i}(z)}{\Delta z_{p,i}} \right) \right] \left[1 + \cos \left(\dfrac{\pi r_p(\varphi, \lambda)}{R_p} \right) \right], & \text{if } r_{z,i}(z) < \tfrac{1}{2}\Delta z_{p,i} \text{ and } r_p(\varphi, \lambda) < R_p, \\ 0, & \text{otherwise,} \end{cases} \tag{51}
$$

for $i \in \{1, 2\}$. The upper-level cloud-like tracer is box-shaped with mixing ratio

$$
q_3(\varphi, \lambda, z) = \begin{cases} 1, & \text{if } r_{z,3}(z) < \tfrac{1}{2}\Delta z_{p,3} \text{ and } r_p(\varphi, \lambda) < R_p, \\ 0, & \text{otherwise.} \end{cases} \tag{52}
$$

The total tracer field is the sum of these three cloud-like tracers

$$
q_4(\varphi, \lambda, z) = q_1(\varphi, \lambda, z) + q_2(\varphi, \lambda, z) + q_3(\varphi, \lambda, z). \tag{53}
$$

Initialization in models using generalized vertical coordinates with terrain-following horizontal velocities

In models with terrain-following vertical coordinates the term "horizontal velocity" is most often interpreted and used in a coordinate-following framework. Consequently, if a constant horizontal velocity with respect to the height above mean sea level is imposed it needs to lead to an implied vertical velocity in the presence of topography. This perceived vertical velocity reflects that the terrain-following coordinates slope up- and downwards. The vertical motion thereby ensures that

there is an exchange of the tracers between the sloping model levels in case of purely horizontal advection. This problem is further described in Appendix B.

In spherical coordinates, the perceived vertical velocity w takes the form

$$w = -\frac{u_\lambda}{a \cos\varphi}\left(\frac{\partial z}{\partial \lambda}\right)_s - \frac{u_\varphi}{a}\left(\frac{\partial z}{\partial \varphi}\right)_s, \tag{54}$$

where u_λ and u_φ are the zonal and meridional velocities with respect to the mean sea level. Here, they coincide with u and v shown in (44) and (45). The derivatives in (54) are taken along the sloping coordinate surfaces (surfaces of the constant generalized vertical coordinate s). Once w is computed the corresponding vertical pressure velocity ω is given by

$$\omega = -\rho g w \tag{55}$$

where $\rho = p/(R_d T_0)$ is the density.

To demonstrate how the perceived vertical velocity is computed, we present it in the height-based orography-following coordinate of Gal-Chen and Somerville [10] (here denoted GC). The formulation for the perceived vertical velocity for the hybrid pressure-based η coordinate [8], which is often used in hydrostatic dynamical cores, is shown in Appendix B. If other vertical coordinates are used the formulation for the vertical velocity needs to be newly derived according to the algorithm given here and in Appendix B.

The GC vertical coordinate $\overline{z} \in [0, z_{\text{top}}]$ maps to the range $z \in [z_s(\lambda, \varphi), z_{\text{top}}]$. It is defined as

$$\overline{z} = z_{\text{top}}\left(\frac{z - z_s(\lambda, \varphi)}{z_{\text{top}} - z_s(\lambda, \varphi)}\right), \tag{56}$$

where $z_s(\lambda, \varphi)$ is the surface elevation, for instance defined by (48), and z_{top} is the height position of the model top. Coordinate surfaces in Cartesian space are defined via the inverse of (56),

$$z = z_s(\lambda, \varphi) + \frac{\overline{z}}{z_{\text{top}}}(z_{\text{top}} - z_s(\lambda, \varphi)). \tag{57}$$

To compute the perceived vertical velocity we differentiate (57) along surfaces of constant $\overline{z}$, obtaining

$$\frac{\partial z}{\partial \lambda} = \frac{\partial z_s}{\partial \lambda}\left(1 - \frac{\overline{z}}{z_{\text{top}}}\right), \tag{58}$$

$$\frac{\partial z}{\partial \varphi} = \frac{\partial z_s}{\partial \varphi}\left(1 - \frac{\overline{z}}{z_{\text{top}}}\right). \tag{59}$$

The final step in this procedure requires one to compute the horizontal derivatives of z_s with respect to λ and φ. Using the Schär mountain profile (48) the derivatives of the surface elevation are

given as follows:

$$
\frac{\partial z_s}{\partial x} = \begin{cases} \left\{ -\dfrac{h_0 \pi}{2R_m} \sin\left(\dfrac{\pi r_m}{R_m}\right) \cos^2\left(\dfrac{\pi r_m}{\zeta_m}\right) - \right. \\ \left. \dfrac{h_0 \pi}{\zeta_m} \left[1 + \cos\left(\dfrac{\pi r_m}{R_m}\right) \right] \cos\left(\dfrac{\pi r_m}{\zeta_m}\right) \sin\left(\dfrac{\pi r_m}{\zeta_m}\right) \right\} \left(\dfrac{\partial r_m}{\partial x} \right), & \text{if } r_m < R_m, \\[2mm] 0, & \text{otherwise.} \end{cases}
$$

(60)

where $x \in \{\lambda, \varphi\}$ and

$$
\frac{\partial r_m}{\partial \lambda} = \frac{\cos \varphi_m \cos \varphi \sin(\lambda - \lambda_m)}{\sqrt{1 - \cos^2(r_m(\lambda, \varphi))}},
$$
(61)

$$
\frac{\partial r_m}{\partial \varphi} = \frac{-\sin \varphi_m \cos \varphi + \cos \varphi_m \sin \varphi \cos(\lambda - \lambda_m)}{\sqrt{1 - \cos^2(r_m(\lambda, \varphi))}}.
$$
(62)

Note that when $r_m(\lambda, \varphi) = 0$ or $\pm\pi$, which will occur at $(\lambda, \varphi) = (\lambda_m, \varphi_m)$ or $(\lambda_m \pm \pi, -\varphi_m)$, we enforce $\frac{\partial r_m}{\partial \lambda} = 0$ and $\frac{\partial r_m}{\partial \varphi} = 0$. At each coordinate (λ, φ) the set of equations (54)-(62) then leads to a unique perceived velocity associated with the terrain-following coordinate transform.

Grid spacings, simulation time, output and diagnostics

This test should be run at $1°$ resolution (~ 110 km equatorial grid spacing) in both horizontal directions with 30, 60, and 120 vertical levels for 12 days. For models using height levels a model top of $z_{\text{top}} = 12000$ m is suggested with a uniformly-spaced vertical grid spacing of Δz in the flat regions away from the mountain range. For the e.g. 60 level setup (L60) this means that the model interfaces are positioned at 0 m, 200 m, 400 m, etc. and that the full model levels are placed at 100 m, 300 m, 500 m, etc. in the flat regions. If the model utilizes orography-following vertical coordinates the grid spacing will be non-uniform over the mountain range. From (1) the height position of the model top corresponds to $p_{\text{top}} \approx 254.944$ hPa. Appendix F.3 outlines how pressure-based levels should be positioned in order to correspond to the equidistant grid spacing Δz. At the L60 resolution the three cloud-like tracers initially occupy 5, 5 and 2 vertical grid points for the lower, middle and upper layers.

Output should be recorded daily (every 86400 s) and needs to include the initial state (13 time snapshots). The desired output variables on model levels are the instantaneous snapshots of $q1, q_2, q_3, q_4$. The following analysis results are suggested:

- Latitude-longitude cross sections of q_4 should be produced at $t = 6$ and 12 days at the model level that is closest to the (non-interpolated) height positions $z = 3100$ m, $z = 5100$ m and $z = 8100$ m.
- Longitude-level cross sections of q_4 should be produced at $t = 6$ and 12 days on model levels along the equator. If q_4 shows that vigorous mixing of the cloud-like tracers q_1, q_2 or q_3 has occured, longitude-height cross sections of q_1, q_2 and q_3 should be plotted on model levels.
- The $q4$ field at the equator should be interpolated to constant height levels in the vertical region between 2000-10000 m. Longitude-height cross sections of q_4 should then be plotted at $t = 6$ and 12 days along the equator. If q_4 shows that vigorous mixing of the cloud-like

tracers q_1, q_2 or q_3 has occured, $q1, q2$ and $q3$ should also be interpolated to height levels, and longitude-height cross sections of q_1, q_2 and q_3 should be plotted.

- Normalized l_1, l_2 and l_∞ error norms should be computed for q_1, q_2, q_3 and q_4 at $t = 12$ days against the initial conditions.

2. TEST CATEGORY 2-X: IMPACT OF OROGRAPHY ON A NON-ROTATING PLANET

The tests in section 2-x examine the impact of mountain profiles on an atmosphere at rest (2-0-0) with a moderately-steep 3D Schär-like [9] circular mountain, an atmosphere at rest with a single steep mountain ridge and more complex temperature structure (2-0-1), and on flow fields with wind shear (2-1) and without vertical wind shear (2-2) in the presence of a 3D Schär-like [9] circular mountain. A non-rotating planet is used for all configurations with $\Omega_{\mathrm{ref}} = 0$ s^{-1}. Test 2-0-0 is conducted on an unscaled regular-size planet and primarily examines the accuracy of the pressure gradient calculation in a steady-state hydrostatically-balanced atmosphere at rest. Test 2-0-1 is similar to test 2-0-0, but focuses on the effects of finite terrain slopes which is especially important for non-hydrostatic models at high resolutions. Test 2-0-1 is therefore run on a small-planet and also includes more complex temperature variations in the vertical direction. Both steady-state tests at rest are especially appealing for models with orography-following vertical coordinates. They increase the complexity of test 1-3, that investigated the impact of an orographic profile on the accuracy of purely-horizontal passive tracer advection.

Tests 2-1 and 2-2 increase the complexity even further since non-zero flow fields are now prescribed with and without vertical wind shear. In order to trigger non-hydrostatic responses the two tests are conducted on a reduced-size planet with reduction factor $X = 500$ which makes the horizontal and vertical grid spacing comparable. This test clearly discriminates between non-hydrostatic and hydrostatic models since the expected response is in the non-hydrostatic regime. Therefore, the flow response is captured differently by hydrostatic models.

2.0. Test 2-0-0: Steady-State Atmosphere at Rest in the Presence of Orography with Moderately-Steep Slopes

Table XII. List of constants used for the steady-state atmosphere at rest in the presence of orography test case (Test $2 - 0 - 0$).

Constant	Value	Description
z_{top}	12000 m	Height position of the model top
p_{top}	≈ 205.448 hPa	Pressure at the model top
X	1	Small-planet scaling factor (regular-size Earth)
Ω	0 s^{-1}	Rotation rate of the Earth
T_0	300 K	Reference surface temperature
p_0	1000 hPa	Reference surface pressure
Γ	0.0065 K m^{-1}	temperature lapse rate
λ_m	$3\pi/2$	Mountain longitude center point
φ_m	0	Mountain latitude center point
h_0	2000 m	Maximum mountain height
R_m	$3\pi/4$	Mountain radius (radians)
ζ_m	$\pi/16$	Mountain oscillation half-width (radians)

The underlying idea behind the steady-state test is similar to the test in [11] which evaluated the accuracy of two discrete approaches to the pressure gradient calculation in the presence of orography. It especially gives insight into the accuracy of the pressure gradient in models with orography-following coordinates due to the complexities of the coordinate transformations and

metric terms. From an analytic viewpoint the atmosphere should remain in its motionless steady-state indefinitely as determined by the continuous equations. In a discretized model, this will generally not be the case due to numerical errors, unless special forms of the equations of motion are chosen, that e.g. utilize the perturbation pressure from the discretely-determined hydrostatic balance. Such models might appear to be 'perfect', which is a consequence of the idealized setup considered here. For there models, this test might not be insightful and should be considered optional. However, for most model designs the test will reveal the numerical characteristics of the discrete pressure gradient terms, and it is furthermore quick to run from a computational viewpoint.

The chosen mountain profile is identical to the one used for test $1 - 3$. For convenience the formulation for the surface height z_s is repeated here

$$
z_s(\lambda, \varphi) = \begin{cases} \dfrac{h_0}{2} \left[1 + \cos \left(\dfrac{\pi r_m}{R_m} \right) \right] \cos^2 \left(\dfrac{\pi r_m}{\zeta_m} \right), & \text{if } r_m < R_m, \\ 0, & \text{otherwise.} \end{cases} \tag{63}
$$

This choice ensures that the topography is flat away from the mountain, but strongly oscillates over the mountain range itself. The surface geopotential is then given by $\Phi_s(\lambda, \varphi) = g z_s(\lambda, \varphi)$. This moderately-steep Schär-like circular mountain is centered around the point (λ_m, φ_m). The great circle distance from the mountain center point (in radians) is defined as

$$
r_m(\lambda, \varphi) = \arccos \left[\sin \varphi_m \sin \varphi + \cos \varphi_m \cos \varphi \cos(\lambda - \lambda_m) \right]. \tag{64}
$$

We initialize the model with a hydrostatically-balanced steady-state at rest. The atmosphere is stratified with a constant lapse rate Γ. The temperature is therefore given by

$$
T(\lambda, \varphi, z) = T_0 - \Gamma z \tag{65}
$$

$$
T(\lambda, \varphi, p) = T_0 \left(\frac{p(\lambda, \varphi, z)}{p_0} \right)^{\frac{R_d \Gamma}{g}} \tag{66}
$$

for height-based and pressure-based vertical coordinates, respectively. T_0 denotes the surface temperature. The hydrostatically-balanced pressure equation then yields

$$
p(\lambda, \varphi, z) = p_0 \left(1 - \frac{\Gamma}{T_0} z(\lambda, \varphi) \right)^{\frac{g}{R_d \Gamma}} \tag{67}
$$

where p_0 stands for the reference pressure at the height position $z_0 = 0$ m. The surface pressure is obtained by substituting $z(\lambda, \varphi) = z_s(\lambda, \varphi)$ into (67). Equation (67) can also be rewritten as

$$
z(\lambda, \varphi, p) = \frac{T_0}{\Gamma} \left[1 - \left(\frac{p}{p_0} \right)^{\frac{R_d \Gamma}{g}} \right]. \tag{68}
$$

The atmosphere is at rest with

$$u = 0 \tag{69}$$

$$v = 0 \tag{70}$$

$$w = \omega = \dot{\eta} = 0 \tag{71}$$

at all grid point positions. Consequently, the relative vorticity and divergence of the flow are zero. In addition, the specific humidity q is set to zero.

For finite-volume-type models it could be advantageous to select a vertical-mean initial state instead of the grid-point values since the vertical-mean might be closer to the discrete hydrostatic balance. However, the vertical-mean is still not identical to a volume-mean in a 3D volume since temperature and pressure also vary in the horizontal direction in orography-following vertical coordinates. For the conditions specified here, the vertical-mean temperature and pressure can be computed analytically. The vertical-mean temperature $\bar{T}$ between the height levels z_{down} and z_{up} (with $z_{\text{down}} < z < z_{\text{up}}$) is

$$\bar{T}(\lambda, \varphi, z) = T_0 - \frac{\Gamma}{2(z_{\text{up}} - z_{\text{down}})} \left(z_{\text{up}}^2 - z_{\text{down}}^2 \right) \tag{72}$$

where the positions z_{down} and z_{up} point to the surrounding model interface levels that enclose the midpoint of the cell at position z. The vertical-mean temperature for pressure-based models is

$$\bar{T}(\lambda, \varphi, p) = \frac{g \, T_0 \, p_0}{(R_d \Gamma + g)(p_{\text{up}} - p_{\text{down}})} \left[\left(\frac{p_{\text{up}}}{p_0} \right)^{\frac{R_d \Gamma}{g} + 1} - \left(\frac{p_{\text{down}}}{p_0} \right)^{\frac{R_d \Gamma}{g} + 1} \right] \tag{73}$$

with the model interface pressures p_{down} and p_{up} that surround the centered pressure position p (with $p_{\text{up}} < p < p_{\text{down}}$). The vertical-mean pressure $\bar{p}$ for non-hydrostatic models is

$$\bar{p}(\lambda, \varphi, z) = \frac{p_0 \, T_0 \, R_d}{(z_{\text{up}} - z_{\text{down}})(R_d \Gamma + g)} \left[\left(1 - \frac{\Gamma}{T_0} z_{\text{down}} \right)^{\frac{g}{R_d \Gamma} + 1} - \left(1 - \frac{\Gamma}{T_0} z_{\text{up}} \right)^{\frac{g}{R_d \Gamma} + 1} \right] \tag{74}$$

The density is given by the ideal gas law

$$\rho(\lambda, \varphi, z) = \frac{p(\lambda, \varphi, z)}{R_d \, T(\lambda, \varphi, z)} \tag{75}$$

which could also be replaced by the approximate vertical-mean density when using $\bar{p}$ and $\bar{T}$ in (75).

Grid spacings, simulation time, output and diagnostics for test 2-0-0

The steady-state test should be run for 6 days (518400 s). A resolution of $1°$ (~ 110 km) with 15 and 30 vertical levels should be chosen. Since the model top is set at $z_{\text{top}} = 12$ km, for models with a height-based vertical coordinate we suggest uniformly spaced levels (in the flat regions away from the mountain range) with thickness $\Delta z = 800$ m and $\Delta z = 400$ m, respectively. For the 15-level setup this means that the model interfaces are positioned at 0 m, 800 m, 1600 m, etc. and that the full model levels are placed at 400 m, 1200 m, 2000 m, etc. (away from the mountain

range). The interface positions for the 30-level configuration are 0 m, 400 m, 800 m, etc. with full model levels at 200 m, 600 m, 1000 m, etc. (away from the mountain range). If the model utilizes orography-following vertical coordinates the grid spacing will be non-uniform over the mountain range. For models utilizing a pressure-based vertical coordinate the corresponding pressure levels can be chosen using (67). The position of the model top for pressure-based models is ≈ 205.448 hPa. Appendix F.3 outlines how pressure-based levels should be positioned in order to correspond to the grid spacing Δz.

Output should be written at 6 hr intervals including the initial state. The output file should contain the instantaneous model-level snapshots of the u, v, w or $\omega, T, p_s, \Phi_s, T_{500}, w_{500}$ or ω_{500} fields and p in case the pressure cannot be reconstructed via the surface pressure. The subscript X_{500} denotes the 500 hPa level. For comparison, we suggest plotting the non-interpolated vertical cross sections (λ-model level) of the zonal wind and vertical velocity along the equator at day 6. We also propose analyzing the structure of the 500 hPa temperature field and plotting longitude-latitude cross sections of the zonal wind, meridional wind and vertical velocity at the lowermost model level and the model level closest to the 500 hPa level (which lies around 5700 m in height-based models) at days 3 and 6. In addition, we suggest evaluating the time series of the global-mean kinetic energy over the 6 simulation days. The global mean (globally-integrated) kinetic energy is defined via the 2D horizontal velocities $0.5(u^2 + v^2)$ in hydrostatic models and the 3D velocities $0.5(u^2 + v^2 + w^2)$ in nonhydrostatic models.

2.0.1. Test 2-0-1: Steady-State Atmosphere at Rest in the Presence of Orography with Steep Slopes

optional test: description to follow, based on ideas by Joseph Klemp (NCAR) and the MPAS modeling group, run on a small planet with $X = 500$ at the resolution $2°$ (≈ 667 m grid spacing) with 30 levels and a model top at 12 km. The vertical temperature profile utilizes a constant lapse rate at low and high levels and includes an embedded isothermal temperature layer at mid-levels.

2.X. Tests 2-1 and 2-2: Non-hydrostatic Mountain Waves over a Schär-type Mountain

The two mountain-induced gravity wave tests 2-1 and 2-2 examine the response of atmospheric models to flow over a mountain profile, with and without vertical wind shear. Their analytical descriptions are almost identical. They are therefore first presented together in their general form, before we highlight the specific settings of the shear parameter c for 2-1 and 2-2 below. In order to ensure the simulated response contains both hydrostatic and non-hydrostatic features, the radius of the Earth is scaled so that the simulation is in the non-hydrostatic domain. We chose a non-rotating reduced-size Earth with radius $a = a_{\text{ref}}/X$. The reduction factor is set to $X = 500$. This choice leads to an Earth with a circumference at the equator of about $2\pi a_{\text{ref}}/X \approx 80$ km. The underlying ideas behind the tests are based on the work of [12], [13] and [14]. Note however that in the presence of vertical wind shear we cannot use isothermal conditions in the spherical domain as suggested by [14]. Such isothermal conditions lead to imbalances of the initial data in spherical geometry. Recall that the Earth's radius and angular velocity must also be redefined in the GCM source code, and that explicit diffusion coefficients (if applied) and the model time step need to be rescaled.

Table XIII. List of constants used for the Non-Hydrostatic Mountain Wave test cases (Tests 2-1 and 2-2).

Constant	Value	Description
z_{top}	30000 m	Height position of the model top
p_{top}	≈ 32.818 hPa	Pressure at the model top at the equator
X	500	Reduced-size planet scaling factor
Ω	0 s^{-1}	Rotation rate of the Earth
λ_c	$\pi/4$	Longitude of Schär-type mountain centerpoint
φ_c	0	Latitude of the Schär-type mountain centerpoint
h_0	250 m	Maximum Schär-type mountain height
d	5000 m	Schär-type mountain half-width
ξ	4000 m	Schär-type mountain wavelength
p_{eq}	1000 hPa	Reference surface pressure at the equator
T_{eq}	300 K	Reference surface temperature at the equator
u_{eq}	20 m s^{-1}	Reference zonal wind velocity
c_s	2.5×10^{-4} m^{-1}	Equatorial surface wind shear (for sheared flow)
z_h	20000 m	Height of the Rayleigh damped layer
τ_0	25 s	Rayleigh friction time scale

For the Schär-type mountain test we specify topography of the form

$$z_s(\lambda, \varphi) = h_0 \exp\left(-\frac{r(\lambda, \varphi)^2}{d^2}\right) \cos^2\left(\frac{\pi r(\lambda, \varphi)}{\xi}\right), \tag{76}$$

where z_s symbolizes the surface elevation and r is the great-circle distance, defined by

$$r = \frac{a_{\mathrm{ref}}}{X} \arccos\left[\sin\varphi_c \sin\varphi + \cos\varphi_c \cos\varphi \cos(\lambda - \lambda_c)\right]. \tag{77}$$

Hence, the surface geopotential is given by $\Phi_s(\lambda, \varphi) = gz_s(\lambda, \varphi)$. Rotation is disabled ($\Omega = 0$ s^{-1}).

This test requires the specification of Rayleigh friction in a rather broad sponge layer which occupies one third of the domain near the model top. It is needed to absorb upward propagating gravity waves and prevent their reflection at the model top. We suggest applying the Rayleigh friction to the horizontal velocity components in hydrostatic models, and to the 3D velocity components in non-hydrostatic formulations, respectively. The Rayleigh friction is defined as an additional forcing term of the momentum equations

$$\frac{\partial \mathbf{u}}{\partial t} = \ldots - \frac{f(z)}{\tau_0}(\mathbf{u} - \mathbf{u}_{\mathrm{ref}}), \tag{78}$$

where $\tau_0 = 25$ s is the damping time scale and $\mathbf{u}$ denotes the 2D or 3D vector form of the velocity, respectively. The damping time scale τ_0 is already scaled for small-planet conditions. The reference profile $\mathbf{u}_{\mathrm{ref}}$ is set identical to the initial velocity field described below. The function

$$f(z) = \begin{cases} \sin^2\left(\frac{\pi}{2}\left(\frac{z - z_h}{z_{\mathrm{top}} - z_h}\right)\right) & \text{if } z > z_h, \\ 0 & \text{if } z \leq z_h, \end{cases} \tag{79}$$

determines the strength of the Rayleigh damping and reaches its maximum at the model top. Here $z_h = 20$ km denotes the altitude of the Rayleigh damped layer and $z_{\mathrm{top}} = 30$ km denotes the

altitude of the model top. For pressure-based models an identical form of the Rayleigh damping should be chosen that utilizes the pressure-height conversion (84) shown below. Note that τ_0 can be adjusted depending on the behavior of the model, but should be chosen to minimize spurious reflections from the model top. Please report the adjusted τ_0 value when providing final results. If a model is formulated in a vorticity-divergence form, the Rayleigh friction mechanism could also be reformulated to force the divergence and vorticity towards their base initial states. Such changes need to be documented. We do not apply any sponge-layer relaxation to the temperature field.

Two wind fields are used for tests 2-1 and 2-2 that only differ by their vertical wind-shear characteristics. Both choices of wind field use a hydrostatically-balanced 3D pressure field of the form

$$p(\lambda, \varphi, z) = p_{eq} \exp\left(-\frac{u_{eq}^2}{2R_d T_{eq}} \sin^2 \varphi - \frac{gz}{R_d T(\varphi)} \right). \tag{80}$$

The surface pressure is obtained from setting $z = z_s(\lambda, \varphi)$ in (80). The temperature field is chosen to be

$$T(\varphi) \;=\; T_{eq}\left(1 - \frac{cu_{eq}^2}{g} \sin^2 \varphi \right) \quad \text{with} \tag{81}$$

$$T(\lambda, \varphi, z) \;=\; T(\lambda, \varphi, p) \;=\; T(\varphi).$$

Note that the temperature only depends on the latitudinal position and is isothermal within each vertical column. The parameter c denotes a prescribed vertical wind shear of the zonal velocity field at the surface. The temperature field is balanced by the initial zonal velocity field

$$u(\lambda, \varphi, z) = u_{eq} \cos(\varphi) \sqrt{\frac{2T_{eq}}{T(\varphi)} cz + \frac{T(\varphi)}{T_{eq}}}. \tag{82}$$

This zonal wind field is characterized by a varying wind shear with altitude. In all cases the meridional and vertical velocities are everywhere zero,

$$v(\lambda, \varphi, z) = 0, \qquad w(\lambda, \varphi, z) = 0, \qquad \omega(\lambda, \varphi, z) = 0. \tag{83}$$

For models with a pressure-based vertical coordinate, (80) can be rearranged to obtain

$$z(\lambda, \varphi, p) = \frac{R_d T(\varphi)}{g} \ln\left(\frac{p_{eq}}{p} \right) - \frac{T(\varphi) \, u_{eq}^2 \sin^2 \varphi}{2 \, T_{eq} \, g}. \tag{84}$$

This height can then be plugged into (82) to obtain the pointwise zonal velocity field. The specific humidity field q needs to be set to zero. The density is defined via the ideal gas law

$$\rho(\lambda, \varphi, z) = \frac{p(\lambda, \varphi, z)}{R_d \, T(\lambda, \varphi, z)}. \tag{85}$$

2.1. Test 2-1: Non-Sheared Background Flow

This non-sheared test case utilizes a vertically-constant zonal velocity with the shear parameter c set to zero ($c = 0$).

2.2. Test 2-2: Sheared Background Flow

This test utilizes a sheared zonal velocity with the shear parameter $c = c_s$ where c_s symbolizes the vertical wind shear at the surface as listed in Table XIII. As noted before the resulting wind shear of the zonal wind is not constant and depends on altitude. The analytic formulation (82) lets the zonal wind vary from $u = 20$ m s^{-1} at the equatorial surface to about 80 m s^{-1} at the height of 30 km.

Grid spacings, simulation time, output and diagnostics for both tests 2-1 and 2-2

For tests 2-1 and 2-2, the model should be run until $t = 7200$ s (in unscaled time units) which corresponds to a simulation length of 1000 hr in scaled time units. A resolution of $1.5°$ (~ 333.6 m) with 60 vertical levels should be chosen. Since the model top is set at $z_{\text{top}} = 30$ km, for models with a height-based vertical coordinate we suggest uniformly spaced levels (in the flat regions away from the mountain range) with thickness $\Delta z = 500$ m. This means that the model interfaces are positioned at 0 m, 500 m, 1000 m, etc. and that the full model levels are placed at 250 m, 750 m, 1250 m, etc. in the flat domain. If the model utilizes orography-following vertical coordinates the grid spacing will be slightly non-uniform over the mountain range. For models utilizing a pressure-based vertical coordinate the corresponding pressure levels can be chosen using (80) with $\varphi = 0$ so that pressure and height levels are coincident at the equator. The position of the model top for pressure-based models is ≈ 32.818 hPa. Appendix F.3 outlines how pressure-based levels should be positioned in order to correspond to the grid spacing Δz.

Output should be written at 100 s (unscaled Earth) intervals including the initial state. This corresponds to an output frequency of 50000 s in scaled Earth units. The output file should contain the instantaneous model-level snapshots of the u, v, w or ω, T, p_s, Φ_s fields and p in case the pressure cannot be reconstructed via the surface pressure. For comparison, we suggest producing $\lambda - z$ plots of the temperature perturbation $T'(\lambda, z) = T - T_{eq}$ at the equator at $t = 2400$ s, $t = 3600$ s and $t = 7200$ s. The time snapshots at $t = 2400$ s and $t = 3600$ s capture the wave before it has fully wrapped around the earth and will be the most informative analysis. The time snapshot $t = 7200$ s captures the wave after it interfered with itself and the absorbing layer. A longitude-height animation of the propagating temperature perturbation along the equator is also very informative. We also recommend analyzing the vertical velocity. Note however, that a pressure-based velocity ω needs to be converted to w if direct comparisons to non-hydrostatic models with height-based coordinates are desired. The temperature perturbation plots avoid any conversions.

3. TEST CATEGORY 3: NON-HYDROSTATIC GRAVITY WAVES

The non-hydrostatic gravity wave test examines the response of models to short time-scale wave-motion triggered by a localized perturbation. The formulation presented in this document is new, but is based on previous approaches by [15], [16] and [17]. The initial state is hydrostatically balanced and in gradient-wind balance. An overlaid potential temperature perturbation then triggers the evolution of gravity waves. We define the initial conditions in the most general form that includes the Coriolis term. Therefore, this initial data equation set can also be used for other test scenarios in the future. However, since we set the Earth's angular velocity to zero it eliminates the impact of the earth's rotation in the initial conditions and simulations considered here. Remember that the Earth's radius and angular velocity must also be redefined in the GCM source code, and that explicit diffusion coefficients (if applied) and the model time step need to be rescaled.

Initial Conditions for Test 3-x

Balanced basic state

The gravity wave test on a reduced-size earth discriminates between hydrostatic and non-hydrostatic responses. We chose a non-rotating Earth with angular velocity $\Omega_{\mathrm{ref}} = 0 \text{ s}^{-1}$ and select a reduced-size Earth with radius $a = a_{\mathrm{ref}}/X$. The reduction factor is set to $X = 125$. This choice leads to an Earth with a circumference at the equator of about $2\pi a_{\mathrm{ref}}/X \approx 320$ km. The temperature field is chosen to have a constant Brunt-Väisälä frequency N, which impacts the phase speed of the gravity wave as discussed below.

Table XIV. List of constants used for the Gravity Wave test case (Test 3-x)

Constant	Value	Description
z_{top}	10000 m	Height position of the model top
p_{top}	≈ 273.759 hPa	Pressure at the model top at the equator
X	125	Reduced-size planet scaling factor
Ω	0 s^{-1}	Rotation rate of the Earth
u_0	20 m s^{-1}	Maximum amplitude of the zonal wind
z_s	0 m	Surface elevation
N	0.01 s^{-1}	Brunt-Väisälä frequency
T_{eq}	300 K	Surface temperature at the equator
p_{eq}	1000 hPa	Reference surface pressure at the equator
d	5000 m	Width parameter for Θ'
λ_c	$2\pi/3$	Longitudinal centerpoint of Θ'
φ_c	0	Latitudinal centerpoint of Θ' (equator)
$\Delta\Theta$	1 K	Maximum amplitude of Θ'
L_z	20000 m	Vertical wave length of the Θ' perturbation

The initial zonal, meridional and vertical wind speeds are

$$u(\lambda, \varphi, z) = u_0 \cos(\varphi), \tag{86}$$

$$v(\lambda, \varphi, z) = 0, \tag{87}$$

$$w(\lambda, \varphi, z) = 0. \tag{88}$$

The corresponding pressure velocity is similarly set to zero everywhere, $\omega(\lambda, \varphi, z) = 0$. No surface topography is present ($z_s = 0$ m), so that the surface geopotential satisfies $\Phi_s = \Phi(z = z_s) = 0$ m^2 s^{-2}. The surface temperature is given by

$$T_s(\lambda, \varphi) = G + (T_{eq} - G) \exp\left(-\frac{u_0 N^2}{4g^2}(u_0 + 2\Omega a)\big(\cos(2\varphi) - 1\big)\right) \tag{89}$$

with

$$G = \frac{g^2}{N^2 c_p} \tag{90}$$

where G denotes the temperature of an isothermal state for a prescribed N. The 3D (unperturbed) background temperature field is represented by

$$T_b(\lambda, \varphi, z) = G\left[1 - \exp\left(\frac{N^2}{g}z\right)\right] + T_s(\lambda, \varphi)\exp\left(\frac{N^2}{g}z\right), \tag{91}$$

$$T_b(\lambda, \varphi, p) = \frac{T_s(\lambda, \varphi)\left(\frac{p}{p_s(\lambda, \varphi)}\right)^\kappa}{\frac{T_s(\lambda, \varphi)}{G}\left(\left(\frac{p}{p_s(\lambda, \varphi)}\right)^\kappa - 1\right) + 1}, \tag{92}$$

in height and pressure coordinates, respectively. The surface pressure is defined by

$$p_s(\lambda, \varphi) = p_{eq} \exp\left\{\frac{u_0}{4GR_d}(u_0 + 2\Omega a)\big(\cos(2\varphi) - 1\big)\right\}\left(\frac{T_s(\lambda, \varphi)}{T_{eq}}\right)^{1/\kappa}. \tag{93}$$

The 3D unperturbed pressure field, in terms of height coordinates, is then

$$p(\lambda, \varphi, z) = p_s(\lambda, \varphi)\left[\frac{G}{T_s(\lambda, \varphi)}\exp\left(-\frac{N^2}{g}z\right) + 1 - \frac{G}{T_s(\lambda, \varphi)}\right]^{1/\kappa}. \tag{94}$$

Note that (94) and (93) can also be combined to give an alternative form of the unperturbed pressure equation

$$p(\lambda, \varphi, z) = p_{eq} \exp\left\{\frac{u_0}{4GR_d}(u_0 + 2\Omega a)\big(\cos(2\varphi) - 1\big)\right\}\left(\frac{T_b(\lambda, \varphi, z)}{T_{eq}}\right)^{1/\kappa}\exp\left(-\frac{gz}{GR_d}\right). \tag{95}$$

Equation (94) can be reformulated to yield a pressure-based expression for the height z

$$z(\lambda, \varphi, p) = -\frac{g}{N^2} \ln\left[\frac{T_s(\lambda, \varphi)}{G}\left\{\left(\frac{p}{p_s(\lambda, \varphi)}\right)^\kappa - 1\right\} + 1\right], \tag{96}$$

which was utilized to derive (92). The expressions for the unperturbed background potential temperature are

$$\Theta_b(\lambda, \varphi, z) = T_s(\lambda, \varphi) \left(\frac{p_0}{p_s(\lambda, \varphi)} \right)^{\kappa} \exp\left(\frac{N^2}{g} z \right) \tag{97}$$

$$\Theta_b(\lambda, \varphi, p) = \frac{T_s(\lambda, \varphi) \left(\frac{p_0}{p_s(\lambda, \varphi)} \right)^{\kappa}}{\frac{T_s(\lambda, \varphi)}{G} \left(\left(\frac{p}{p_s(\lambda, \varphi)} \right)^{\kappa} - 1 \right) + 1} \tag{98}$$

for height-based and pressure-based models.

For models in vorticity-divergence form, the relative vorticity ζ and divergence δ are defined by

$$\zeta(\lambda, \varphi, z) = \frac{2u_0 \sin \varphi}{a_{\text{ref}}/X} = \frac{2X u_0 \sin \varphi}{a_{\text{ref}}} \tag{99}$$

$$\delta(\lambda, \varphi, z) = 0 \text{ s}^{-1}. \tag{100}$$

The specific humidity field q needs to be set to zero. The background (unperturbed) density is defined via the ideal gas law

$$\rho(\lambda, \varphi, z) = \frac{p(\lambda, \varphi, z)}{R_d \, T_b(\lambda, \varphi, z)}. \tag{101}$$

Test 3-1: Overlaid potential temperature perturbation at the equator

In order to trigger the propagation of a gravity wave, a small-amplitude potential temperature perturbation Θ' is added to the balanced background potential temperature field to yield

$$\Theta(\lambda, \varphi, z) = \Theta_b(\lambda, \varphi, z) + \Theta'(\lambda, \varphi, z) \tag{102}$$

$$\Theta(\lambda, \varphi, p) = \Theta_b(\lambda, \varphi, p) + \Theta'(\lambda, \varphi, p) \tag{103}$$

depending on the choice of the vertical coordinate. The analytic expression for the height-based potential temperature perturbation is

$$\Theta'(\lambda, \varphi, z) = \Delta\Theta \, s(\lambda, \varphi) \sin\left(\frac{2\pi z}{L_z} \right), \tag{104}$$

where L_z is the vertical wave length of the perturbation. The horizontal shape function $s(\lambda, \varphi)$ is defined as

$$s(\lambda, \varphi) = \frac{d^2}{d^2 + r^2}, \tag{105}$$

where d is a width parameter for the bell-shaped potential temperature perturbation and r symbolizes the great circle distance between a position (λ, φ) and the center of the perturbation, initially set to (λ_c, φ_c) along the equator. The great circle distance r is defined as

$$r = \frac{a_{\text{ref}}}{X} \arccos\left[\sin \varphi_c \sin \varphi + \cos \varphi_c \cos \varphi \cos(\lambda - \lambda_c) \right]. \tag{106}$$

For pressure-based vertical coordinates, the potential temperature perturbation is given as

$$\Theta'(\lambda, \varphi, p) = \Delta\Theta \, s(\lambda, \varphi) \sin\left(\frac{2\pi \, z(\lambda, \varphi, p)}{L_z}\right), \tag{107}$$

which utilizes (96) to evaluate the height z at a given pressure p.

The corresponding temperature perturbations for models with a prognostic temperature field are

$$T'(\lambda, \varphi, z) = \Theta'(\lambda, \varphi, z)\left(\frac{p(\lambda, \varphi, z)}{p_0}\right)^{\kappa}, \tag{108}$$

$$T'(\lambda, \varphi, p) = \Theta'(\lambda, \varphi, p)\left(\frac{p}{p_0}\right)^{\kappa}, \tag{109}$$

depending on the choice of the vertical coordinate. These perturbations are added to the background temperature field

$$T(\lambda, \varphi, z) = T_b(\lambda, \varphi, z) + T'(\lambda, \varphi, z) \tag{110}$$

$$T(\lambda, \varphi, p) = T_b(\lambda, \varphi, p) + T'(\lambda, \varphi, p). \tag{111}$$

Grid spacings, simulation time and output

The suggested grid spacings are $1.125° \times 1.125°$ in the horizontal direction which yields a physical horizontal grid spacing of about 1 km near the equator. On a latitude-longitude grid this corresponds to 160×320 grid points (without pole points) or 161×320 (including pole points). In the vertical, a grid spacing of $\Delta z = 1$ km with a model top at $z_{\text{top}} = 10$ km is suggested which gives 10 full model levels at the positions 0.5, 1.5, 2.5 km and so on. The position of the model top corresponds to half a wave length $z_{\text{top}} = L_z/2$. Using $N = 0.01$ s^{-1} the top level (interface) pressure p_{top} is $p_{\text{top}} = p(z_{\text{top}}) \approx 273.759$ hPa according to (94). Here, the position of the model top is computed for $p_s = p_{eq}$. Appendix F.3 outlines how pressure-based levels should be positioned in order to correspond to the equidistant grid spacing Δz.

The simulation should be run until $t = 3600$ s in unscaled Earth units which corresponds to 125 hours in scaled time units. The output should be recorded every 100 s (in unscaled units) including the initial state. The output file should contain the instantaneous model-level snapshots of the u, v, w or ω, T, p_s fields and p in case the pressure cannot be reconstructed via the surface pressure.

This test can also be run in many variants if the perturbation is placed away from the equator. E.g. Θ' could be placed at $\varphi = 45°$ in models with cubed-sphere coordinates to evaluate the potential impact of the cubed-sphere corners on the propagation of the wave. It is left to the modeler's discretion if more than variant 3-1 should be tested. Additional test case numbers can then be defined.

Diagnostics

Along the equator, the gravity wave propagates to the west and east of its initial location with a longitudinal phase speed of

$$c_x = u \pm \frac{N L_z}{2\pi}, \tag{112}$$

which corresponds to about 31.8 m s^{-1} without the background flow u. The inclusion of the background flow leads to asymmetric phase speeds which are about -11.8 m s^{-1} (towards the west) and 51.8 m s^{-1} towards the east along the equator. We suggest analyzing the potential temperature deviations from the base state in form of a longitude-height cross section along the equator with $\varphi = 0°$ at time $t = 3000$ s (and optionally other times). The deviations are given by

$$\Theta'_m = \Theta_m - \Theta, \tag{113}$$

where

$$\Theta_m = T \left(\frac{p_0}{p} \right)^{\kappa} \tag{114}$$

is the modeled potential temperature, and the base state Θ is either defined by (97) or (98) depending on the choice of the vertical coordinate. In addition, a line plot of the Θ'_m at the height level $z = 5.5$ km along the equator at time $t = 3000$ s is suggested. For models with pressure-based levels the corresponding model level closest to $p = 512.085$ hPa should be selected without any vertical interpolations since it corresponds almost exactly to the position $z = 5.5$ km at the equator.

4. TEST CATEGORY 4-X: BAROCLINIC INSTABILITY

The baroclinic instability test of [18, 19] and its rotated version described in [20] have been used extensively to test the response of 3D atmospheric models to a controlled, evolving instability. This test is specified in pressure-based η-coordinates for the vertical, defined by

$$\eta = \frac{p}{p_s(\lambda, \varphi)}. \tag{115}$$

Hence, the η coordinates is equal to unity at the surface and approaches zero as $p \to 0$. For models using a height-based or isentropic vertical coordinate, an iterative procedure as described in Appendix F.5 and Appendix F.6 is required in order to initialize this test.

Table XV. List of constants used for the Baroclinic Instability test cases (Test $4 - x$).

Constant	Value	Description
z_{top}	44000 m	Recommended height position of the model top
p_{top}	≈ 2.26 hPa	Recommended pressure at the model top
X	various	Reduced-size planet scaling factor, see below
a	a_{ref}/X	Scaled radius of the Earth
Ω	$\Omega_{\text{ref}} X$	Scaled angular speed of the Earth
p_s	1000 hPa	Surface pressure (constant)
p_0	1000 hPa	Reference pressure (constant)
η_0	0.252	Value of η at a reference level (position of the jet)
η_t	0.2	Value of η at the tropopause
η_s	1	Value of η at the surface
u_0	35 m s^{-1}	Maximum amplitude of the zonal wind
u_p	1 m s^{-1}	Maximum amplitude of the zonal wind perturbation
λ_c	$\pi/9$	Longitude of the zonal wind perturbation centerpoint (20° E)
φ_c	$2\pi/9$	Latitude of the zonal wind perturbation centerpoint (40° N)
R	$a/10$	Radius of the zonal wind perturbation
T_0	288 K	Horizontal-mean temperature at the surface
Γ	0.005 K m^{-1}	Temperature lapse rate
ΔT	4.8×10^5 K	Empirical temperature difference

An auxiliary variable η_ν is defined by

$$\eta_\nu = (\eta - \eta_0)\frac{\pi}{2}. \tag{116}$$

The zonal velocity field consists of two symmetric zonal jets in the midlatitudes which are overlaid by a Gaussian-type zonal wind perturbation. The zonal wind u is defined as

$$u(\lambda, \varphi, \eta) = u_0 \cos^{\frac{3}{2}} \eta_\nu \, \sin^2(2\varphi) + u_p \exp\left(-\left(\frac{r}{R}\right)^2\right). \tag{117}$$

The meridional and vertical velocity is everywhere zero,

$$v(\lambda, \varphi, z) = 0, \qquad w(\lambda, \varphi, z) = 0, \qquad \omega(\lambda, \varphi, z) = 0. \tag{118}$$

Here r is the great circle distance from the zonal wind perturbation centerpoint, defined by

$$r = a \arccos \left(\sin \varphi_c \sin \varphi + \cos \varphi_c \cos \varphi \cos(\lambda - \lambda_c) \right). \tag{119}$$

In addition, the specific humidity field q is set to zero for the dry test variants 4-1-x, and the surface pressure is set to the constant $p_s = p_0 = 1000$ hPa.

The total temperature distribution comprises the horizontal-mean temperature and a horizontal variation at each level. It is given by

$$
\begin{aligned}
T(\lambda, \varphi, \eta) \;=\; & \overline{T}(\eta) + \frac{3}{4} \frac{\eta \pi u_0}{R_d} \sin \eta_\nu \cos^{\frac{1}{2}} \eta_\nu \times \\
& \left\{ 2 u_0 \cos^{\frac{3}{2}} \eta_\nu \left(-2 \sin^6 \varphi \left(\cos^2 \varphi + \frac{1}{3} \right) + \frac{10}{63} \right) + \right. \\
& \left. a\Omega \left(\frac{8}{5} \cos^3 \varphi \left(\sin^2 \varphi + \frac{2}{3} \right) - \frac{\pi}{4} \right) \right\}.
\end{aligned}
\tag{120}
$$

The horizontally averaged temperature $\overline{T}(\eta)$ is split into two representations for the lower (121) and middle atmosphere (122). It is given by

$$\overline{T}(\eta) = T_0 \eta^{\frac{R_d \Gamma}{g}}, \qquad \qquad \text{(for } 1 \geq \eta \geq \eta_t) \tag{121}$$

$$\overline{T}(\eta) = T_0 \eta^{\frac{R_d \Gamma}{g}} + \Delta T (\eta_t - \eta)^5, \qquad \text{(for } \eta_t > \eta) \tag{122}$$

The density ρ is defined by the ideal gas law

$$\rho(\lambda, \varphi, \eta) = \frac{p(\lambda, \varphi, \eta)}{R_d\, T(\lambda, \varphi, \eta)}. \tag{123}$$

The geopotential $\Phi = gz$ completes the description of the steady-state initial conditions, where z symbolizes the elevation at model level η. The total geopotential distribution $\Phi = \overline{\Phi} + \Phi'$ consists of the horizontal-mean geopotential $\overline{\Phi}$ and a horizontal variation Φ' at each level. It is given by

$$
\begin{aligned}
\Phi(\lambda, \varphi, \eta) \;=\; & \overline{\Phi}(\eta) + u_0 \cos^{\frac{3}{2}} \eta_\nu \times \\
& \left\{ u_0 \cos^{\frac{3}{2}} \eta_\nu \left(-2 \sin^6 \varphi \left(\cos^2 \varphi + \frac{1}{3} \right) + \frac{10}{63} \right) + \right. \\
& \left. a\Omega \left(\frac{8}{5} \cos^3 \varphi \left(\sin^2 \varphi + \frac{2}{3} \right) - \frac{\pi}{4} \right) \right\},
\end{aligned}
\tag{124}
$$

with horizontal-mean geopotential

$$\overline{\Phi}(\eta) = \frac{T_0 g}{\Gamma} \left(1 - \eta^{\frac{R_d \Gamma}{g}} \right), \qquad \qquad \text{(for } 1 \geq \eta \geq \eta_t), \tag{125}$$

$$\overline{\Phi}(\eta) = \frac{T_0 g}{\Gamma} \left(1 - \eta^{\frac{R_d \Gamma}{g}} \right) - \Delta\Phi(\eta), \qquad \text{(for } \eta_t > \eta), \tag{126}$$

where

$$\Delta\Phi(\eta) = R_d \Delta T \left\{ \left(\ln\left(\frac{\eta}{\eta_t} \right) + \frac{137}{60} \right) \eta_t^5 - 5\eta_t^4 \eta + 5\eta_t^3 \eta^2 - \frac{10}{3} \eta_t^2 \eta^3 + \frac{5}{4} \eta_t \eta^4 - \frac{1}{5} \eta^5 \right\}. \tag{127}$$

The test requires the initialization of the surface geopotential Φ_s. The orography field balances the non-zero zonal wind at the surface and is determined by (124) when evaluated at the surface with $\eta_s = 1$. It is given by

$$
\begin{aligned}
\Phi_s(\lambda, \varphi) = u_0 \; \cos^{\frac{3}{2}} \left((\eta_s - \eta_0) \frac{\pi}{2} \right) \times \\
\left\{ u_0 \; \cos^{\frac{3}{2}} \left((\eta_s - \eta_0) \frac{\pi}{2} \right) \left(-2 \sin^6 \varphi \; (\cos^2 \varphi + \frac{1}{3}) + \frac{10}{63} \right) + \right. \\
\left. a \, \Omega \left(\frac{8}{5} \cos^3 \varphi \; (\sin^2 \varphi + \frac{2}{3}) - \frac{\pi}{4} \right) \right\}.
\end{aligned}
\tag{128}
$$

Note that the use of a scaling parameter $X > 1$ does not impact the initialization of u, v, T, ps or Φ_s since the rescaled radius is always multiplied with the rescaled angular velocity.

4.1. Test 4-1-x: Dry Baroclinic Instability on a Small Planet with Dynamic Tracers

The baroclinic instability on a small planet is initialized as above, except we vary the scaling parameter X (defined in Table III) to redefine the radius and rotation rate of the Earth, relative to real-world reference values. This change needs to be implemented in the GCM code. Analogously, we define a *small planet timescale* according to $t_s = t/X$ which reflects the faster development of the baroclinic instability associated with contraction of the length scale. Since both the radius $a = a_{ref}/X$ and the rotation rate $\Omega = \Omega_{ref} X$ are impacted by the scaling factor X, their product $a\Omega$ remains the same. It means that the initial conditions on small planets will be identical to the initial conditions on the regular-size planet with the exception of the Ertel potential vorticity field used as an invariant dynamic tracer (see below).

In hydrostatic models variations in X should have very minor effects on the model output. The most dominant differences to a regular-size planet experiment are that the amplitude of the vertical velocity approximately scales with X and thereby increases in strength on small planets. In addition, the amplitude of the Ertel potential vorticity tracer increases by the factor X. While these changes do not seem to impact the overall development of the baroclinic wave in hydrostatic models, the evolution of the wave has been observed to become very different in non-hydrostatic models with increased scaling factor X. The investigation of the regime shifts in the baroclinic wave development are of particular interest here.

Invariant tracers

Test 4-1-x includes two invariant tracer fields, potential temperature ($q_1 = \Theta$) and the absolute value of Ertel's potential vorticity ($q_2 = |\text{EPV}|$). That is, it follows from the primitive equations that each of the invariant tracers inherently satisfies the advection equation with no exterior source terms. Since the numerical simulation is inexact, we expect there to be a deviation between the invariant tracer field and the dynamically computed tracer over time. Comparing these two quantities yields insight into how well a model conserves the invariant relationships with time.

The initial distribution of potential temperature can be immediately computed from the temperature field (120)-(122),

$$
q_1(\lambda, \varphi, \eta) = \Theta(\lambda, \varphi, \eta) = \overline{T}(\eta)\eta^{-\kappa} + \frac{3}{4} \frac{\pi u_0}{R_d} \eta^{1-\kappa} \sin \eta_v \cos^{\frac{1}{2}} \eta_v Y,
\tag{129}
$$

where

$$Y = \left(-2\sin^6\varphi\left[\cos^2\varphi + \frac{1}{3}\right] + \frac{10}{63}\right)2u_0\cos^{3/2}\eta_v + \left(\frac{8}{5}\cos^3\varphi\left[\sin^2\varphi + \frac{2}{3}\right] - \frac{\pi}{4}\right)a\Omega. \quad (130)$$

The definition of the absolute value of the hydrostatic variant of Ertel's potential vorticity on pressure levels is

$$q_2(\lambda,\varphi,\eta) = |\text{EPV}(\lambda,\varphi,\eta)| = \left|g\left\{\frac{1}{a\cos\varphi}\frac{\partial v}{\partial p}\left(\frac{\partial\Theta}{\partial\lambda}\right)_p - \frac{1}{a}\frac{\partial u}{\partial p}\left(\frac{\partial\Theta}{\partial\varphi}\right)_p + (f+\zeta_p)\left(-\frac{\partial\Theta}{\partial p}\right)\right\}\right|,$$
$$(131)$$

where ζ_p is the relative vorticity computed at constant pressure [21] and $f = 2\Omega\sin(\varphi)$ is the Coriolis parameter. The subscript p denotes that these partial derivatives are taken at constant pressure levels. We consider the analytic initial conditions and EPV formulation described in [18] and [22]. Since the basic initial state is hydrostatically balanced and the pressure does not vary along the η-levels, this formulation for the initial EPV field is also valid for non-hydrostatic shallow-atmosphere models. As noted before the scaling parameter X leads to an increase of EPV by the factor X as both $a = a_{\text{ref}}/X$ and $\Omega = \Omega_{\text{ref}}X$ are present in (131).

Note that the initial potential temperature does not vary in the longitudinal direction ($\partial\Theta/\partial\lambda = 0$) and that ∂p can be expressed as $p_0\partial\eta$ since the surface pressure is constant. Using all simplifications in (131), the initial absolute value of the EPV tracer yields

$$q_2(\lambda,\varphi,\eta) = |\text{EPV}(\lambda,\varphi,\eta)| = \left|\frac{g}{p_0}\left\{-\frac{1}{a}\frac{\partial u}{\partial\eta}\left(\frac{\partial\Theta}{\partial\varphi}\right)_p - (f+\zeta_p)\frac{\partial\Theta}{\partial\eta}\right\}\right|. \quad (132)$$

The total velocity components for the test case are given by (117) and (118). As also specified in [18] this immediately leads to the relative vorticity in the outward direction (perpendicular to the pressure surfaces in this case) being given by

$$\begin{aligned}
\zeta(\lambda,\varphi,\eta) &= \zeta_b(\lambda,\varphi,\eta) + \zeta'(\lambda,\varphi,\eta) \\
&= -4\frac{u_0}{a}\cos^{\frac{3}{2}}\eta_v\sin\varphi\cos\varphi(2 - 5\sin^2\varphi) + \frac{u_p}{a}\exp\left(-\left(\frac{r}{R}\right)^2\right) \times \\
&\quad \left\{\tan(\varphi) - 2\left(\frac{a}{R}\right)^2\arccos(K)\frac{\sin\varphi_c\cos\varphi - \cos\varphi_c\sin\varphi\cos(\lambda-\lambda_c)}{\sqrt{1-K^2}}\right\}(133)
\end{aligned}$$

where ζ_b is the unperturbed background relative vorticity, ζ' denotes the relative vorticity perturbation, and K is defined as $K = \sin\varphi_c\sin\varphi + \cos\varphi_c\cos\varphi\cos(\lambda-\lambda_c)$. For the singular points (λ_c,φ_c) and $(\lambda_c + \pi, -\varphi_c)$ with $K^2 = 1$, $\zeta'(\lambda_c,\varphi_c) = u_p\tan\varphi/a$ is well-defined and $\lim_{\lambda\to\lambda_c+\pi,\varphi\to-\varphi_c}\zeta'$ is zero. Similarly, $\lim_{\varphi\to\pm\frac{\pi}{2}}\zeta'$ is zero at the poles. These limits need to be enforced in the implementation of the initial conditions.

The vertical derivative of the zonal wind yields

$$\frac{\partial u}{\partial\eta} = -u_0\sin^2(2\varphi)\frac{3\pi}{4}\cos^{\frac{1}{2}}\eta_v\sin\eta_v. \quad (134)$$

The vertical derivative of the potential temperature is calculated from (129) as

$$
\begin{aligned}
\frac{\partial \Theta}{\partial \eta} = {} & \frac{\partial \overline{\Theta}}{\partial \eta} + \frac{3}{4} \frac{\pi u_0}{R_d} (1 - \kappa) \, \eta^{-\kappa} \sin \eta_v \cos^{\frac{1}{2}} \eta_v Y + \frac{3}{8} \frac{\pi^2 u_0}{R_d} \eta^{1-\kappa} \cos^{\frac{3}{2}} \eta_v Y \\
& - \frac{3}{16} \frac{\pi^2 u_0}{R_d} \eta^{1-\kappa} \sin^2 \eta_v \cos^{-\frac{1}{2}} \eta_v Y \\
& - \frac{9}{8} \frac{\pi^2 u_0^2}{R_d} \eta^{1-\kappa} \sin^2 \eta_v \cos \eta_v \left(-2 \sin^6 \varphi \left[\cos^2 \varphi + \frac{1}{3} \right] + \frac{10}{63} \right)
\end{aligned}
\tag{135}
$$

where

$$
\frac{\partial \overline{\Theta}}{\partial \eta} =
\begin{cases}
T_0 \left(\frac{R_d \Gamma}{g} - \kappa \right) \eta^{(R_d \Gamma / g - \kappa) - 1} & \text{for } \eta_s \geq \eta \geq \eta_t \\[2mm]
T_0 \left(\frac{R_d \Gamma}{g} - \kappa \right) \eta^{(R_d \Gamma / g - \kappa) - 1} & \\
\quad - \Delta T \left(5(\eta_t - \eta)^4 \eta^{-\kappa} + \kappa (\eta_t - \eta)^5 \eta^{-\kappa - 1} \right) & \text{for } \eta_t > \eta.
\end{cases}
\tag{136}
$$

The derivative of potential temperature with respect to the latitudinal direction is also computed as

$$
\begin{aligned}
\frac{\partial \Theta}{\partial \varphi} = {} & \frac{3}{4} \frac{\pi u_0}{R_d} \eta^{1-\kappa} \sin \eta_v \cos^{\frac{1}{2}} \eta_v \\
& \times \left\{ 2 u_0 \cos^{\frac{3}{2}} \eta_v \left(-12 \cos \varphi \sin^5 \varphi \left[\cos^2 \varphi + \frac{1}{3} \right] + 4 \cos \varphi \sin^7 \varphi \right) \right. \\
& \left. + a \Omega \left(-\frac{24}{5} \sin \varphi \cos^2 \varphi \left[\sin^2 \varphi + \frac{2}{3} \right] + \frac{16}{5} \cos^4 \varphi \sin \varphi \right) \right\}.
\end{aligned}
\tag{137}
$$

Combining all of these terms as illustrated in (132) we can define the initial EPV distribution analytically. The EPV is positive in the Northern Hemisphere, and negative in the Southern Hemisphere. However, we initialize the EPV tracer field with the absolute value of EPV in order to avoid model errors arising from negative tracer constituents. In this case the tracer distribution will only correspond to the dynamically computed EPV in the Northern Hemisphere, and to the absolute value of the dynamic EPV field in the Southern Hemisphere.

We suggest running the dry baroclinic instability test with the following small-planet scaling factors:

Test Name	Scaling Factor
Test 4-1-0	$X = 1$
Test 4-1-1	$X = 10$
Test 4-1-2	$X = 100$
Test 4-1-3	$X = 1000$

Grid spacings, simulation time and output

The simulation should be run for $t_s = 30$ small planet days, which corresponds to $t = (2592000/X)$ seconds in unscaled Earth units. Output should be written every small planet day (each $86400/X$ seconds in unscaled Earth units) including the initial state. The output file should contain the instantaneous model-level snapshots of the q_1, q_2, u, v, w or ω, T, p_s, Φ_s fields and p in case the pressure cannot be reconstructed via the surface pressure. In addition, we ask for 2D fields at the

850 hPa pressure level if available as output quantities. They are u, v, T, w or ω at the interpolated 850 hPa level.

The grid resolution is chosen to be roughly $1°$ at the equator with 30 vertical levels arranged in approximate correspondence with Appendix F.1. The model top in height-based models should be at least 30 km high. However, a higher model top of about 44 km is the preferred choice since it mimics the model top in the pressure-based L30 setup (Table XVIII) more closely. The position of the model top in pressure-based models should lie around 2.26 hPa as specified by the level distribution in Table XVIII. Appendix F.2 makes suggestions for the placement of the 30 model levels in height-based models.

Diagnostics

Surface pressure, the 850 hPa temperature, 850 hPa vertical velocity and 850 hPa relative vorticity should be plotted at small planet days 7, 9, 12 and 15 for each of these simulations. Further, we are interested in the consistency between the dynamic tracers Θ and EPV and the dynamics themselves. We suggest plotting Θ and q_1 at the small planet days 7, 9, 12 and 15 at the 850 hPa level. In addition, we suggest interpolating q_1 to the $\Theta_0 = 315$ K isentropic level to evaluate the deviations of the tracer q_1 from Θ_0 at this isentropic level. The 315 K isentropic level does not intersect with the ground and lies close to the 900 hPa pressure surface in the tropics and between 400-500 hPa in mid- and high latitudes. The deviation $(q_1 - \Theta_0)$ along the Θ_0 isentropic level should be plotted at the small planet days 7, 9, 12 and 15 as a longitude-latitude cross section. Error measures for $(q_1 - \Theta_0)$, like the normalized l_2 error norm , might be considered while acknowledging that the vertical interpolation contributes to the overall error. However, its effect might be small in comparison to the dynamic inconsistency errors depending on the model formulation.

We suggest comparing the tracer EPV and dynamic EPV fields at the $\Theta_0 = 315$ K isentropic level in the Northern Hemisphere. The dynamic EPV field can be computed from the output quantities. Such analysis routines will be provided in form of NCL scripts. Of course, if an analysis of the dynamic EPV field is already provided in the model, we ask for it as an output quantity. We suggest plotting both the 315 K dynamic and tracer EPV fields in the Northern Hemisphere ($\varphi \in [0°, 90°]$) at small Earth days 8, 12 and 15. In addition, we suggest creating x-y scatter plots of the dynamic 315 K EPV (x-axis) versus the tracer EPV (y-axis) field in the region $\varphi \in [30°, 90°]$ at the small planet days 8, 12 and 15. The spread on these scatter plots is an indication of dynamic inconsistencies in the model as discussed in [22].

In order to gain an appreciation for the dissipation characteristics of the model, we also propose plotting the 700 hPa kinetic energy (KE) spectrum at small planet day 30. The selected rather low-lying pressure level is selected since the baroclinic wave is most pronounced at the lower levels. Such plots can be directly compared to KE-spectra analyses in [23].

4.2. Test 4-2: Moist Variant of the Baroclinic Wave Test Case with Large-Scale Condensation

Moist initial conditions

The initial conditions for the moist baroclinic wave are almost identical to the initial conditions for the dry baroclinic wave. We utilize the regular-size planet with the scaling factor $X = 1$. The differences to the dry baroclinic wave test case 4-1 are that the original temperature equation T

Table XVI. List of additional constants used for the Moist Baroclinic Instability test cases (Test $4-2$), see also Table XV.

Constant	Value	Description
X	1	small-planet scaling factor (regular-size Earth)
φ_w	$2\pi/9$	Specific humidity latitudinal width parameter ($40°$)
p_w	340 hPa	Specific humidity vertical pressure width parameter
q_0	0.021 kg/kg	Maximum specific humidity amplitude
p_0	1000 hPa	Surface pressure

now gets interpreted as an equation for the virtual temperature T_v, the formally dry surface pressure $p_s = p_0$ gets interpreted as the surface pressure of the moist air, the definition of the density needs to utilize the virtual temperature instead of the temperature, and an analytic equation for the specific humidity q is added. The wind initialization of the moist baroclinic wave is identical to the dry case. No passive tracers q_1 or q_2 are specified.

The specific humidity field is

$$q(\lambda, \varphi, \eta) \;=\; q_0 \exp\left[-\left(\frac{\varphi}{\varphi_w}\right)^4\right] \exp\left[-\left(\frac{(\eta-1)p_0}{p_w}\right)^2\right] \tag{138}$$

with the latitudinal width parameter $\varphi_w = 2\pi/9$ (corresponding to $40°$ latitude) and the pressure-based width parameter $p_w = 340$ hPa. Since the surface pressure of the moist air p_s is constant with $p_s = p_0 = 1000$ hPa the vertical coordinate η is represented by $\eta = p/p_0$. The functional form of q and its parameters were inspired by observations. This moisture fields leads to maximum relative humidities around 90% in the lower levels of the midlatitudes, and around 70% in the topics.

This virtual temperature T_v field is given by the original temperature definition in (120)-(122),

$$
\begin{aligned}
T_v(\lambda, \varphi, \eta) \;=\;& \langle T_v(\eta)\rangle + \frac{3}{4}\frac{\eta\,\pi\,u_0}{R_d}\ \sin\eta_v\ \cos^{\frac{1}{2}}\eta_v\ \times \\
& \left\{\left(-2\sin^6\varphi\,(\cos^2\varphi + \frac{1}{3}) + \frac{10}{63}\right)2\,u_0\,\cos^{\frac{3}{2}}\eta_v\ + \right. \\
& \left.\left(\frac{8}{5}\cos^3\varphi\,(\sin^2\varphi + \frac{2}{3}) - \frac{\pi}{4}\right)a\,\Omega\right\}
\end{aligned}
\tag{139}
$$

with the horizontal-mean virtual temperature

$$\langle T_v(\eta)\rangle \;=\; T_0\,\eta^{\frac{R_d\Gamma}{g}} \qquad\qquad \text{(for } \eta_s \geq \eta \geq \eta_t) \tag{140}$$

$$\langle T_v(\eta)\rangle \;=\; T_0\,\eta^{\frac{R_d\Gamma}{g}} + \Delta T\,(\eta_t - \eta)^5 \qquad \text{(for } \eta_t > \eta). \tag{141}$$

The density of the moist air is defined by the ideal gas law

$$\rho(\lambda, \varphi, \eta) = \frac{p(\lambda, \varphi, \eta)}{R_d\,T_v(\lambda, \varphi, \eta)}. \tag{142}$$

and utilizes the pressure of the moist air and the virtual temperature.

The formulation of the virtual temperature and specific humidity leads to the analytic representation of the temperature

$$T(\lambda, \varphi, \eta) = \frac{T_v(\lambda, \varphi, \eta)}{1 + 0.608\, q(\lambda, \varphi, \eta)} \tag{143}$$

This temperature is colder than the original dry temperature. However, note that in the moist case the virtual temperature and moist pressure determine the strength of the pressure gradient term in the momentum equations. Since these are identical to the temperature and pressure in the dry case, the forcing by the pressure gradient term is the same in both the dry and moist variant of the baroclinic wave. The moist variant of the baroclinic wave without the temperature forcing from large-scale condensation should lead to almost identical results when compared to the dry version. Very small variations are expected since the moisture gets independently transported as a passive tracer in this case and some models utilize the moist variant of the physical constant c_p. If possible, the dry c_p should be used. Comparing the evolution of the dry baroclinic wave to its moist variant (without large-scale condensation) can serve as a first sensibility check.

Inclusion of large-scale condensation

The underlying idea of the moist baroclinic wave test case is to provide a feedback mechanism between the equations of motion and moisture. This is achieved via the inclusion of a large-scale condensation process which is triggered in the case of supersaturation. If large-scale condensation is invoked, the excess moisture is removed as large-scale precipitation without a cloud stage or re-evaporation, and the released heat forces the thermodynamic variable. The suggested approach can be considered one of the simplest possible tests of the coupled moist physics-dynamics system. The scheme for large-scale condensation is based on the scheme of [3], and is described in Appendix C. The large-scale condensation mechanism is also provided as part of the Fortran template routine simple_physics_v5.f90 (updated on July/8/2012) that is provided on the DCMIP web page.

After the large-scale condensation is computed and moisture is removed from the system care needs to be taken to ensure that the model conserves the total dry air mass or its analog, the global average of the dry surface pressure. This is especially true if the moist surface pressure is predicted in the dynamical core. If needed the 'dry air adjustment' should take place in either the dynamical core or after the large-scale condensation was applied as a 'physics' package. This depends on the design of the model. Most often, GCMs already provide a mechanism to ensure that the total dry air mass is conserved, such as global mass fixers or explicit dry air adjustment routines as discussed in e.g. [24]. If not, such a mechanism needs to be supplied and invoked after each 'physics' time step.

Grid spacings, simulation time, output and diagnostics

We suggest running this test until $t = 15$ days, which corresponds to 1296000 seconds with output at 6-hourly time intervals (every 21600 seconds) including the initial state. Two grid resolutions should be chosen. The first experiment should be run at roughly $1°$ at the equator (110 km equatorial grid spacing) with 30 vertical levels arranged in approximate correspondence with Appendix F.1. This is also discussed above in section 4.1. The second experiment doubles the horizontal resolution and sets the horizontal grid spacing to $\approx 0.5°$ (≈ 55 km) while keeping the L30 level configuration.

If height-based coordinates are used we recommend a model top of about 44 km. The lowermost full model level should lie around 60-70 m above the ground to mimic the position of the lowermost level in the pressure-based level distribution (Table XVIII) most closely. Appendix F.2 makes suggestions for the placement of the 30 model levels in height-based models.

The output file should contain instantaneous model-level snapshots of the q, u, v, w or $\omega, T, p_s, \Phi_s, P_{ls}$ fields and p in case the pressure cannot be reconstructed via the surface pressure field. In addition, we ask for 2D fields at the 850 hPa pressure level, if available, as output quantities. They are u, v, T, w or ω fields at the interpolated 850 hPa level. Surface pressure, the 850 hPa temperature, 850 hPa vertical velocity and large-scale precipitation rate P_{ls} should be plotted at days 6, 9, 12 and 15. In addition, we recommend plotting the time history of the surface pressure field at selected locations in the Northern midlatitudes (positions to be determined).

4.3. Optional Test 4-3: Moist Variant of the Baroclinic Wave Test Case, driven by "Simple-Physics"

The setup of test 4-3 is formally identical to test 4-2 on a regular-size Earth (see section 4.2), but now assumes that the Earth is a water-covered aqua-planet. The only difference to test 4-2 is that additional simplified physical forcing mechanisms are applied at each physics time step. These incorporate simple surface fluxes of momentum, latent and sensible heat, as well as a simplified boundary layer diffusion mechanism which mixes the horizontal velocities, the temperature and specific humidity via a second-order vertical diffusion. The design of this "simple-physics" package has been introduced by [3] and is described in the Appendices C-E. However, there is one difference. Instead of using a constant sea surface temperature (SST), the prescribed and time-independent SST field needs to be initialized via (143) evaluated at the surface level $\eta = 1$. All test specific parameters are listed in Tables XV and XVI. Section 0.6 provides practical recommendations on the provided template routine for the "simple-physics" package.

As before in test 4-2, after physical forcings are computed and moisture is removed from the system care needs to be taken to ensure that the model conserves the total dry air mass or its analog, the global average of the dry surface pressure. This is especially true if the moist surface pressure is predicted in the dynamical core. If needed this 'dry air adjustment' should take place in either the dynamical core or after the large-scale condensation was applied as a 'physics' package. This depends on the design of the model. Most often, GCMs already provide a mechanism to ensure that the total dry air mass is conserved, such as global mass fixers or explicit dry air adjustment routines as discussed in e.g. [24]. If not, such a mechanism needs to be supplied and invoked after each 'physics' time step.

Grid spacings, simulation time, output and diagnostics

We suggest running this test until $t = 15$ days, which corresponds to 1296000 seconds with output at 6-hourly time intervals (every 21600 seconds). The output file should include the initial state. Two grid resolutions are recommended. The first experiment should be run at roughly $1°$ at the equator (110 km equatorial grid spacing) with 30 vertical levels arranged in approximate correspondence with Appendix F.1. This is also discussed above in section 4.1. The second experiment doubles the

horizontal resolution and sets the horizontal grid spacing to $\approx 0.5°$ (≈ 55 km) while keeping the L30 level configuration.

If height-based coordinates are used we recommend a model top of about 44 km. As before, the lowermost full model level should lie around 60-70 m above the ground to mimic the position of the lowermost level in the pressure-based level distribution (Table XVIII) most closely. Since the position of the lowest model level enters the computation of the simple-physics forcings, there might be sensitivities to the level placement. Appendix F.2 makes suggestions for the placement of the 30 model levels in height-based models.

The output file should contain the instantaneous model-level snapshots of q, u, v, w or $\omega, T, p_s, \Phi_s, P_{ls}, SST$, and p in case the pressure cannot be reconstructed via the surface pressure field. In addition, we ask for 2D fields at the 850 hPa pressure level, if available, as output quantities. They are u, v, T, w or ω fields at the interpolated 850 hPa level. Surface pressure, the 850 hPa temperature, 850 hPa vertical velocity and large-scale precipitation rate P_{ls} should be plotted at days 6, 9, 12 an 15. In addition, we recommend plotting the time history of the surface pressure field at selected locations in the Northern midlatitudes (positions to be determined).

5. TEST CATEGORY 5-X: IDEALIZED TROPICAL CYCLONE EXPERIMENTS

The simplified tropical cyclone test case on a regular-size Earth is based on the work of [3, 25, 26, 27]. In this test an analytic vortex is initialized in a background environment which is tractable to a rapid intensification of tropical cyclones. Two test variants are suggested. The first test variant 5-1 has intermediate complexity, requiring simplified physical forcings in order to drive the tropical storm. This simplified physics parameterization suite called "simple-physics" is described in detail in [3], although the important components have been reproduced here in Appendices C-E. In short, the simple-physics suite provides a large-scale condensation process, surface fluxes and boundary layer mixing. The use of the simplified parameterization package guarantees that the model results can be intercompared.

The second test variant 5-2 is optional, and might be considered if the GCM is configurable as an aqua-planet model described by [28]. The only differences to [28] are that the SST field needs to be set to 29 C$^\circ$ and that the model is only integrated for 10 days. We propose using the analytic initial vortex in combination with the model's own complex physical parameterization package in this aqua-planet mode. Of course, the physical parameterization packages in GCMs vary widely and cannot be compared directly. However, such an experiment gives valuable insight into the structural uncertainty among the DCMIP models that are run at comparable horizontal and vertical resolutions. The structural uncertainties are therefore triggered by the designs of the dynamical cores, the physical parameterizations, and their complex nonlinear interactions. Since the models start with identical initial conditions, utilize an identical forcing at the lower boundary via the prescribed SST, and share the same external forcing parameters like the solar constant or greenhouse gas concentrations (defined in [28]) the initial data and boundary data uncertainties are eliminated.

Table XVII. List of constants used for the Simplified Tropical Cyclone Experiments (Tests 5-1 and 5-2)

Constant	Value	Description
X	1	small-planet scaling factor (regular-size Earth)
z_t	15000 m	Tropopause height
q_0	0.021 kg/kg	Maximum specific humidity amplitude
q_t	10^{-11} kg/kg	Specific humidity in the upper atmosphere
T_0	302.15 K	Surface temperature of the air
T_s	302.15 K	Sea surface temperature (SST), 29 C$^\circ$
z_{q1}	3000 m	Height related to the linear decrease of q with height
z_{q2}	8000 m	Height related to the quadratic decrease of q with height
Γ	0.007 K m^{-1}	Virtual temperature lapse rate
p_b	1015 hPa	Background surface pressure
φ_c	$\pi/18$	Initial latitude of vortex center
λ_c	π	Initial longitude of vortex center
Δp	11.15 hPa	Pressure perturbation at vortex center
r_p	282000 m	Horizontal half-width of pressure perturbation
z_p	7000 m	Height related to the vertical decay rate of p perturbation
ϵ	10^{-25}	Small threshold value

Initial Conditions for Test 5-1 and 5-2

Background state

The background state consists of a prescribed specific humidity profile, virtual temperature and pressure profile. These parameters are chosen to roughly match an observed tropical sounding documented in [29]. The background specific humidity profile $\overline{q}(z)$ as a function of height z is

$$\overline{q}(z) = q_0 \exp\left(-\frac{z}{z_{q1}}\right) \exp\left(-\left(\frac{z}{z_{q2}}\right)^2\right) \qquad \text{for } 0 \leq z \leq z_t,$$

$$\overline{q}(z) = q_t \qquad\qquad\qquad\qquad\qquad \text{for } z_t < z. \tag{144}$$

The background virtual temperature sounding $\overline{T}_v(z)$ is split into two different representations for the lower and upper atmosphere. It is given by

$$\overline{T}_v(z) = T_{v0} - \Gamma z \qquad \text{for } 0 \leq z \leq z_t,$$
$$\overline{T}_v(z) = T_{vt} = T_{v0} - \Gamma z_t \quad \text{for } z_t < z, \tag{145}$$

with the virtual temperature at the surface $T_{v0} = T_0(1 + 0.608\, q_0)$ and the virtual temperature at the tropopause level $T_{vt} = T_{v0} - \Gamma z_t$. As a result, the background temperature profile $\overline{T}(z)$ is

$$\overline{T}(z) = \frac{\overline{T}_v(z)}{1 + 0.608\, \overline{q}(z)}. \tag{146}$$

The specific humidity values correspond to relative humidities of about 80% at lower levels and prescribe a warm and moist environment.

The background vertical pressure profile $\overline{p}(z)$ of the moist air is computed using the hydrostatic balance and the virtual temperature equation (145). The profile is given by

$$\overline{p}(z) = p_b \left(\frac{T_{v0} - \Gamma z}{T_{v0}}\right)^{\frac{g}{R_d \Gamma}} \quad \text{for } 0 \leq z \leq z_t,$$

$$\overline{p}(z) = p_t \exp\left(\frac{g(z_t - z)}{R_d T_{vt}}\right) \quad \text{for } z_t < z. \tag{147}$$

The pressure at the tropopause level z_t is continuous and given by

$$p_t = p_b \left(\frac{T_{vt}}{T_{v0}}\right)^{\frac{g}{R_d \Gamma}}, \tag{148}$$

which, for the given set of parameters, is approximately 130.5 hPa.

Axisymmetric Vortex

The pressure equation $p(r, z)$ for the moist air is comprised of the background pressure profile (147) plus a 2D pressure perturbation $p'(r, z)$,

$$p(r, z) = \overline{p}(z) + p'(r, z), \tag{149}$$

where r symbolizes the radial distance (or radius) to the center of the prescribed vortex. On the sphere r is defined using the great circle distance

$$r = a \arccos \left(\sin \varphi_c \sin \varphi + \cos \varphi_c \cos \varphi \cos \left(\lambda - \lambda_c \right) \right). \tag{150}$$

The perturbation pressure is defined as

$$p'(r, z) = -\Delta p \exp \left(-\left(\frac{r}{r_p} \right)^{3/2} - \left(\frac{z}{z_p} \right)^2 \right) \left(\frac{T_{v0} - \Gamma z}{T_{v0}} \right)^{\frac{g}{R_d \Gamma}} \qquad \text{for } 0 \le z \le z_t,$$

$$p'(r, z) = 0 \qquad \qquad \text{for } z_t < z. \tag{151}$$

The pressure perturbation depends on the pressure difference Δp between the background surface pressure p_b and the pressure at the center of the initial vortex, the pressure change in the radial direction r_p and the pressure decay with height within the vortex z_p. The moist surface pressure $p_s(r)$ is computed by setting $z = 0$ m in (149), which gives

$$p_s(r) = p_b - \Delta p \exp \left(-\left(\frac{r}{r_p} \right)^{3/2} \right). \tag{152}$$

The axisymmetric virtual temperature $T_v(r, z)$ is computed using the hydrostatic equation and ideal gas law

$$T_v(r, z) = -\frac{g p(r, z)}{R_d} \left(\frac{\partial p(r, z)}{\partial z} \right)^{-1}. \tag{153}$$

Again it can be written as a sum of the background state and a perturbation,

$$T_v(r, z) = \overline{T}_v(z) + T'_v(r, z), \tag{154}$$

where the virtual temperature perturbation is defined as

$$T'_v(r, z) = (T_{v0} - \Gamma z) \left\{ \left[1 + \frac{2 R_d (T_{v0} - \Gamma z) z}{g z_p^2 \left[1 - \frac{p_b}{\Delta p} \exp \left(\left(\frac{r}{r_p} \right)^{3/2} + \left(\frac{z}{z_p} \right)^2 \right) \right]} \right]^{-1} - 1 \right\} \quad \text{for } 0 \le z \le z_t,$$

$$T'_v(r, z) = 0 \qquad \qquad \text{for } z_t < z. \tag{155}$$

The axisymmetric specific humidity $q(r, z)$ is set to the background profile everywhere

$$q(r, z) = \overline{q}(z). \tag{156}$$

Consequently, the temperature can be written as

$$T(r, z) = \overline{T}(z) + T'(r, z), \tag{157}$$

with the temperature perturbation

$$T'(r,z) = \frac{T_{v0} - \Gamma z}{1 + 0.608\overline{q}(z)} \left\{ \left[1 + \frac{2R_d(T_{v0} - \Gamma z)z}{gz_p^2 \left[1 - \frac{p_b}{\Delta p} \exp\left(\left(\frac{r}{r_p}\right)^{3/2} + \left(\frac{z}{z_p}\right)^2 \right) \right]} \right]^{-1} - 1 \right\} \quad \text{for } 0 \le z \le z_t,$$

$$T'(r,z) = 0 \qquad\qquad\qquad\qquad\qquad\qquad\qquad\qquad\qquad\qquad \text{for } z_t < z. \tag{158}$$

Due to the small specific humidity value in the upper atmosphere (10^{-11} kg/kg for $z > z_t$) the virtual temperature equals the temperature to a very good approximation in this region. The formulation presented here is equivalent to the one presented in [3].

If the density of the moist air needs to be initialized its formulation is based on the ideal gas law

$$\rho(r,z) = \frac{p(r,z)}{R_d T_v(r,z)} \tag{159}$$

which utilizes the moist pressure (149) and virtual temperature (154). The surface elevation z_s and thereby the surface geopotential $\Phi_s = gz_s$ are set to zero.

Finally, the tangential velocity field $v_T(r,z)$ of the axisymmetric vortex is defined by utilizing the gradient-wind balance, which depends on the pressure (149) and the virtual temperature (155). The tangential velocity is given by

$$v_T(r,z) = -\frac{f_c r}{2} + \sqrt{\frac{f_c^2 r^2}{4} + \frac{R_d T_v(r,z)\, r}{p(r,z)} \frac{\partial p(r,z)}{\partial r}}, \tag{160}$$

where $f_c = 2\Omega \sin(\varphi_c)$ is the Coriolis parameter at the constant latitude φ_c. Substituting $T_v(r,z)$ and $p(r,z)$ into (160) gives

$$v_T(r,z) = -\frac{f_c r}{2} + \sqrt{\frac{f_c^2 r^2}{4} - \frac{\frac{3}{2}\left(\frac{r}{r_p}\right)^{3/2}(T_{v0} - \Gamma z)R_d}{1 + \frac{2R_d(T_{v0}-\Gamma z)z}{gz_p^2} - \frac{p_b}{\Delta p}\exp\left(\left(\frac{r}{r_p}\right)^{3/2} + \left(\frac{z}{z_p}\right)^2\right)}} \quad \text{for } 0 \le z \le z_t,$$

$$v_T(r,z) = 0 \qquad\qquad\qquad\qquad\qquad\qquad\qquad\qquad\qquad\qquad \text{for } z_t < z. \tag{161}$$

The last step is to split the tangential velocity (161) into its zonal and meridional wind components $u(\lambda, \varphi, z)$ and $v(\lambda, \varphi, z)$. Similar to [30] these are computed using the following expressions,

$$d_1 = \sin\varphi_c \cos\varphi - \cos\varphi_c \sin\varphi \cos(\lambda - \lambda_c) \tag{162}$$

$$d_2 = \cos\varphi_c \sin(\lambda - \lambda_c) \tag{163}$$

$$d = \max\left(\epsilon, \sqrt{d_1^2 + d_2^2}\right), \tag{164}$$

which are utilized in the projections

$$u(\lambda, \varphi, z) \quad = \quad \frac{v_T(\lambda, \varphi, z)\, d_1}{d} \tag{165}$$

$$v(\lambda, \varphi, z) \quad = \quad \frac{v_T(\lambda, \varphi, z)\, d_2}{d}\, . \tag{166}$$

A small $\epsilon = 10^{-25}$ value avoids divisions by zero. The vertical velocity is set to zero.

Test 5-1: Coupling to the "Simple-Physics" Physical Parameterizations

Without external physical forcing, the vortex initialized by the procedure above will simply dissipate with time. Test 5-1 makes use of very simplified physical parameterizations which provide essential forcing mechanisms relevant to tropical cyclone intensification. In particular, this test requires parameterizations of large-scale condensation (Appendix C), idealized fluxes from a ocean surface (Appendix D) and a representation of the planetary boundary layer (Appendix E). The design of the simple-physics suite is discussed in detail in [3]. Section 0.6 provides practical recommendations on the provided template routine for the "simple-physics" package.

An additional design choice needs to be made concerning the physics-dynamics coupling strategy. If no prior constraint exists, we recommend coupling the simple-physics suite to the dynamical core with a time-split coupling strategy [4]. This means that the dynamical core already updates the model state before the physical parameterizations are called and vice versa. However, a process-split coupling strategy (both the dynamical core and the physics package work with the identical state variables before the state is advanced for one time step) is also acceptable if required by the GCM design. A hybrid between the two approaches is also possible. The design choice needs to be documented.

As before in tests 4-1 and 4-2, after physical forcings are computed and moisture is removed from the system care needs to be taken to ensure that the model conserves the total dry air mass or its analog, the global average of the dry surface pressure. This is especially true if the moist surface pressure is predicted in the dynamical core. If needed the 'dry air adjustment' should take place in either the dynamical core or after the large-scale condensation was applied as a 'physics' package. This depends on the design of the model. Most often, GCMs already provide a mechanism to ensure that the total dry air mass is conserved, such as global mass fixers or explicit dry air adjustment routines as discussed in e.g. [24]. If not, such a mechanism needs to be supplied and invoked after each 'physics' time step.

Grid spacings, simulation time, output and diagnostics

We suggest running this test until day 10, which corresponds to 864000 seconds with output written at 6-hourly time intervals (every 21600 seconds). The output should include the initial state. Three grid resolutions are suggested. The first experiment should be run at roughly $1°$ at the equator (110 km equatorial grid spacing) with 30 vertical levels arranged in approximate correspondence with Appendix F.1. The second experiment doubles the horizontal resolution and sets the horizontal grid spacing to $\approx 0.5°$ while keeping the L30 level configuration. The third experiment sets the resolution to $\approx 0.25°$ with the identical L30 levels.

If height-based coordinates are used we recommend a model top of about 44 km. The lowermost full model level should lie around 60-70 m above the ground to mimic the position of the lowermost level in the pressure-based level distribution (Table XVIII) most closely. Since the position of the lowest model level enters the computation of the simple-physics forcings, there might be sensitivities to the level placement. Appendix F.2 makes suggestions for the placement of the 30 model levels in height-based models.

The output file should contain the instantaneous model-level snapshots of q, u, v, w or ω, T, p_s, P_{ls} and p in case the pressure cannot be reconstructed via the surface pressure. In addition, we ask for 2D fields at the 850 hPa pressure level if available as output quantities. They are u, v, T, w or ω at the interpolated 850 hPa level. Surface pressure and the 100 m horizontal wind speed ($\sqrt{u^2 + v^2}$) should be plotted at days 3, 5, 7 and 10. The latter necessitates a vertical interpolation to the 100 m level. In addition, we recommend plotting the longitude-height cross sections of the horizontal wind speed through the center latitude of the vortex at days 3, 5, 7 and 10. NCL scripts will be provided.

Test 5-2: Using the Model's Full-Physics Aqua-Planet Mode with a constant SST of 29 C$^\circ$

The second test variant 5-2 is optional, and as mentioned above, might be considered if the GCM is configurable as an aqua-planet model described by [28]. We propose using the analytic initial vortex in combination with the model's own complex physical parameterization package in aqua-planet mode. The only differences to the aqua-planet specification in [28] are that the SST field needs to be set to 29 C$^\circ$ and that the model is run in a short deterministic mode for only 10 days.

Some physical parameterization schemes might have difficulty handling the zero vertical wind shear that is present in the background environment. E.g. the gravity wave drag scheme or the computation of the Richardson number in the planetary boundary layer routine might be set up to divide by the discretely computed wind shear, which could lead to divisions by zero. Most often though, the physical parameterization packages provide thresholds to avoid such difficulties.

Grid spacings, simulation time, output and diagnostics

We suggest running this experiment at a single resolution with the grid spacing $\approx 0.5^\circ$ (55 km) in the horizontal directions and the L30 level setup as used before in test 5-1.

The output file should contain the instantaneous model-level snapshots of q, u, v, w or ω, T, p_s and p in case the pressure cannot be reconstructed via the surface pressure. In addition, we ask for 2D fields at the 850 hPa pressure level if available as output quantities. They are u, v, T, w or ω at the interpolated 850 hPa level. In addition, we suggest including the surface fluxes of latent and sensible heat, and momentum. The precipitation rate is likely split into the components 'total', 'large-scale' and 'convective' precipitation rate. We recommend adding all three to the output file if available.

Surface pressure and the 100 m horizontal wind speed ($\sqrt{u^2 + v^2}$) should be plotted at days 3, 5, 7 and 10. The latter necessitates a vertical interpolation to the 100 m level. In addition, we recommend plotting the longitude-height cross sections of the horizontal wind speed through the center latitude of the vortex at days 3, 5, 7 and 10. NCL scripts will be provided. We leave other plots to the modeler's discretion.

REFERENCES

1. NetCDF. NetCDF data format. World Wide Web 2012. URL: http://www.unidata.ucar.edu/software/netcdf/.

2. NetCDF-CF. NetCDF data format, Climate and Forecast (CF) Metadata Convention. World Wide Web 2012. URL: http://cf-pcmdi.llnl.gov/.

3. Reed KA, Jablonowski C. Idealized tropical cyclone simulations of intermediate complexity: a test case for AGCMs. *J. Adv. Model. Earth Syst.* 2012; **4**:M04 001, doi:10.1029/2011MS000099. Available online at http://www.agu.org/pubs/crossref/2012/2011MS000099.shtml.

4. Williamson D. Time-split versus process-split coupling of parameterizations and dynamical core. *Mon. Wea. Rev.* 2002; **130**:2779–2799.

5. Lin SJ. A "vertically Lagrangian" finite-volume dynamical core for global models. *Mon. Wea. Rev.* October 2004; **132**:2293–2307.

6. Nair RD, Lauritzen PH. A class of deformational flow test cases for linear transport problems on the sphere. *J. Comput. Phys.* 2010; **229**(23):8868–8887.

7. Phillips NA. A coordinate system having some special advantages for numerical forecasting. *J. Meteor.* 1957; **14**:184–185.

8. Simmons AJ, Burridge DM. An energy and angular-momentum conserving vertical finite-difference scheme and hybrid vertical coordinates. *Mon. Wea. Rev.* April 1981; **109**:758–766.

9. Schär C, Leuenberger D, Fuhrer O, Lüthi D, Girard C. A new terrain-following vertical coordinate formulation for atmospheric prediction models. *Mon. Wea. Rev.* 2002; **130**:2459–2480.

10. Gal-Chen T, Somerville RCJ. On the use of a coordinate transformation for the solution of the Navier-Stokes equations. *J. Comput. Phys.* Feb 1975; **17**:209–228, doi:10.1016/0021-9991(75)90037-6.

11. Lin SJ. A finite volume integration method for computing pressure gradient forces in general vertical coordinates. *Quart. J. Roy. Meteor. Soc.* 1997; **123**:1749–1762.

12. Schär C, Leuenberger D, Fuhrer O, Lüthi D, Girard C. A new terrain-following vertical coordinate formulation for atmospheric prediction models. *Mon. Weather Rev.* 2002; **130**:2459–2480, doi:10.1175/1520-0493(2002)130⟨2459: ANTFVC⟩2.0.CO;2.

13. Wedi NP, Smolarkiewicz PK. A framework for testing global non-hydrostatic models. *Quart. J. Roy. Meteor. Soc.* 2009; **135**:469–484.

14. Wedi NP, Yassad K, Untch A. The nonhydrostatic global IFS/ARPEGE: model formulation and testing. *Technical Report*, European Centre for Medium-Range Weather Forecasts 2009. Technical memorandum No. 594.

15. Skamarock WC, Weisman ML, Klemp JB. Three-dimensional evolution of simulated long-lived squall lines. *J. Atmos. Sci.* 1994; **51**(17):2563–2584.

16. Tomita H, Satoh M. A new dynamical framework of nonhydrostatic global model using the icosahedral grid. *Fluid Dyn. Res.* 2004; **34**:357–400.

17. Jablonowski C, Lauritzen PH, Nair RD, Taylor MA. Idealized test cases for the dynamical cores of Atmospheric General Circulation Models: A proposal for the NCAR ASP 2008 summer colloquium 2008. Available online at http://www-personal.umich.edu/~cjablono/cv.html#Publication.

18. Jablonowski C, Williamson DL. A baroclinic instabilitiy test case for atmospheric model dynamical cores. *Quart. J. Roy. Meteor. Soc.* 2006; **132**(621C):2943–2975.

19. Jablonowski C, Williamson DL. A baroclinic wave test case for dynamical cores of General Circulation Models: Model intercomparisons. *NCAR Tech. Note NCAR/TN-469+STR*, National Center for Atmospheric Research, Boulder, Colorado January 2006. 89 pp., available from http://www.ucar.edu/library/collections/technotes/technotes.jsp.

20. Lauritzen PH, Jablonowski C, Taylor MA, Nair RD. Rotated versions of the Jablonowski steady-state and baroclinic wave test cases: A dynamical core intercomparison. *J. Adv. Model. Earth Syst.* 2010; **2**:34. #15, available from URL:http://james.agu.org/index.php/JAMES/volume/view/2010.

21. Hoskins BJ, McIntyre ME, Robertson AW. On the use and significance of isentropic potential vorticity maps. *Quart. J. Roy. Meteor. Soc.* 1985; **111**:877–946.

22. Whitehead JP, Jablonowski C, Kent J, Rood RB. Potential vorticity: A diagnostic tool for general circulation models. *Quart. J. Roy. Meteorol. Soc.* 2012; In review.

23. Jablonowski C, Williamson DL. The pros and cons of diffusion, filters and fixers in atmospheric general circulation models. *Numerical Techniques for Global Atmospheric Models*, *Lecture Notes in Computational Science and Engineering*, vol. 80, Lauritzen PH, Jablonowski C, Taylor MA, Nair RD (eds.). Springer, 2011; 381–493.

24. Neale RB, Chen CC, Gettelman A, Lauritzen PH, Park S, Williamson DL, Conley AJ, Garcia R, Kinnison D, Lamarque JF, *et al.*. Description of the NCAR Community Atmosphere Model (CAM 5.0). *NCAR Technical Note NCAR/TN-486+STR*, National Center for Atmospheric Research, Boulder, Colorado June 2010. 268 pp., available from http://www.cesm.ucar.edu/models/cesm1.0/cam/.

25. Reed KA, Jablonowski C. An analytic vortex initialization technique for idealized tropical cyclone studies in AGCMs. *Mon. Wea. Rev.* 2011; **139**:689–710.
26. Reed KA, Jablonowski C. Impact of physical parameterizations on idealized tropical cyclones in the Community Atmosphere Model. *Geophys. Res. Lett.* 2011; **38**:L04 805, doi:10.1029/2010GL046297.
27. Reed KA, Jablonowski C. Assessing the Uncertainty of Tropical Cyclone Simulations in NCAR's Community Atmosphere Model. *J. Adv. Model. Earth Syst.* 2011; **3**:Art. 2011MS000 076, 16 pp.
28. Neale RB, Hoskins BJ. A standard test for AGCMs including their physical parameterizations: I: The proposal. *Atmos. Sci. Lett.* 2000; **1**:101–107.
29. Jordan CL. Mean soundings for the west indies area. *J. Atmos. Sci.* 1958; **15**:91–97, doi:10.1175/1520-0469(1958) 015.
30. Nair RD, Jablonowski C. Moving vortices on the sphere: A test case for horizontal advection problems. *Mon. Wea. Rev.* 2008; **136**:699–711.
31. Lauritzen PH, Thuburn J. Evaluating advection/transport schemes using interrelated tracers, scatter plots and numerical mixing diagnostics. *Quart. J. Roy. Meteor. Soc.* 2012; doi:10.1002/qj.986. In press.
32. Holton JR. *An introduction to dynamic meteorology*. Fourth edn., Academic Press, Inc., 2004. 535 pp.
33. Majewski D, Liermann D, Prohl P, Ritter B, Buchhold M, Hanisch T, Paul G, Wergen W, Baumgardner J. The operational global icosahedral-hexagonal gridpoint model GME: Description and high-resolution tests. *Mon. Wea. Rev.* February 2002; **130**:319–338.
34. Kasahara A. Various vertical coordinate systems used for numerical weather prediction. *Mon. Wea. Rev.* 1974; **102**:509–522.
35. Laprise R, Girard C. A spectral General Circulation Model using the piecewise-constant finite-element representation on a hybrid vertical coordinate system. *J. Climate* 1990; **3**:32–52.
36. NCO. NetCDF Operator (NCO). World Wide Web 2012. URL: http://nco.sourceforge.net/.

A. MIXING DIAGNOSTICS AND CORRELATION PLOTS

Mixing diagnostics and correlation plots are described by [31] as a method for determining the nature of numerical mixing errors which are introduced by an advection scheme. These errors are of particular importance in atmospheric chemistry modeling, since they represent important functional relationships between tracer species.

By defining nonlinearly correlated tracer fields (χ, ξ), one can determine how well the numerical scheme preserves these correlations over the duration of the simulation. For the deformational flow test (Test 1-1), we have specified a tracer field $q_1(\lambda, \varphi, z)$ and a field $q_2(\lambda, \varphi, z)$ which satisfies the initial relationship

$$q_2(\lambda, \varphi, z) = \psi(q_1(\lambda, \varphi, z)) \equiv 0.9 - 0.8q_1(\lambda, \varphi, z)^2. \qquad (167)$$

We define the *correlation plot* of q_1 and q_2 as the scatter plot obtained from plotting the mixing ratios $(q_1)_k = \chi_k$ against $(q_2)_k = \xi_k$ for each cell k. For the given distribution, one will initially obtain a curve similar to the one in Figure 1. As the simulation progresses, the nonlinear correlation between these tracers will be lost due to numerical errors and so the scatter plot will drift from its initial distribution. The final correlation plot reveals important information on how well the scheme preserves these correlations.

A measure of the types of numerical mixing which occur during the simulation can be quantitatively obtained using mixing diagnostics. We first define ΔA_k as the area of grid cell k and A as the total area of the domain. Further, we define d_k as the normalized shortest distance between the point (χ_k, ξ_k) and the initial $(\chi, \psi(\chi))$ correlation curve. For the initial distribution given in (167), d_k is defined as

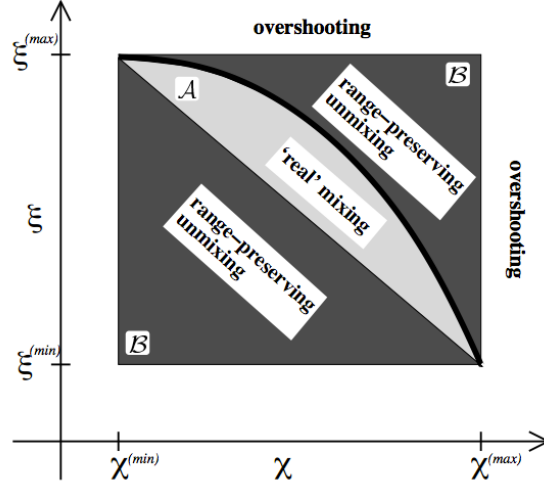$$d_k = L(\chi_k^{(\psi)}, \chi_k, \xi_k), \qquad (168)$$

Figure 1. Classifications of numerical mixing based on an original paired tracer distribution $((q_1)_k, (q_2)_k) = (\chi_k, \xi_k)$ (for all grid cells k) which initially follows the thick black curve. Mixing ratio pairs (χ_k, ξ_k) in region $\mathcal{A}$ have undergone numerical mixing which resembles "real" mixing. Mixing ratio pairs in region $\mathcal{B}$ have undergone numerical mixing which is inherently unphysical. Mixing ratio pairs outside of these regions have overshot the original distribution due to an insufficient shape-preserving filter. This figure is reproduced from [31].

where

$$C(\chi_k, \xi_k) = \frac{1}{12}\left[432\chi_k + 6\sqrt{750(2\xi_k - 1)^3 + 5184\chi_k^2}\right]^{1/3}, \qquad (169)$$

$$\chi_k^{(root)}(\chi_k, \xi_k) = C(\chi_k, \xi_k) + \frac{1}{C(\chi_k, \xi_k)}\left(\frac{5}{24} - \frac{5}{12}\xi_k\right), \qquad (170)$$

$$\chi_k^{(\psi)}(\chi_k, \xi_k) = \min\left[\max\left(\chi^{(min)}, \chi_k^{(root)}(\chi_k, \xi_k)\right), \chi^{(max)}\right], \qquad (171)$$

and

$$L(\chi, \chi_k, \xi_k) = \sqrt{\left(\frac{\chi_k - \chi}{\chi^{(max)} - \chi^{(min)}}\right)^2 + \left(\frac{\xi_k - \psi(\chi)}{\xi^{(max)} - \xi^{(min)}}\right)^2}. \qquad (172)$$

The constant mixing ratios which bound the initial profile are

$$\chi^{(min)} = 0, \qquad \chi^{(max)} = 1.0, \qquad \xi^{(min)} = 0.1, \qquad \xi^{(max)} = 0.9. \qquad (173)$$

We chose to constrict our analysis to the five equidistantly-spaced model levels at 4500, 4700, 4900, 5100 and 5300 m when calculating the mixing diagnostics and correlation plots. The mixing diagnostics work based on the classification of each element pair (χ_k, ξ_k) into region $\mathcal{A}$, $\mathcal{B}$ or $(\mathcal{A} \cup \mathcal{B})'$ (see Figure 1). For a mathematical description of these regions see [31].

The diagnostic for mixing that resembles 'real' mixing is defined as

$$\ell_r \equiv \frac{1}{A}\sum_k \begin{cases} d_k\Delta A_k, & \text{if } (\chi_k, \xi_k) \in \mathcal{A}, \\ 0 & \text{otherwise.} \end{cases} \qquad (174)$$

The diagnostic for mixing that is range-preserving is

$$\ell_u \equiv \frac{1}{A} \sum_k \begin{cases} d_k \Delta A_k, & \text{if } (\chi_k, \xi_k) \in \mathcal{B}, \\ 0 & \text{otherwise.} \end{cases} \tag{175}$$

Finally the diagnostic for overshooting is

$$\ell_o \equiv \frac{1}{A} \sum_k \begin{cases} d_k \Delta A_k, & \text{if } (\chi_k, \xi_k) \notin \mathcal{A} \cup \mathcal{B}, \\ 0 & \text{otherwise.} \end{cases} \tag{176}$$

In all cases the summation is taken over all cell k.

B. COORDINATE-FOLLOWING VELOCITIES

B.1. Cartesian decomposition of a terrain-following horizontal velocity field

In this Appendix we are interested in writing a purely horizontal velocity field $\mathbf{u}$ in both a coordinate-following and a Cartesian basis. This procedure will allow us to identify the source of the "perceived" vertical velocities which may be caused by an underlying terrain-following vertical coordinate system with sloping coordinate surfaces.

Observe that the basis vector following coordinate lines can be decomposed into a purely horizontal velocity and a purely vertical velocity in accordance with Figure 2. Mathematically, this takes the form

$$\mathbf{g}_s = \left(\frac{\partial z}{\partial x} \right)_s \mathbf{g}_z + \mathbf{g}_x, \tag{177}$$

where x is an arbitrary horizontal coordinate, z is the height coordinate, s denotes the quantity which is constant along coordinate lines and $\mathbf{g}_s$, $\mathbf{g}_z$ and $\mathbf{g}_x$ denote basis vectors along surfaces of constant s, z and x, respectively.
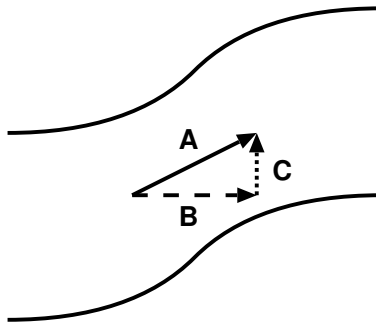

Figure 2. A depiction of horizontal velocities in the coordinate-following frame and constant height frame. Here (A) is the velocity field following coordinate lines, (B) is the purely horizontal component of the velocity field and (C) is the purely vertical component of the velocity field.

Given a velocity field in coordinate-following spherical coordinates (with basis vectors $\mathbf{g}_{\hat{\lambda}}$ and $\mathbf{g}_{\hat{\varphi}}$) we have

$$\mathbf{g}_{\hat{\lambda}} = \frac{1}{a\cos\varphi}\left(\frac{\partial z}{\partial \lambda}\right)_s \mathbf{g}_z + \mathbf{g}_\lambda, \tag{178}$$

$$\mathbf{g}_{\hat{\varphi}} = \frac{1}{a}\left(\frac{\partial z}{\partial \varphi}\right)_s \mathbf{g}_z + \mathbf{g}_\varphi. \tag{179}$$

We impose a purely horizontal velocity field $\mathbf{u} = u_\lambda \mathbf{g}_\lambda + u_\varphi \mathbf{g}_\varphi$ on the sphere (horizontal with respect to the "main sea level"). Consequently, in coordinate-following spherical coordinates we have

$$\mathbf{u} = u_\lambda\left(\mathbf{g}_{\hat{\lambda}} - \frac{1}{a\cos\varphi}\left(\frac{\partial z}{\partial \lambda}\right)_s \mathbf{g}_z\right) + u_\varphi\left(\mathbf{g}_{\hat{\varphi}} - \frac{1}{a}\left(\frac{\partial z}{\partial \varphi}\right)_s \mathbf{g}_z\right), \tag{180}$$

$$= u_\lambda \mathbf{g}_{\hat{\lambda}} + u_\varphi \mathbf{g}_{\hat{\varphi}} + \left[-\frac{u_\lambda}{a\cos\varphi}\left(\frac{\partial z}{\partial \lambda}\right)_s - \frac{u_\varphi}{a}\left(\frac{\partial z}{\partial \varphi}\right)_s\right]\mathbf{g}_z. \tag{181}$$

The basis vector for the last term in (181) is $\mathbf{g}_z$. Therefore, we observe that in coordinate-following form we have introduced the additional "perceived" vertical velocity

$$w = -\frac{u_\lambda}{a\cos\varphi}\left(\frac{\partial z}{\partial \lambda}\right)_s - \frac{u_\varphi}{a}\left(\frac{\partial z}{\partial \varphi}\right)_s, \tag{182}$$

which depends on how coordinate surfaces vary with height. Intuitively we should observe a downward vertical velocity when a horizontal velocity field encounters coordinate lines are sloped upward in the direction of the flow and an upward vertical velocity when coordinate lines are sloped downward. One can quickly verify that this is the case.

B.2. Perceived vertical velocity under hybrid pressure-based η coordinates

Calculation of the perceived vertical velocity under hybrid-η coordinates requires us to compute the horizontal derivatives of z with respect to λ and φ. Under hybrid-η coordinates we use the fact that $p = a(\eta)p_0 + b(\eta)p_s(\lambda, \varphi)$ [8]. Combining this with the pressure equation for isothermal conditions with temperature T_0 and the reference surface pressure p_0

$$p = p_0 \exp\left(\frac{-gz}{R_d T_0}\right), \tag{183}$$

we obtain

$$z = -\frac{R_d T_0}{g}\ln\left[a(\eta) + b(\eta)\frac{p_s(\lambda, \varphi)}{p_0}\right]. \tag{184}$$

Consequently,

$$\left(\frac{\partial z}{\partial \lambda}\right)_\eta = -\frac{R_d T_0}{g}\left[a(\eta) + b(\eta)\frac{p_s(\lambda, \varphi)}{p_0}\right]^{-1}\frac{b(\eta)}{p_0}\frac{\partial p_s}{\partial \lambda}, \tag{185}$$

$$\left(\frac{\partial z}{\partial \varphi}\right)_\eta = -\frac{R_d T_0}{g}\left[a(\eta) + b(\eta)\frac{p_s(\lambda, \varphi)}{p_0}\right]^{-1}\frac{b(\eta)}{p_0}\frac{\partial p_s}{\partial \varphi}. \tag{186}$$

Equivalently,

$$\left(\frac{\partial z}{\partial \lambda}\right)_\eta = -\frac{R_d T_0}{g p(\eta, \lambda, \varphi)} b(\eta) \frac{\partial p_s}{\partial \lambda}, \tag{187}$$

$$\left(\frac{\partial z}{\partial \varphi}\right)_\eta = -\frac{R_d T_0}{g p(\eta, \lambda, \varphi)} b(\eta) \frac{\partial p_s}{\partial \varphi}. \tag{188}$$

Since the surface profile is given in terms of height z, we need to use

$$\frac{\partial p_s}{\partial x} = -\frac{g p_0}{R_d T_0} \exp\left(\frac{-g z_s}{R_d T_0}\right) \frac{\partial z_s}{\partial x}, \tag{189}$$

where $x \in \{\lambda, \varphi\}$. Since pressure is constant with time, we also have that pressure velocity is related to vertical velocity via

$$\omega = -\rho g w. \tag{190}$$

In practice the following steps can be used to apply the perceived vertical velocity under a hybrid-η vertical coordinate:

1. Compute the surface height derivatives from (60)-(62).
2. Compute the surface pressure derivatives from (189).
3. For each coordinate line (vertical edge) compute (187)-(188).
4. Compute the perceived vertical velocity w from (54).
5. Compute the perceived pressure velocity ω from (190).

C. LARGE-SCALE CONDENSATION

The forcing by large-scale condensation is described in [3] which is partly reproduced here. The parameterization of the large-scale condensation leads to the forcing mechanisms

$$\frac{\partial T}{\partial t} = \frac{L}{c_p} C \tag{191}$$

$$\frac{\partial q}{\partial t} = -C, \tag{192}$$

where L is the latent heat of vaporization at $0\,°C$ ($= 2.5 \times 10^6$ J kg^{-1}) and c_p is the specific heat of dry air ($= 1004.5$ J kg^{-1} K^{-1}). The condensation rate C is the rate at which the saturation specific humidity q_{sat} changes with time t

$$C = \frac{\mathrm{d} q_{sat}}{\mathrm{d} t}. \tag{193}$$

If the air is found to be supersaturated (that is $q > q_{sat}(T)$) T and q need to be adjusted to their saturation values, which will lead to the updated values T^{n+1} and q^{n+1} at the future time level

$n+1$

$$T^{n+1} = T + \Delta T \tag{194}$$

$$q^{n+1} = q + \Delta q. \tag{195}$$

The time index of the T and q values on the right hand side (RHS) of these equations depends upon the AGCM design which might enforce constraints on the suitable physics-dynamics coupling strategy. Two coupling strategies are common which are called process-split and time-split [4]. In models with process-split physics-dynamics coupling T and q represent either the values at the current time level (n) for two-time-level schemes or the values at the previous time level ($n-1$) for three-time-level schemes, like e.g. the leapfrog method used in CAM 5 EUL [24]. In time-split models, the values of T and q are already partially updated by the time tendencies of the dynamical core before physical forcings are invoked. We leave the specific choice of the physics-dynamics coupling to the modeling group. However, in case no prior constraints exist we recommend the time-split approach.

The correction factors ΔT and Δq are given by

$$\Delta T = -\frac{L}{c_p}\Delta q \tag{196}$$

$$\Delta q = q_{sat}(T^{n+1}) - q. \tag{197}$$

Here $q_{sat}(T^{n+1})$ is approximated by a first-order Taylor series

$$q_{sat}(T^{n+1}) \cong q_{sat}(T) + \frac{\mathrm{d}q_{sat}(T)}{\mathrm{d}T}\Delta T. \tag{198}$$

The forms of T^{n+1} and q^{n+1} are then represented by

$$T^{n+1} = T + \frac{L}{c_p}\left(\frac{q - q_{sat}(T)}{1 + \frac{L}{c_p}\frac{\mathrm{d}q_{sat}(T)}{\mathrm{d}T}}\right) \tag{199}$$

$$q^{n+1} = q - \frac{q - q_{sat}(T)}{1 + \frac{L}{c_p}\frac{\mathrm{d}q_{sat}(T)}{\mathrm{d}T}}. \tag{200}$$

This leads to the expression of the condensation rate for models with two-time-level schemes

$$C = \frac{1}{\Delta t}\left(\frac{q - q_{sat}(T)}{1 + \frac{L}{c_p}\frac{\mathrm{d}q_{sat}(T)}{\mathrm{d}T}}\right) \tag{201}$$

where Δt symbolizes the discrete physics time step. Note that the physics time step may be different from the dynamics or tracer advection time steps as it is the case in the model CAM 5 FV [24]. In models with a three-time-level leapfrog scheme, Δt needs to be replaced with $2\Delta t$.

We now need to define the derivative of the saturated specific humidity with respect to temperature. From [32] we approximate this to be

$$\frac{\mathrm{d}q_{sat}}{\mathrm{d}T} \approx \frac{\varepsilon}{p}\frac{\mathrm{d}e_s}{\mathrm{d}T} = \frac{Lq_{sat}}{R_\nu T^2} \tag{202}$$

where p is pressure, e_s is the saturation vapor pressure, R_ν is the gas constant for water vapor ($= 461.5$ J kg^{-1} K^{-1}) and ε is the ratio of the gas constant for dry air R_d to that for water vapor ($\varepsilon = R_d/R_\nu \approx 0.622$). We approximate the saturation specific humidity by utilizing the Clausius-Clapeyron equation for the saturation vapor pressure in the form

$$q_{sat}(T) \approx \varepsilon \frac{e_s}{p} \approx \frac{\varepsilon}{p} e_0^* e^{-(L/R_\nu)[(1/T)-(1/T_0)]} \tag{203}$$

where e_0^* ($= 6.1078$ hPa) is the saturation vapor pressure at $T_0 = 273.16$ K. As mentioned before, it is assumed that all of the condensed water vapor immediately falls out as precipitation without re-evaporation. The large-scale precipitation rate P_{ls} is therefore given as

$$P_{ls} = \frac{1}{\rho_{water}} \int_0^\infty C\rho \mathrm{d}z = \frac{1}{\rho_{water} g} \int_0^{p_s} C \mathrm{d}p \tag{204}$$

where the hydrostatic relation is used to eliminate the air density ρ, $\rho_{water} = 1000$ kg m^{-3} is the density of water, and p_s is the surface pressure. The units of P_{ls} are meters of water per second (m_{H_2O} s^{-1}). The quantity P_{ls} can be used as a diagnostic quantity.

D. SURFACE FLUXES ON AN AQUA-PLANET WITH PRESCRIBED SEA SURFACE TEMPERATURES

The forcing by surface fluxes from an idealized ocean is described in [3] and is partly reproduced here. We use a model configuration which corresponds to an aqua-planet setup with prescribed sea surface temperatures (SSTs). This forcing by the surface fluxes is applied to the state variables in the lowermost model level using a partially implicit formulation to avoid numerical instabilities. Throughout this section we use the subscript a to denote variables defined on the lowermost model level.

The surface fluxes depend on the *drag coefficient C_d*, defined as

$$\begin{aligned} C_d &= C_{d0} + C_{d1}|\vec{v}_a| \quad \text{for } |\vec{v}_a| < 20 \text{ m s}^{-1} \\ C_d &= 0.002 \qquad\qquad \text{for } |\vec{v}_a| \geq 20 \text{ m s}^{-1}, \end{aligned} \tag{205}$$

where C_{d0} and C_{d1} are 7.0×10^{-4} (unitless) and 6.5×10^{-5} s m^{-1}, respectively, and $|\vec{v}_a|$ is the magnitude of the horizontal wind at the lowermost model level. In terms of the zonal wind u_a and meridional wind v_a, it is defined as

$$|\vec{v}_a| = \sqrt{u_a^2 + v_a^2}. \tag{206}$$

For both evaporation and sensible heat the bulk coefficient is set to

$$C_E = C_H = 0.0011. \tag{207}$$

The formulation of the surface fluxes makes use of the height of the lowermost full model level z_a (in m). For pressure-based models, z_a can be expressed with the help of the hydrostatic equation

in terms of pressure

$$z_a = \frac{R_d T_{\nu,a}}{g} \frac{(\ln p_s - \ln p_-)}{2}, \tag{208}$$

where $T_{\nu,a} = T_a(1 + 0.608 q_a)$ is the virtual temperature at the lowermost full model level and p_- is the edge pressure at the model level interface between the lowest and second lowest full model levels. This notation and all following equations assume that the temperature, horizontal wind components and the specific humidity in the physical parameterization package are co-located in both the vertical and horizontal directions, as is the case for the Lorenz grid. The height of the lowest full model level should ideally lie between 60-70m above the ground to make the results comparable to those in the literature.

As described in [3], the surface fluxes can be written as

$$\frac{\partial \vec{v}_a}{\partial t} = -\frac{C_d |\vec{v}_a| \vec{v}_a}{z_a} \tag{209}$$

$$\frac{\partial T_a}{\partial t} = \frac{C_H |\vec{v}_a| (T_s - T_a)}{z_a} \tag{210}$$

$$\frac{\partial q_a}{\partial t} = \frac{C_E |\vec{v}_a| (q_{sat,s} - q_a)}{z_a}. \tag{211}$$

We note that the wind at the surface is taken to be zero and therefore does not appear explicitly in (209). In these equations T_s denotes the prescribed sea surface temperature (SST) and $q_{sat,s}$ is the saturation specific humidity defined by (203) and computed with the SST value.

The final form of the surface fluxes will vary for models with other choices of prognostic variables. For example, if potential temperature Θ_a is used (210) takes the form

$$\frac{\partial \Theta_a}{\partial t} = \frac{C_H |\vec{v}_a| (T_s - T_a)}{z_a} \left(\frac{p_0}{p_a} \right)^{R_d/c_p} \tag{212}$$

where $p_0 = 1000$ hPa is a reference pressure. This conversion uses the assumption that the pressure is time-invariant when individual physics parameterizations are applied. For other choices of prognostic variables like $(\rho u)_a$, $(\rho v)_a$, $(\rho \Theta)_a$ and $(\rho q)_a$ the right-hand-side of (209), (212) and (211) would need to be multiplied by the density of the air ρ.

In order to ensure numerical stability, each of the aforementioned surface fluxes are applied via a semi-implicit operator. We demonstrate this procedure on the temperature evolution equation (210). First, the time derivative is expanded using a backward Euler operator,

$$\frac{T_a^{n+1} - T_a^n}{\Delta t} = \frac{C_H |\vec{v}_a^n| (T_s - T_a^{n+1})}{z_a}. \tag{213}$$

The superscripts n and $n+1$ represent the current time step (after the update from the large-scale condensation scheme) and the future time step, respectively. Note, that on the right-hand-side of the equation the only variable taken implicitly is T_a. $|\vec{v}_a^n|$ is evaluated at the current time step and C_H is constant. The equation can now be solved for T_a^{n+1}

$$T_a^{n+1} = \frac{T_a^n + C_H |\vec{v}_a^n| T_s \frac{\Delta t}{z_a}}{1 + C_H |\vec{v}_a^n| \frac{\Delta t}{z_a}}. \tag{214}$$

Similar equations for $\vec{v}_a$ and q_a can be calculated

$$\vec{v}_a^{n+1} \quad = \quad \frac{\vec{v}_a^n}{1 + C_d^n|\vec{v}_a^n|\frac{\Delta t}{z_a}} \tag{215}$$

$$q_a^{n+1} \quad = \quad \frac{q_a^n + C_E|\vec{v}_a^n|q_{sat,s}^n\frac{\Delta t}{z_a}}{1 + C_E|\vec{v}_a^n|\frac{\Delta t}{z_a}}, \tag{216}$$

with the time-level dependent coefficient C_d^n. Notice that the second term in the numerator of (215) is absent in the case of the zonal and merdional wind. This is because the wind is set to zero at the surface.

E. SIMPLIFIED MIXING IN THE PLANETARY BOUNDARY LAYER

The forcing by the planetary boundary layer is described in [3] and is partly reproduced here. To parameterize the surface fluxes that impact the zonal velocity u, the meridional velocity v and moisture q we start with the time rate of change equations

$$\frac{\partial u}{\partial t} \quad = \quad -\frac{1}{\rho}\frac{\partial \rho \,\overline{w'u'}}{\partial z} \tag{217}$$

$$\frac{\partial v}{\partial t} \quad = \quad -\frac{1}{\rho}\frac{\partial \rho \,\overline{w'v'}}{\partial z} \tag{218}$$

$$\frac{\partial q}{\partial t} \quad = \quad -\frac{1}{\rho}\frac{\partial \rho \,\overline{w'q'}}{\partial z}. \tag{219}$$

Potential temperature, as opposed to temperature, is used in the boundary layer parameterization because the vertical profile of the potential temperature is a suitable indicator of static stability. This adds the time rate of change equation

$$\frac{\partial \Theta}{\partial t} \quad = \quad -\frac{1}{\rho}\frac{\partial \rho \,\overline{w'\Theta'}}{\partial z}. \tag{220}$$

Here u', v', w', Θ' and q' symbolize the deviations of the zonal velocity, meridional velocity, vertical velocity, potential temperature and specific humidity from their averages, respectively. The average is indicated by an overbar. The eddy turbulence surface momentum fluxes on the RHS of (217)-(219) are approximated by the bulk aerodynamic formulae in kinematic units

$$\overline{w'u'} \quad = \quad -C_d|\vec{v}|u \tag{221}$$

$$\overline{w'v'} \quad = \quad -C_d|\vec{v}|v, \tag{222}$$

where C_d is again defined by (205). Evaporation occurs at the surface and is similarly described by the kinematic eddy flux of water vapor. It is expressed via the bulk formula for latent heat

$$\overline{w'q'} = C_E|\vec{v}|(q_{sat} - q), \tag{223}$$

where C_E is defined by (207), q_{sat} is again defined by (203) and q is the specific humidity. The kinematic eddy sensible heat flux at the surface is defined by the formula

$$\overline{w'\Theta'} = C_H |\vec{v}|(\Theta_s - \Theta), \tag{224}$$

where Θ_s is the potential temperature at the surface. Assuming pressure is held constant (which is a common assumption in physical parameterizations), the potential temperature time tendency can be converted back to a temperature tendency of the following form

$$\frac{\partial T}{\partial t} = -\frac{1}{\rho}\left(\frac{p}{p_0}\right)^{\kappa} \frac{\partial \rho \, \overline{w'\Theta'}}{\partial z}. \tag{225}$$

with the reference pressure $p_0 = 1000$ hPa.

We suggest implementing the boundary layer scheme with an implicit temporal discretization to avoid numerical instabilities. The details of this discretization are somewhat complicated, and so we refer to implementation details in Appendix D of [3]. In addition, we supply the DCMIP modeling groups with the complete "simple-physics" package as used in the model CAM which can serve as a template routine.

F. INFORMATION ON THE PLACEMENT OF THE VERTICAL LEVELS

F.1. Hybrid Coefficients for the L30 Setup with a Stretched Vertical Grid

Test cases 4-1-x, 4-2, 4-3 and 5 utilize a stretched vertical grid that provides 9 model levels below 700 hPa and is gradually stretched in the vertical direction. We suggest using a stretched vertical grid that is based on the hybrid η coordinate used in NCAR's Community Atmosphere Model (CAM) [24]. This hybrid orography-following η-coordinate [8] comprises a pure pressure coordinate and a σ-component with $\sigma = p/p_s$. The pressure p at a vertical level η is given by

$$p(\lambda, \varphi, \eta, t) = a(\eta)\, p_0 + b(\eta)\, p_s(\lambda, \varphi, t) \tag{226}$$

where the coefficients $a(\eta)$ and $b(\eta)$ are height-dependent and provided in tabular form (e.g. see Table XVIII for the suggested L30 configuration). Most commonly the reference pressure p_0 is set to 1000 hPa which is chosen here. If a different p_0 is generally implemented in a GCM (like 1013.25 hPa), it needs to be changed to $p_0 = 1000$ hPa. In case, the initial surface pressure p_s is set to the constant p_0, as it is the case for the baroclinic wave experiments (tests 4-x), this leads to the simplified expression

$$p(\lambda, \varphi, \eta, t = 0) = (a(\eta) + b(\eta))\, p_0 = \eta\, p_0\,. \tag{227}$$

In the discrete representation, the vertical direction is subdivided into N_{lev} model levels which are bounded by $N_{lev} + 1$ interface levels (denoted by the half indices $k + \frac{1}{2}$ below). The index increases downwards. The pressure at the interfaces is then given by

$$p_{k+\frac{1}{2}} = a_{k+\frac{1}{2}}\, p_0 + b_{k+\frac{1}{2}}\, p_s \quad \equiv \quad \eta_{k+\frac{1}{2}}\, p_0(\text{ if } p_s = p_0) \tag{228}$$

with $\eta_{k+\frac{1}{2}} = a_{k+\frac{1}{2}} + b_{k+\frac{1}{2}}$ and $k = 0, 1, 2, \cdots N_{lev}$. The corresponding η_k values at the centers are determined via the average $\eta_k = \frac{1}{2}\left(\eta_{k+\frac{1}{2}} + \eta_{k-\frac{1}{2}}\right)$. For $p_s = p_0$ follows $p_k = \eta_k\, p_0$.

For the baroclinic wave tests and the tropical cyclone test case a 30 model level setup (L30) is chosen. The corresponding coefficients for the model interfaces $a_{k+\frac{1}{2}}$ and $b_{k+\frac{1}{2}}$ are listed in Table XVIII. Here it is important to note that some GCMs (for example [33]) employ the alternative notation $p_{k+\frac{1}{2}} = a_{k+\frac{1}{2}} + b_{k+\frac{1}{2}}\, p_s$ where the coefficients $a_{k+\frac{1}{2}}$ are given in Pa. If such a setup is encountered, the $a_{k+\frac{1}{2}}$ coefficients in Table XVIII need to be multiplied by p_0.

Table XVIII. Suggested vertical hybrid coefficients at 31 level interfaces for a 30-level (L30) setup. The coefficient $a_{i+\frac{1}{2}}$ represents the pure pressure component and $b_{i+\frac{1}{2}}$ denotes the σ-pressure component, with the subscript $i+\frac{1}{2}$ defining the model interface between two full model levels. $i = 0$ indicates the model top (interface level).

i	$a_{i+\frac{1}{2}}$	$b_{i+\frac{1}{2}}$
0	0.00225523952394724	0.
1	0.00503169186413288	0.
2	0.0101579474285245	0.
3	0.0185553170740604	0.
4	0.0306691229343414	0.
5	0.0458674766123295	0.
6	0.0633234828710556	0.
7	0.0807014182209969	0.
8	0.0949410423636436	0.
9	0.11169321089983	0.
10	0.131401270627975	0.
11	0.154586806893349	0.
12	0.181863352656364	0.
13	0.17459799349308	0.0393548272550106
14	0.166050657629967	0.0856537595391273
15	0.155995160341263	0.140122056007385
16	0.14416541159153	0.204201176762581
17	0.130248308181763	0.279586911201477
18	0.113875567913055	0.368274360895157
19	0.0946138575673103	0.47261056303978
20	0.0753444507718086	0.576988518238068
21	0.0576589405536652	0.672786951065063
22	0.0427346378564835	0.753628432750702
23	0.0316426791250706	0.813710987567902
24	0.0252212174236774	0.848494648933411
25	0.0191967375576496	0.881127893924713
26	0.0136180268600583	0.911346435546875
27	0.00853108894079924	0.938901245594025
28	0.00397881818935275	0.963559806346893
29	0.	0.985112190246582
30	0.	1.

F.2. Suggestion: L30 Level Distribution for Height-Based Models

It is not possible to exactly match the pressure-based L30 distribution shown in Table XVIII in a height-based model. However, here we provide some guidance how the height-based positions might be chosen via discrete fractional height positions or an analytical function. Modelers might also decide to choose their own level distributions. If this is the case we ask to pick 30 vertical levels with a model top at about 44 km to make the results comparable to others. A finer grid spacing should be placed near the surface (we recommend about 9 full levels below 700 hPa or $\approx$ 3000 m) and the grid might be stretched in the vertical direction. The lowest full model level should be placed at roughly $60 - 70$ m above the ground. This will be important for tests 4-3 and 5 since the applied "simple-physics" physical parameterization suite utilizes the height position of the lowest level.

If the model accepts discrete positions for the vertical levels we recommend the fractional height positions $(z - z_s)/(z_{\text{top}} - z_s)$ listed in Table XIX (right column). These fractional height positions are based on the positions of the pressure levels listed in Table XVIII which have been evaluated with the help of (124) and $z = \Phi/g$ in midlatitudes at $\varphi = \pi/4$. Note though that the order of the level index is reversed here in contrast to Table XVIII. The level index here counts the levels in a bottom-up approach whereas the pressure levels are listed in a top-down order. These fractional height positions are the preferred choice since they are the closest match to the pressure-based level distribution. We note that the height thicknesses of the model layers are given by the distances of the neighboring model interface levels which are listed in the middle column in Table XIX. These are in this example about 122 m, 146 m, 170 m, etc. and thereby stretched in the vertical direction.

However, if an analytic mapping function is required we suggest defining the positions of the model level interfaces via the following formula

$$z_n = z_{\text{top}} \frac{\sqrt{\phi(n/30)^2 + 1} - 1}{\sqrt{\phi + 1} - 1}, \tag{229}$$

where $\phi = 15$ is a flattening parameter and $n = \{0, 1, \ldots, 30\}$ is the model interface level (with the surface at $n = 0$ counting upwards). The function provides about 6-7 full levels below 3000 m (somewhat coarser than the pressure-level distribution) and tends to a uniform distribution of levels at upper levels. Using $z_{\text{top}} = 44$ km the thickness of the lowest model level between the surface and the next interface level is about 121.7 m. This places the lowermost full model level at about 60.9 m above the ground. Full model levels are always placed at the midpoint within each layer that is enclosed by the model interfaces.

F.3. Analytic Conversion from z to p Levels: Hybrid Coefficients

If level spacings are prescribed in z-coordinates as in tests 1-x, 2-x and 3, the z positions can be analytically translated into a pressure-based system. This is possible for initial conditions with rather simple temperature profiles. For isothermal conditions (within the vertical column) the vertical pressure profiles at the equator in tests 1-x, 2-1 and 2-2 are given by

$$p(z) = p_{eq} \exp\left(\frac{-gz}{R_d T_0}\right) \tag{230}$$

Table XIX. List of the altitudes of 31 model interface levels corresponding to the pressure levels prescribed in Appendix F.1 for the baroclinic instability test (Test 4-x), evaluated at $\varphi = 45°$. Note that interface level 0 is located at the surface which is different from the order in Table XVIII.

Interface Level	Altitude z in m	Fraction of total height $\frac{z-z_s}{z_{\text{top}}-z_s}$
0	$z_s = -50.154680940719$ (surface)	0.0
1	71.859873718723	0.00277313208750091
2	217.90597770021	0.00609245033059798
3	387.795626858368	0.00995368179374962
4	581.338418392235	0.0143524990250550
5	798.321401584915	0.0192840621062922
6	1038.53239060309	0.0247435485034241
7	1301.74464384305	0.0307258048606185
8	1775.35740259496	0.0414900185399455
9	2455.30741876575	0.0569438405286354
10	3336.07885762681	0.0769619075999979
11	4410.44563738228	0.101379986238196
12	5638.88811825063	0.129299878835001
13	6844.44565652005	0.156699645215562
14	8026.11085495629	0.183556389376999
15	9183.13736386181	0.209853148373368
16	10315.0862542580	0.235579946279765
17	11421.7993603143	0.260733188322264
18	12503.3408461626	0.285314332815515
19	13560.0640574031	0.309331410555718
20	14593.6667576978	0.332823008110694
21	15608.7432468909	0.355893544173383
22	16612.8461828224	0.378714674640579
23	17615.1909141375	0.401495844845236
24	19127.5085718247	0.435867618235090
25	21206.0521276769	0.483108505570857
26	23947.4486879917	0.545414636074529
27	27595.1338254421	0.628318784091769
28	32199.6060034172	0.732968672610087
29	37699.3990101633	0.857967304979478
30	$z_{\text{top}} = 43948.6707661513$ (model top)	1.0

which is based on (1) and (80). p_{eq} is a reference surface pressure at the equator and T_0 is the equatorial reference surface temperature. For temperature profiles with a constant lapse rate Γ (test 2-0-0) the pressure equation (67) is

$$p(z) = p_0 \left(1 - \frac{\Gamma}{T_0} z \right)^{\frac{g}{R_d \Gamma}} \tag{231}$$

where p_0 and T_0 stand for the surface pressure and surface temperature. For an atmosphere with a constant Brunt-Väisälä frequency N (Test 3-1) the pressure profile (94) at the equator is

$$p(z) = p_{eq} \left[\frac{G}{T_{eq}} \exp \left(-\frac{N^2 z}{g} \right) + 1 - \frac{G}{T_{eq}} \right]^{\frac{1}{\kappa}} \tag{232}$$

with the temperature parameter $G = g^2/(c_p N^2)$. As before, T_{eq} and p_{eq} symbolize the surface temperature and a reference surface pressure at the equator.

Using (230)-(232) the corresponding σ-levels according to [34] are

$$\sigma(z) = \frac{p(z) - p(z_{\text{top}})}{p_s - p(z_{\text{top}})} \tag{233}$$

where z_{top} denotes the height position of the model top. For hybrid vertical coordinate systems like

$$p(\eta) = A(\eta)\,p_0 + B(\eta)\,p_s \tag{234}$$

we recommend using the hybrid coefficients A and B

$$A(\eta) = \eta - B(\eta) \tag{235}$$

$$B(\eta) = \left(\frac{\eta - \eta_{\text{top}}}{1 - \eta_{\text{top}}}\right)^c \tag{236}$$

for the interface levels as suggested by [35]. For $p_s = p_0$, the definitions are $\eta = p(z)/p_s$ and $\eta_{\text{top}} = p(z_{\text{top}})/p_s$. We recommend these definitions of η and η_{top} as the chosen reference settings even if orography is present. The exponent c determines the smoothness of the transition between the σ-coordinate at low levels to the pressure coordinate near the upper boundary. We recommend choosing $c = 1$ which closely resembles the σ-system. Bigger coefficients $c > 1$ would allow for a more gradual transition and could potentially also be tested (e.g. $c = 2$).

This hybrid coordinate system is a variant of the one used by [8]. It guarantees the conditions $p(\eta = \eta_{\text{top}}) = p_{\text{top}}$ and $p(\eta = 1) = p_s$ at the top and bottom boundaries. The hybrid coefficients at the full model levels can then be computed via the linear average

$$A_k = \frac{1}{2}\big(A_{k+1/2} + A_{k-1/2}\big), \tag{237}$$

$$B_k = \frac{1}{2}\big(B_{k+1/2} + B_{k-1/2}\big) \tag{238}$$

where the index k denotes the discrete full model level which is surrounded by the two interface levels shown with half indices. The linear average guarantees that vertical differencing operations conserve energy. We note that some models, e.g. [33], use the alternative definition of (234)

$$p(\eta) = A(\eta) + B(\eta)\,p_s. \tag{239}$$

where the coefficients A have pressure units. Then (235) is represented by $A(\eta) = p_0[\eta - B(\eta)]$.

F.4. Iterative Conversion from p to z Levels: Tropical Cyclone Test Case (Test 5-x)

For GCMs that are built upon pressure-based vertical coordinates, such as the σ-coordinate [7] or the hybrid σ-pressure (η) coordinate [8], the equivalent height position for each pressure position along the model levels must be found to initialize the tropical cyclone experiment. The conversion is analytic for the background conditions of the idealized tropical vortex and in the upper atmosphere

above the tropopause height z_t, but requires straightforward fixed-point iterations in the vortex-covered region.

Given the background pressure profile (147) where p_0 is now generalized to be surface pressure p_s, the analytic conversion between pressure p and height z is given by

$$
\begin{aligned}
z &= \tfrac{T_{v0}}{\Gamma} \left(1 - \left(\tfrac{p}{p_s} \right)^{\frac{R_d \Gamma}{g}} \right) && \text{for } p_s \geq p \geq p_t, \\
z &= z_t + \tfrac{R_d T_{vt}}{g} \ln \left(\tfrac{p_t}{p} \right) && \text{for } p_t > p.
\end{aligned}
\tag{240}
$$

The pressure p denotes the pressure position of a GCM grid point, which can be computed via the analytically prescribed surface pressure (152) and the prescribed positions of the σ- or η-levels (see Table XVIII and the explanations in Appendix F.1). The z-value (240) that corresponds to the pressure position p can then be plugged into the equations for the specific humidity, temperature and horizontal velocities according to (156), (157), (165) and (166).

This analytic conversion is not accurate within the vortex due to its pressure perturbation and warm-core structure. Within the vortex the z-value at each model level needs to be computed iteratively via Newton's method

$$
z^{n+1} = z^n - \frac{F(\lambda, \varphi, z^n)}{\partial F / \partial z(\lambda, \varphi, z^n)}.
\tag{241}
$$

The superscript $n = 0, 1, 2, 3,...$ indicates the iteration count. The function F is determined by

$$
F(\lambda, \varphi, z) = p_{model} - p(\lambda, \varphi, z).
\tag{242}
$$

p_{model} is the pressure of the GCM grid point at a given longitude λ, latitude φ and model level, and $p(\lambda, \varphi, z)$ represents (149) evaluated with the great circle distance r. Therefore, $\partial F / \partial z$ is defined by

$$
\frac{\partial F(\lambda, \varphi, z)}{\partial z} = -\frac{\partial p(\lambda, \varphi, z)}{\partial z},
\tag{243}
$$

which can be computed analytically from (149). The analytic form of $\partial p / \partial z$ in terms of the great circle distance r is

$$
\begin{aligned}
\frac{\partial p(r, z)}{\partial z} =\ & \frac{2 \Delta p\, z}{z_p^2} \exp\left(-\left(\frac{r}{r_p} \right)^{3/2} \right) \exp\left(-\left(\frac{z}{z_p} \right)^2 \right) \left(\frac{T_{v0} - \Gamma z}{T_{v0}} \right)^{\frac{g}{R_d \Gamma}} \\
& -\frac{g}{R_d T_{v0}} \left[p_0 - \Delta p \exp\left(-\left(\frac{r}{r_p} \right)^{3/2} \right) \exp\left(-\left(\frac{z}{z_p} \right)^2 \right) \right] \left(\frac{T_{v0} - \Gamma z}{T_{v0}} \right)^{\frac{g}{R_d \Gamma} - 1}.
\end{aligned}
\tag{244}
$$

(241) is iterated until it converges to $|z^{n+1} - z^n| / |z^{n+1}| < \epsilon_n$ where ϵ_n is set to 2×10^{-13} (close to machine precision for double precision arithmetic). We recommend starting the iterations with the start value z^0 equal to z given in (240). Typically, the computations converge within the ϵ_n precision in under ten iterations. We apply the iterative technique below z_t (equivalent to $p_{model} > p_t$ where p_t is the pressure at the tropopause level) within a great circle distance of $r \leq 1000$ km from the vortex

center. It represents the distance at which the pressure (151) and temperature (158) perturbations become negligible.

F.5. Iterative Conversion from z to Pressure-Based η Levels (Test 4-x)

If models utilize a height-based vertical coordinate, the height position z needs to be translated into a pressure and thereby η position for the baroclinic wave experiments (Test 4-x). The initial conditions for the baroclinic instability are given in terms of pressure-based vertical coordinates with $\eta = p/p_0$ with $p_0 = 1000$ hPa. To find the corresponding η level for a given height z, we must implicitly solve a nonlinear equation relating η and z. Here we choose to use the iterative Newton fixed-point strategy as described before in Appendix F.4, which is now given by

$$\eta^{n+1} = \eta^n - \left[\frac{\partial F}{\partial \eta}(\lambda, \varphi, \eta^n)\right]^{-1} F(\lambda, \varphi, \eta^n), \tag{245}$$

where $n = 0, 1, 2, \ldots$ is the iteration count. The functions F and $\partial F/\partial \eta$ are determined by

$$F(\lambda, \varphi, \eta^n) = -gz + \Phi(\lambda, \varphi, \eta^n), \tag{246}$$

$$\frac{\partial F}{\partial \eta}(\lambda, \varphi, \eta^n) = -\frac{R_d}{\eta^n} T(\lambda, \varphi, \eta^n). \tag{247}$$

Here Φ and T are given by (124) and (120), respectively. The starting value of $\eta^0 = 10^{-7}$ is used for all Newton iterations, corresponding to a model top of about 100 km. If a higher model top is required, the value of η^0 needs to be decreased. Convergence is deemed to have occurred if $|\eta^{n+1} - \eta^n| \le 10^{-14}$, and usually takes about 10 iterations in most cases.

Once the $\eta(\lambda, \varphi, z)$ position is determined via the iterative technique at the grid point location (λ, φ, z) the temperature can be evaluated according to (120). The pressure p, density ρ and potential temperature Θ at position (λ, φ, z) are then given by

$$p(\lambda, \varphi, \eta) = \eta(\lambda, \varphi, z)p_0, \tag{248}$$

$$\rho(\lambda, \varphi, \eta) = \frac{p(\lambda, \varphi, \eta)}{R_d\, T(\lambda, \varphi, \eta)}, \tag{249}$$

$$\Theta(\lambda, \varphi, \eta) = T(\lambda, \varphi, \eta) \left(\frac{p_0}{p(\lambda, \varphi, \eta)}\right)^{\kappa}. \tag{250}$$

The formal initialization procedure for T, Θ and p is identical for both the dry and moist variants of the baroclinic wave. The main difference is that T, Θ and p are interpreted differently in the moist case since they then symbolize the virtual temperature T_v, virtual potential temperature Θ_v and the pressure of the moist air. This leads to the density equation for moist air

$$\rho(\lambda, \varphi, \eta) = \frac{p(\lambda, \varphi, \eta)}{R_d\, T_v(\lambda, \varphi, \eta)}. \tag{251}$$

F.6. Iterative Conversion from Θ to Pressure-Based η Levels (Test 4-x)

If isentropic levels are utilized the same fixed-point iteration strategy

$$\eta^{n+1} = \eta^n - \left[\frac{\partial F}{\partial \eta}(\lambda, \varphi, \eta^n) \right]^{-1} F(\lambda, \varphi, \eta^n), \tag{252}$$

can be employed where $n = 0, 1, 2, \ldots$ is the iteration count. The function F is defined by

$$F(\lambda, \varphi, \eta^n) = -\Theta + (\eta^n)^{-\kappa} T(\lambda, \varphi, \eta^n). \tag{253}$$

For $\partial F / \partial \eta$ it follows

$$\frac{\partial F}{\partial \eta}(\lambda, \varphi, \eta^n) = V(\eta^n) - \frac{3\,\pi\,u_0}{4\,R_d\,(\eta^n)^\kappa} \cos^{\frac{1}{2}} \eta_v^n \left\{ \frac{3\,\pi}{2} u_0 \eta^n A \sin^2 \eta_v^n \, \cos^{\frac{1}{2}} \eta_v^n - \tag{254} \right.$$

$$\left. \left(2A\,u_0 \cos^{\frac{3}{2}} \eta_v^n + B\,a\,\Omega \right) \left((1-\kappa) \sin \eta_v^n + \frac{\pi\,\eta^n}{4 \cos \eta_v^n} (2 - 3\sin^2 \eta_v^n) \right) \right\}$$

with $A = \left(-2\sin^6 \varphi \, (\cos^2 \varphi + \frac{1}{3}) + \frac{10}{63} \right)$, $B = \left(\frac{8}{5} \cos^3 \varphi \, (\sin^2 \varphi + \frac{2}{3}) - \frac{\pi}{4} \right)$ and $\eta_v^n = ((\eta^n - \eta_0)\,\pi/2)$. V symbolizes the vertical derivative of the horizontal-mean potential temperature $\langle \Theta(\eta) \rangle = \eta^{-\kappa} \langle T(\eta) \rangle$. It is given by

$$V(\eta^n) = T_0 \left(\frac{R_d\,\Gamma}{g} - \kappa \right) (\eta^n)^{\left(\frac{R_d\Gamma}{g} - \kappa - 1\right)} \qquad \text{(for } \eta_s \geq \eta^n \geq \eta_t) \tag{255}$$

$$V(\eta^n) = T_0 \left(\frac{R_d\,\Gamma}{g} - \kappa \right) (\eta^n)^{\left(\frac{R_d\Gamma}{g} - \kappa - 1\right)} - \frac{\Delta T}{(\eta^n)^{(\kappa+1)}} \left(\eta_t - \eta^n \right)^4 \left(\kappa\,\eta_t + \eta^n (5 - \kappa) \right)$$

$$\text{(for } \eta_t > \eta^n). \tag{256}$$

The starting value of $\eta^0 = 10^{-7}$ is used for all Newton iterations, corresponding to a model top of about 100 km. Convergence is deemed to have occurred if $|\eta^{n+1} - \eta^n| \leq 10^{-14}$, and usually takes about 10 iterations in most cases.

G. REQUIRED NETCDF OUTPUT FORMAT

As mentioned in section 0.4 a fundamental requirement for the exchange of scientific data is the ability to precisely describe the physical quantities being represented. We require data in the 'Network Common Data Form' (netCDF) [1] that adhere to the netCDF Climate and Forecast (CF) metadata convention (if possible to version 1.6 from Dec. 2011 [2]). NetCDF files should have the file name extension ".nc". In particular, netCDF metadata need to be present. If models cannot adhere to the CF standards, we will work with these modeling groups before the DCMIP workshop and evaluate the application of 'NCO' (netCDF operator [36]) tools to help make the output netCDF-CF compliant after the model execution.

G.1. Global attributes

We ask for netCDF "global attributes" that make the output files self-describing and searchable by cyberinfrastructure tools. We ask for the inclusion of the global attributes

- model
- test_case
- horizontal_resolution
- levels
- grid
- native_grid
- equation
- time_frequency
- description

The entries "model, test_case, horizontal_resolution, levels, grid, native_grid, equation" need to follow the file naming convention outlined in Tables IV and V. The "native_grid" attribute indicates the computational base grid that was used for the computations. An example is "cubed" for a cubed-sphere model. The models will then be searchable on the DCMIP webpage according to their computational meshes. The "time_frequency" attribute indicates the output frequency in seconds (s), hours (hr) or days (day), and needs be specified as e.g.

```
time_frequency = "1hr"
time_frequency = "6hr"
time_frequency = "day"
time_frequency = "100s"
```

for the 1-hourly, 6-hourly, daily, or 100-second output. The last "100s" entry refers to the unscaled time in the non-rotating small-planet experiments 21, 22 and 31. However, the rotating small-planet experiments (411, 412, 413) with the scaled "daily" output need to be specified with the scaled time_frequency attribute "day" to make the comparison to the unscaled experiment 410 simple. Other global attributes might also be present as shown in the example in section G.3.

G.2. Coordinates, variable names, metadata

The standard netCDF variable names (here denoted as "acronyms"), the requested physical 'units' attribute, a suggested 'long_name' and the standardized netCDF attribute 'standard_name' are listed in Tables XX and XXI. The entry for the netCDF attribute 'long_name' can be freely selected. However, if 'standard_name' is present its value must come from the standard netCDF CF-compliant entries listed below. The 'units' and 'long_name' attributes need to be part of the metadata of the netCDF output file. The 'standard_name' might be added as an option. Remember that the case is significant in netCDF names, and that all variable listed in Tables XX and XXI are written with upper case letters, all others like the dimensions or coordinates are written with lower case letters.

Table XX. List of symbols and corresponding netCDF attributes

Symbol	Acronym	'units'	Suggested 'long_name'	NetCDF 'standard_name'
λ	lon	degrees_east	longitude	longitude
φ	lat	degrees_north	latitude	latitude
p_s	PS	Pa	Surface pressure	surface_air_pressure
Φ_s	PHIS	m2/m2	Surface geopotential	surface_geopotential
u	U	m/s	Zonal wind	eastward_wind
v	V	m/s	Meridional wind	northward_wind
w	W	m/s	Vertical velocity	upward_air_velocity
ω	OMEGA	Pa/s	Vertical pressure velocity	lagrangian_tendency_of_air_pressure
p	P	Pa	Pressure	air_pressure
T	T	K	Temperature	air_temperature
q	Q	kg/kg	Specific humidity	specific_humidity
P_{ls}	PRECL	m/s	Large-scale precipitation rate	rainfall_rate
$q1$	Q1	kg/kg	Tracer mixing ratio q1	
$q2$	Q2	kg/kg	Tracer mixing ratio q2	
$q3$	Q3	kg/kg	Tracer mixing ratio q3	
$q4$	Q4	kg/kg	Tracer mixing ratio q4	
$q5$	Q5	kg/kg	Tracer mixing ratio q5	

Table XXI. Optional model variables: List of symbols and corresponding netCDF attributes

Symbol	Acronym	'units'	Suggested 'long_name'
SST	SST	K	Sea surface temperature
u_{850}	U850	m/s	Zonal wind at 850 hPa
v_{850}	V850	m/s	Meridional wind at 850 hPa
w_{500}	W500	m/s	Vertical velocity at 500 hPa
w_{850}	W850	m/s	Vertical velocity at 850 hPa
ω_{500}	OMEGA500	Pa/s	Vertical pressure velocity at 500 hPa
ω_{850}	OMEGA850	Pa/s	Vertical pressure velocity at 850 hPa
T_{500}	T500	K	Temperature at 500 hPa
T_{850}	T850	K	Temperature at 850 hPa
Z_{500}	Z500	m	Geopotential height at 500 hPa

G.3. Example: Selected entries of a netCDF file with latitude-longitude grid

An example of selected entries of an NCAR CAM-FV output file 'cam-fv.42.medium.L30' is shown below. The simulation was run at the medium resolution on a regular 181×360 latitude-longitude grid with grid spacing $1° \times 1°$ (including the poles) and 30 hybrid η-levels. Note that this output data set also lists the approximate (reference) pressure positions of the 30 full levels (lev) and 31 model interface levels (ilev) as well as the hybrid coefficients for the full (hyam, hybm) and half levels (hyai, hybi). The latter can be used in combination with the surface pressure to reconstruct the actual pressure at each grid point as explained in section F.1 (where hyam and hybm correspond to the coefficients A_k and B_k in (237) and (238)). The surface geopotential PHIS is provided as a 3D data set despite its time-independency. The time-dependent data sets PS, U, V, T and OMEGA (actual data not listed) contain 61 instantaneous 6-hourly snapshots between day 0 and 15. In addition, the NetCDF header also lists variables on the 850 hPa pressure surface.

Desirable output quantities are the time step 'mdt' used for the simulation (here it represents the physics time step 1800 s), and the 'gw' field. The latter contains the latitudinal area-based

("Gaussian") weights that need to be used for area-averages on the latitude-longitude grid. The sum of these 'gw' weights is 2.

Example of a NetCDF file (header and selected entries and data sets):

```
netcdf cam-fv.42.medium.L30.latlon.hydro.4th_order_div_damping.nc {
dimensions:
  lat = 181 ;
  lon = 360 ;
  lev = 30 ;
  ilev = 31 ;
  time = UNLIMITED ; // (61 currently)
variables:
  double P0 ;
    P0:long_name = "reference pressure" ;
    P0:units = "Pa" ;
  double lat(lat) ;
    lat:long_name = "latitude" ;
    lat:units = "degrees_north" ;
  double lon(lon) ;
    lon:long_name = "longitude" ;
    lon:units = "degrees_east" ;
  double lev(lev) ;
    lev:long_name = "hybrid level at midpoints(1000*(A+B))" ;
    lev:units = "level" ;
    lev:positive = "down" ;
    lev:standard_name = "atmosphere_hybrid_sigma_pressure_coordinate" ;
    lev:formula_terms = "a: hyam b: hybm p0: P0 ps: PS" ;
  double ilev(ilev) ;
    ilev:long_name = "hybrid level at interfaces (1000*(A+B))" ;
    ilev:units = "level" ;
    ilev:positive = "down" ;
    ilev:standard_name = "atmosphere_hybrid_sigma_pressure_coordinate" ;
    ilev:formula_terms = "a: hyai b: hybi p0: P0 ps: PS" ;
  double time(time) ;
    time:long_name = "time" ;
    time:units = "days since 2000-01-01 00:00:00" ;
    time:calendar = "noleap" ;
  double mdt ;
    mdt:long_name = "timestep" ;
    mdt:units = "s" ;
  double hyai(ilev) ;
    hyai:long_name = "hybrid A coefficient at layer interfaces" ;
  double hybi(ilev) ;
```

```
   hybi:long_name = "hybrid B coefficient at layer interfaces" ;
double hyam(lev) ;
   hyam:long_name = "hybrid A coefficient at layer midpoints" ;
double hybm(lev) ;
   hybm:long_name = "hybrid B coefficient at layer midpoints" ;
double gw(lat) ;
   gw:long_name = "gauss weights" ;
float PHIS(lat, lon) ;
   PHIS:units = m2/s2" ;
   PHIS:long_name = "Surface geopotential" ;
float PS(time, lat, lon) ;
   PS:units = "Pa" ;
   PS:long_name = "Surface pressure" ;
float PRECL(time, lat, lon) ;
   PRECL:units = "m/s" ;
   PRECL:long_name = "Large-scale precipitation rate" ;
float Q(time, lev, lat, lon) ;
   Q:units = "kg/kg" ;
   Q:long_name = "Specific humidity" ;
float T(time, lev, lat, lon) ;
   T:units = "K" ;
   T:long_name = "Temperature" ;
float U(time, lev, lat, lon) ;
   U:units = "m/s" ;
   U:long_name = "Zonal wind" ;
float V(time, lev, lat, lon) ;
   V:units = "m/s" ;
   V:long_name = "Meridional wind" ;
float OMEGA(time, lev, lat, lon) ;
   OMEGA:units = Pa/s" ;
   OMEGA:long_name = "Vertical pressure velocity" ;
float OMEGA850(time, lat, lon) ;
   OMEGA850:units = Pa/s" ;
   OMEGA850:long_name = "Vertical pressure velocity at 850 hPa" ;
float T850(time, lat, lon) ;
   T850:units = "K" ;
   T850:long_name = "Temperature at 850 hPa" ;
float U850(time, lat, lon) ;
   U850:units = "m/s" ;
   U850:long_name = "Zonal wind at 850 hPa" ;
float V850(time, lat, lon) ;
   V850:units = "m/s" ;
   V850:long_name = "Meridional wind at 850 hPa" ;
```

```
// global attributes:
                :Conventions = "CF-1.0" ;
                :model = "cam-fv" ;
                :test_case = "42" ;
                :horizontal_resolution= "medium" ;
                :levels = "L30" ;
                :grid = "latlon" ;
                :native_grid = "latlon" ;
                :equation = "hydro";
                :time_frequency = "6hr";
                :description = "4th-oder divergence damping" ;

data:

 P0 = 100000 ;

 lat = -90.0, -89.0, -88.0, -87.0, -86.0, -85.0, -84.0, -83.0,
      -82.0, -81.0, -80.0, -79.0, -78.0, -77.0, -76.0, -75.0,
      -74.0, -73.0, -72.0, -71.0, -70.0, -69.0, -68.0, -67.0,
      -66.0, -65.0, -64.0, -63.0, -62.0, -61.0, -60.0, -59.0,
      -58.0, -57.0, -56.0, -55.0, -54.0, -53.0, -52.0, -51.0,
      -50.0, -49.0, -48.0, -47.0, -46.0, -45.0, -44.0, -43.0,
      -42.0, -41.0, -40.0, -39.0, -38.0, -37.0, -36.0, -35.0,
      -34.0, -33.0, -32.0, -31.0, -30.0, -29.0, -28.0, -27.0,
      -26.0, -25.0, -24.0, -23.0, -22.0, -21.0, -20.0, -19.0,
      -18.0, -17.0, -16.0, -15.0, -14.0, -13.0, -12.0, -11.0,
      -10.0,  -9.0,  -8.0,  -7.0,  -6.0,  -5.0,  -4.0,  -3.0,
       -2.0,  -1.0,   0.0,   1.0,   2.0,   3.0,   4.0,   5.0,
        6.0,   7.0,   8.0,   9.0,  10.0,  11.0,  12.0,  13.0,
       14.0,  15.0,  16.0,  17.0,  18.0,  19.0,  20.0,  21.0,
       22.0,  23.0,  24.0,  25.0,  26.0,  27.0,  28.0,  29.0,
       30.0,  31.0,  32.0,  33.0,  34.0,  35.0,  36.0,  37.0,
       38.0,  39.0,  40.0,  41.0,  42.0,  43.0,  44.0,  45.0,
       46.0,  47.0,  48.0,  49.0,  50.0,  51.0,  52.0,  53.0,
       54.0,  55.0,  56.0,  57.0,  58.0,  59.0,  60.0,  61.0,
       62.0,  63.0,  64.0,  65.0,  66.0,  67.0,  68.0,  69.0,
       70.0,  71.0,  72.0,  73.0,  74.0,  75.0,  76.0,  77.0,
       78.0,  79.0,  80.0,  81.0,  82.0,  83.0,  84.0,  85.0,
       86.0,  87.0,  88.0,  89.0,  90.0;

 lon =   0.,    1.,    2.,    3.,    4.,    5.,    6.,    7.,    8.,    9.,
        10.,   11.,   12.,   13.,   14.,   15.,   16.,   17.,   18.,   19.,
```

```
 20.,  21.,  22.,  23.,  24.,  25.,  26.,  27.,  28.,  29.,
 30.,  31.,  32.,  33.,  34.,  35.,  36.,  37.,  38.,  39.,
 40.,  41.,  42.,  43.,  44.,  45.,  46.,  47.,  48.,  49.,
 50.,  51.,  52.,  53.,  54.,  55.,  56.,  57.,  58.,  59.,
 60.,  61.,  62.,  63.,  64.,  65.,  66.,  67.,  68.,  69.,
 70.,  71.,  72.,  73.,  74.,  75.,  76.,  77.,  78.,  79.,
 80.,  81.,  82.,  83.,  84.,  85.,  86.,  87.,  88.,  89.,
 90.,  91.,  92.,  93.,  94.,  95.,  96.,  97.,  98.,  99.,
100., 101., 102., 103., 104., 105., 106., 107., 108., 109.,
110., 111., 112., 113., 114., 115., 116., 117., 118., 119.,
120., 121., 122., 123., 124., 125., 126., 127., 128., 129.,
130., 131., 132., 133., 134., 135., 136., 137., 138., 139.,
140., 141., 142., 143., 144., 145., 146., 147., 148., 149.,
150., 151., 152., 153., 154., 155., 156., 157., 158., 159.,
160., 161., 162., 163., 164., 165., 166., 167., 168., 169.,
170., 171., 172., 173., 174., 175., 176., 177., 178., 179.,
180., 181., 182., 183., 184., 185., 186., 187., 188., 189.,
190., 191., 192., 193., 194., 195., 196., 197., 198., 199.,
200., 201., 202., 203., 204., 205., 206., 207., 208., 209.,
210., 211., 212., 213., 214., 215., 216., 217., 218., 219.,
220., 221., 222., 223., 224., 225., 226., 227., 228., 229.,
230., 231., 232., 233., 234., 235., 236., 237., 238., 239.,
240., 241., 242., 243., 244., 245., 246., 247., 248., 249.,
250., 251., 252., 253., 254., 255., 256., 257., 258., 259.,
260., 261., 262., 263., 264., 265., 266., 267., 268., 269.,
270., 271., 272., 273., 274., 275., 276., 277., 278., 279.,
280., 281., 282., 283., 284., 285., 286., 287., 288., 289.,
290., 291., 292., 293., 294., 295., 296., 297., 298., 299.,
300., 301., 302., 303., 304., 305., 306., 307., 308., 309.,
310., 311., 312., 313., 314., 315., 316., 317., 318., 319.,
320., 321., 322., 323., 324., 325., 326., 327., 328., 329.,
330., 331., 332., 333., 334., 335., 336., 337., 338., 339.,
340., 341., 342., 343., 344., 345., 346., 347., 348., 349.,
350., 351., 352., 353., 354., 355., 356., 357., 358., 359.;

gw = 0.3807694E-04, 0.3045981E-03, 0.6091034E-03, 0.9134232E-03,
     0.1217465E-02, 0.1521135E-02, 0.1824343E-02, 0.2126994E-02,
     0.2428998E-02, 0.2730262E-02, 0.3030694E-02, 0.3330203E-02,
     0.3628698E-02, 0.3926087E-02, 0.4222280E-02, 0.4517187E-02,
     0.4810718E-02, 0.5102784E-02, 0.5393296E-02, 0.5682164E-02,
     0.5969302E-02, 0.6254621E-02, 0.6538035E-02, 0.6819458E-02,
     0.7098804E-02, 0.7375987E-02, 0.7650923E-02, 0.7923528E-02,
     0.8193721E-02, 0.8461417E-02, 0.8726535E-02, 0.8988996E-02,
```

```
       0.9248719E-02, 0.9505624E-02, 0.9759633E-02, 0.1001067E-01,
       0.1025866E-01, 0.1050352E-01, 0.1074518E-01, 0.1098357E-01,
       0.1121862E-01, 0.1145024E-01, 0.1167838E-01, 0.1190297E-01,
       0.1212392E-01, 0.1234118E-01, 0.1255469E-01, 0.1276437E-01,
       0.1297016E-01, 0.1317200E-01, 0.1336983E-01, 0.1356358E-01,
       0.1375321E-01, 0.1393864E-01, 0.1411983E-01, 0.1429672E-01,
       0.1446925E-01, 0.1463738E-01, 0.1480104E-01, 0.1496020E-01,
       0.1511480E-01, 0.1526480E-01, 0.1541015E-01, 0.1555080E-01,
       0.1568672E-01, 0.1581785E-01, 0.1594417E-01, 0.1606564E-01,
       0.1618221E-01, 0.1629385E-01, 0.1640052E-01, 0.1650220E-01,
       0.1659886E-01, 0.1669045E-01, 0.1677697E-01, 0.1685837E-01,
       0.1693464E-01, 0.1700575E-01, 0.1707168E-01, 0.1713241E-01,
       0.1718792E-01, 0.1723819E-01, 0.1728322E-01, 0.1732298E-01,
       0.1735746E-01, 0.1738666E-01, 0.1741056E-01, 0.1742915E-01,
       0.1744244E-01, 0.1745041E-01, 0.1745307E-01, 0.1745041E-01,
       0.1744244E-01, 0.1742915E-01, 0.1741056E-01, 0.1738666E-01,
       0.1735746E-01, 0.1732298E-01, 0.1728322E-01, 0.1723819E-01,
       0.1718792E-01, 0.1713241E-01, 0.1707168E-01, 0.1700575E-01,
       0.1693464E-01, 0.1685837E-01, 0.1677697E-01, 0.1669045E-01,
       0.1659886E-01, 0.1650220E-01, 0.1640052E-01, 0.1629385E-01,
       0.1618221E-01, 0.1606564E-01, 0.1594417E-01, 0.1581785E-01,
       0.1568672E-01, 0.1555080E-01, 0.1541015E-01, 0.1526480E-01,
       0.1511480E-01, 0.1496020E-01, 0.1480104E-01, 0.1463738E-01,
       0.1446925E-01, 0.1429672E-01, 0.1411983E-01, 0.1393864E-01,
       0.1375321E-01, 0.1356358E-01, 0.1336983E-01, 0.1317200E-01,
       0.1297016E-01, 0.1276437E-01, 0.1255469E-01, 0.1234118E-01,
       0.1212392E-01, 0.1190297E-01, 0.1167838E-01, 0.1145024E-01,
       0.1121862E-01, 0.1098357E-01, 0.1074518E-01, 0.1050352E-01,
       0.1025866E-01, 0.1001067E-01, 0.9759633E-02, 0.9505624E-02,
       0.9248719E-02, 0.8988996E-02, 0.8726535E-02, 0.8461417E-02,
       0.8193721E-02, 0.7923528E-02, 0.7650923E-02, 0.7375987E-02,
       0.7098804E-02, 0.6819458E-02, 0.6538035E-02, 0.6254621E-02,
       0.5969302E-02, 0.5682164E-02, 0.5393296E-02, 0.5102784E-02,
       0.4810718E-02, 0.4517187E-02, 0.4222280E-02, 0.3926087E-02,
       0.3628698E-02, 0.3330203E-02, 0.3030694E-02, 0.2730262E-02,
       0.2428998E-02, 0.2126994E-02, 0.1824343E-02, 0.1521135E-02,
       0.1217465E-02, 0.9134232E-03, 0.6091034E-03, 0.3045981E-03,
       0.3807694E-04;

  lev = 3.64346569404006, 7.59481964632869, 14.3566322512925,
     24.6122200042009, 38.2682997733355, 54.5954797416925, 72.0124505460262,
     87.8212302923203, 103.317126631737, 121.547240763903, 142.994038760662,
     168.225079774857, 197.908086702227, 232.828618958592, 273.910816758871,
```

322.241902351379, 379.100903868675, 445.992574095726, 524.687174707651,
   609.778694808483, 691.389430314303, 763.404481112957, 820.858368650079,
   859.53476652503, 887.020248919726, 912.644546944648, 936.198398470879,
   957.485479535535, 976.325407391414, 992.556095123291 ;

ilev = 2.25523952394724, 5.03169186413288, 10.1579474285245,
   18.5553170740604, 30.6691229343414, 45.8674766123295, 63.3234828710556,
   80.7014182209969, 94.9410423636436, 111.69321089983, 131.401270627975,
   154.586806893349, 181.863352656364, 213.952820748091, 251.704417169094,
   296.117216348648, 348.366588354111, 409.83521938324, 482.149928808212,
   567.22442060709, 652.332969009877, 730.445891618728, 796.363070607185,
   845.353666692973, 873.715866357088, 900.324631482363, 924.964462406933,
   947.432334534824, 967.538624536246, 985.112190246582, 1000 ;

hyai = 0.00225523952394724, 0.00503169186413288, 0.0101579474285245,
   0.0185553170740604, 0.0306691229343414, 0.0458674766123295,
   0.0633234828710556, 0.0807014182209969, 0.0949410423636436,
   0.11169321089983, 0.131401270627975, 0.154586806893349,
   0.181863352656364, 0.17459799349308, 0.166050657629967,
   0.155995160341263, 0.14416541159153, 0.130248308181763,
   0.113875567913055, 0.0946138575673103, 0.0753444507718086,
   0.0576589405536652, 0.0427346378564835, 0.0316426791250706,
   0.0252212174236774, 0.0191967375576496, 0.0136180268600583,
   0.00853108894079924, 0.00397881818935275, 0, 0 ;

hybi = 0, 0, 0, 0, 0, 0, 0, 0, 0, 0, 0, 0, 0, 0.0393548272550106,
   0.0856537595391273, 0.140122056007385, 0.204201176762581,
   0.279586911201477, 0.368274360895157, 0.47261056303978,
   0.576988518238068, 0.672786951065063, 0.753628432750702,
   0.813710987567902, 0.848494648933411, 0.881127893924713,
   0.911346435546875, 0.938901245594025, 0.963559806346893,
   0.985112190246582, 1 ;

hyam = 0.00364346569404006, 0.00759481964632869, 0.0143566322512925,
   0.0246122200042009, 0.0382682997733355, 0.0545954797416925,
   0.0720124505460262, 0.0878212302923203, 0.103317126631737,
   0.121547240763903, 0.142994038760662, 0.168225079774857,
   0.178230673074722, 0.170324325561523, 0.161022908985615,
   0.150080285966396, 0.137206859886646, 0.122061938047409,
   0.104244712740183, 0.0849791541695595, 0.066501695662736,
   0.0501967892050743, 0.037188658490777, 0.028431948274374,
   0.0222089774906635, 0.016407382208854, 0.0110745579004288,
   0.00625495356507599, 0.00198940909467638, 0 ;

```
 hybm = 0, 0, 0, 0, 0, 0, 0, 0, 0, 0, 0, 0, 0.0196774136275053,
    0.062504293397069, 0.112887907773256, 0.172161616384983,
    0.241894043982029, 0.323930636048317, 0.420442461967468,
    0.524799540638924, 0.624887734651566, 0.713207691907883,
    0.783669710159302, 0.831102818250656, 0.864811271429062,
    0.896237164735794, 0.92512384057045, 0.951230525970459,
    0.974333998296738, 0.992556095123291 ;

 time = 0, 0.25, 0.5, 0.75, 1, 1.25, 1.5, 1.75, 2, 2.25,
    2.5, 2.75, 3, 3.25, 3.5, 3.75, 4, 4.25, 4.5, 4.75,
    5, 5.25, 5.5, 5.75, 6, 6.25, 6.5, 6.75, 7, 7.25,
    7.5, 7.75, 8, 8.25, 8.5, 8.75, 9, 9.25, 9.5, 9.75,
    10, 10.25, 10.5, 10.75, 11, 11.25, 11.5, 11.75, 12, 12.25,
    12.5, 12.75, 13, 13.25, 13.5, 13.75, 14, 14.25, 14.5, 14.75,
    15 ;

 mdt = 1800 ;

}
```

Note that the notation of the variables uses the NetCDF-specific order of the dimensions (time,lev,lat,lon). We ask for output data (like U, V, T, PS, etc.) with single precision (float) accuracy using 4 bytes per datum. This uses the storage space more economically than double-precision (double) data.

G.4. Dimensions & metadata & time stamp

The NetCDF file must contain information about the grid and time dimensions. For a regular latitude-longitude grid (either as the native computational grid or as the result of interpolations) the dimensions need to utilize the keywords (see also the in section G.3)

```
dimensions:
  lat = 181 ;
  lon = 360 ;
  lev = 30 ;
  ilev = 31 ;
  time = UNLIMITED ; // (61 currently)
```

where "lat" and "lon" denote the number of latitudes and longitudes, "lev" and "ilev" symbolize the number of full model levels and interface levels, and 'time' denotes the number of time snapshots. These keywords for the dimensions are also used to define the size of the coordinate arrays like

```
  double lat(lat) ;
    lat:long_name = "latitude" ;
    lat:units = "degrees_north" ;
```

```
double lon(lon) ;
  lon:long_name = "longitude" ;
  lon:units = "degrees_east" ;
```

and to define the dimensions of the model output variables like

```
float U(time, lev, lat, lon) ;
  U:units = "m/s" ;
  U:long_name = "Zonal wind" ;
```

As in the example above, the coordinates and model output variables need to be accompanied by metadata that describe, at a minimum, the "units" and "long_name" of the entry, except "units" are not necessary for non-dimensional quantities. The "standard_name" as listed in Table XX might also be included.

Idealized test cases are not associated with a particular date. However, a date must be chosen as a reference date, e.g.

```
double time(time) ;
  time:long_name = "time" ;
  time:units = "days since 2000-01-01 00:00:00" ;
  time:calendar = "none" ;
```

so that the data entries for the "time" variable can read

```
time = 0, 0.25, 0.5, 0.75, 1, 1.25, 1.5, 1.75, 2, 2.25,
   2.5, 2.75, 3, 3.25, 3.5, 3.75, 4, 4.25, 4.5, 4.75,
   5, 5.25, 5.5, 5.75, 6, 6.25, 6.5, 6.75, 7, 7.25,
   7.5, 7.75, 8, 8.25, 8.5, 8.75, 9, 9.25, 9.5, 9.75,
   10, 10.25, 10.5, 10.75, 11, 11.25, 11.5, 11.75, 12, 12.25,
   12.5, 12.75, 13, 13.25, 13.5, 13.75, 14, 14.25, 14.5, 14.75,
   15 ;
```

for 6-hourly snapshots. We recommend picking the reference date "2000-01-01 00:00:00". This date is arbitrary and irrelevant for practical purposes, since the model simulations are idealized. However, a sensible date such as this must be picked to avoid potential problems in the DCMIP visualization tools. Daily time snapshots (e.g. 13 snapshots for 12 days including the initial state) need to be listed as

```
time = 0, 1, 2, 3, 4, 5, 6, 7, 8, 9, 10, 11, 12;
```

G.5. Computational grid

The netCDF file must list the longitudinal and latitudinal positions of the horizontal grid (in degrees) and must contain sufficient information about the vertical grid. In orography-following hybrid $\sigma - p$ (η) coordinates, as shown in the example in section G.3, the necessary information for the reconstruction of the pressure values along the full model and interface levels is the surface pressure PS, the surface geopotential PHIS and the list of the 'a' and 'b' hybrid coefficients, here called HYAM, HYBM, HYAI, HYBI. The key point is that the vertical positions of the grid, either in

pressure coordinates (for most hydrostatic model) or height coordinates (for most non-hydrostatic models), need to be reconstructable based on the information in the netCDF output file. Details on the vertical grids and the equations for the reconstruction of the pressure or height values need to be provided, possibly in form of a model documentation or a journal paper. In addition, the netCDF file needs to define whether the order of the vertical levels is positive downwards ("down"), as in the example above, or positive upwards ("up"). The metadata entry 'positive =' as shown in

```
double lev(lev) ;
  lev:long_name = "hybrid level at midpoints(1000*(A+B))" ;
  lev:units = "level" ;
  lev:positive = "down" ;
  lev:standard_name = "atmosphere_hybrid_sigma_pressure_coordinate" ;
  lev:formula_terms = "a: hyam b: hybm p0: P0 ps: PS" ;
```

defines this order, and needs to be present. If the vertical arrangement can be freely chosen, the 'down' numbering system is recommended (level counter increases downwards).

G.6. Example: NetCDF data structure for a non-latitude-longitude grid

An example netCDF data structure for a non-latitude-longitude (e.g. spherical geodesic) grid is given below.

```
dimensions:
   cell = 2562 ;  // number of grid cells
   lev = 30 ;
   ilev = 31 ;
   time = UNLIMITED ; // (11 currently)
variables:
  double lon(cell) ;
    lon:long_name = "longitude" ;
    lon:units = "degrees_east" ;
    lon:bounds="lon_vertices" ;
  double lat(cell) ;
    lat:long_name = "latitude" ;
    lat:units = "degrees_north" ;
    lat:bounds="lat_vertices" ;
  double time(time) ;
    time:long_name = "time" ;
    time:units = "days since 2000-01-01 00:00:00" ;
  double cell_area(cell) ;
    cell_area:long_name = "area of grid cell" ;
    cell_area:standard_name="area";
    cell_area:units = "m2"
  float PS(time,cell) ;
    PS:units = "Pa" ;
```

```
    PS:coordinates = "lon lat" ;
    PS:cell_measures = "area: cell_area" ;
    PS:long_name = "Surface pressure" ;
 float T(time, lev, cell) ;
    T:units = "K" ;
    T:coordinates = "lon lat" ;
    T:cell_measures = "area: cell_area" ;
    T:long_name = "Temperature" ;
```

On non-latitude-longitude grids the area weight "cell_area" of cell should be included in the netCDF output file. This allows for the computation of global error norms based on the original grid point locations. Here, the data structure for the non-orthogonal grid utilizes a single index "cell" for all positions of the horizontal grid. The longitudinal and latitudinal positions are listed according this single array index. Other data structures are also possible.